

Structural and Functional Characterization of Extracellular Domains of Vascular Endothelial Growth Factor Receptor 1 and 2

Inauguraldissertation

zur

Erlangung der Würde eines Doktors der Philosophie

vorgelegt der

Philosophisch-Naturwissenschaftlichen Fakultät

der Universität Basel

von

Mayanka Asthana

von Indien

2019

Genehmigt von der Philosophisch-Naturwissenschaftlichen Fakultät

auf Antrag von

Prof. Dr. Kurt Ballmer-Hofer

(Fakultätsverantwortlicher & Dissertationsleiter)

Prof. Dr. Timm Maier

(Korreferent)

Basel, 25. Juni 2019

Prof. Dr. Martin Spiess

The Dean of Faculty

1. Table of content

1.	Table of content	1
2.	Abbreviations	5
3.	Summary.....	11
4.	Zusammenfassung.....	13
5.	Introduction	17
5.1.	Molecular basis of angiogenesis	17
5.2.	Pathological angiogenesis	20
5.3.	Therapeutic approaches	21
5.4.	VEGFs/VEGFR signaling cascade.....	23
5.4.1.	The ligands.....	24
5.4.2.	VEGFRs.....	29
5.5.	Aims of the thesis.....	34
6.	Materials and Methods	37
6.1.	Cloning, expression and purification of VEGFR-2 ECD subdomains for crystallization experiments	37
6.1.1.	Cloning of a VEGFR-2 ECD subdomain construct for insect cell expression.....	37
6.1.2.	Cloning of VEGFR-2 constructs for baculovirus mediated transduction in mammalian (HEK293S GnTi-) cells	37
6.1.3.	Cloning of mouse mVEGFR-2 ECD constructs for expression in mammalian (HEK293 EBNA) cells	38
6.1.4.	Cloning of glycosylation lacking VEGFR-2 constructs for mammalian (HEK293 EBNA) cell expression	40
6.1.5.	Protein production of ligands.....	41
6.1.6.	Production and purification of human VEGFR-2 ECD subdomain proteins in insect cells.....	41
6.1.7.	Production and purification of mouse VEGFR-2 ECD subdomains in mammalian cells	42
6.1.8.	Cloning, expression and purification of soluble Fab.....	43
6.2.	Biochemical and biophysical characterization of recombinant proteins	44
6.2.1.	Limited proteolysis	44

6.2.2.	Differential scanning fluorimetry.....	44
6.2.3.	Isothermal titration microcalorimetry	45
6.2.4.	Microscale thermophoresis (MST)	45
6.3.	Functional analysis of Ig-homology domain 5 mutants of VEGFR-1 and 2 46	
6.3.1.	Cloning of VEGFR-1 mutants for functional analysis	46
6.3.2.	Cloning of VEGFR-2 mutants for functional analysis	48
6.3.3.	Cloning of VEGFR-1/2 chimeric constructs for functional analysis	51
6.3.4.	Cloning of VEGFR-1 for lenti viral expression.....	51
6.3.5.	Cell Culture	52
6.3.6.	Transient transfections.....	52
6.3.7.	Generation of stably transfected PAE cells by chemical transfections..	53
6.3.8.	Generation of stably transfected PAE cells by lentiviral transductions..	53
6.3.9.	Immunocytochemistry	54
6.3.10.	VEGF receptor activity assay.....	54
7.	Results	57
7.1.	Structural characterization of VEGFR-2 ECD complexes	57
7.1.1.	Expression and purification in insect cells.....	57
7.1.2.	Expression and purification in mammalian cells.....	61
7.1.2.1.	Baculovirus mediated gene expression of VEGFR-2 ECD subdomains in mammalian cells	61
7.1.2.2.	Expression and purification of mouse VEGFR-2 ECD subdomains in HEK293 EBNA cells	64
	66	
7.1.3.	Crystallization of VEGFR-2 ECD complexes.....	67
7.1.3.1.	Co-crystallization of VEGFR-2 ECD subdomains with ligands.....	68
7.1.3.2.	Co-crystallization of VEGFR-2 ECD/VEGF-E with scFV	72
7.1.3.3.	Co-crystallization of VEGFR-2 ECD/VEGF-A ₁₂₁ with Fab.....	73
7.2.	Biochemical and biophysical characterization of VEGFR-2 ECD complexes.....	76
7.2.1.	Analysis of unstructured regions in VEGFR-2 ECD	76
7.2.1.1.	Limited proteolysis	77
7.2.2.	Thermal stability assay	80
7.2.3.	Thermodynamic analysis of VEGFR-2 ECD complexes	81

7.3.	Functional analysis of ligand binding and receptor activation of VEGFR-1	84
7.3.1.	Functional analysis of VEGFR-1 domain 5 mutants.....	84
7.3.2.	Functional analysis of chimeric VEGFR-1/2 domain 5 mutants	90
7.3.3.	Functional analysis of VEGFR-2 domain 5 mutants.....	92
7.4	Structure of the Full-length VEGFR-1 ECD in Complex with VEGF-A ..	95
8.	Discussion and Outlook.....	121
8.1.	Crystallization of VEGFR-2 ECD ligand complexes	121
8.2.	Role of VEGFR-2 ECD in receptor dimerization and activation	124
8.3.	Functional role of homotypic interactions in the VEGFR-1 ECD	126
9.	Conclusion	131
10.	Acknowledgement.....	133
11.	References.....	135

2. Abbreviations

Akt	Protein kinase B
AMD	Age-related macular degeneration
ANG	Angiopoietin
AP	Alkaline phosphatase
BacMam	Baculovirus mediated gene transduction of mammalian cell
BCA	Bicinchoninic Acid
BM	Basement membrane
c-Kit	Stem cell growth factor receptor
Co-IP	Co-immunoprecipitation
C-terminal	Carboxy-terminal
CTLA	Cytotoxic T lymphocyte protein
DAG	Diacylglycerol
DLL4	Delta-like ligand 4
DMEM	Dulbecco's modified Eagle's medium
DNase	Deoxyribonuclease
DSS	Distal splice site
DTT	Dithiothreitol
EBNA-1	Epstein-Barr nuclear antigen 1
EBV	Epstein-Barr virus
<i>E.coli</i>	<i>Escherichia coli</i>
ECD	Extracellular domain
ECM	Extracellular matrix
EC(s)	Endothelial cell(s)

EDTA	Ethylenediamine tetraacetic acid
EM	Electron microscopy
Endo F	Endoglycosidase F
eNOS	Endothelial nitric oxide synthase
EPCs	Endothelial precursor cells
Eph	Ephrin
ERK	Extracellular signal-regulated kinase
Fab	Fragment antigen-binding antibody
FAK	Focal adhesion kinase
FATP	Fatty acid transport protein
FBS	Fetal bovine serum
Fc	Fragment crystallizable
FGFs	Fibroblast growth factors
Flk-1	Fetal liver kinase-1
Flt-1	Fms-like tyrosine kinase-1
Fyn	Proto-oncogene tyrosine-protein kinase
Grb	Growth factor receptor bound
HEK293	Human embryonic kidney cells
HEPES	4-(2-Hydroxyethyl) piperazine-1-ethanesulfonic acid
HIF	Hypoxia-inducible factor
HRP	Horseradish peroxidase
HSPG	Heparin sulfate proteoglycan
Ig	Immunoglobulin
IMAC	Immobilized metal ion affinity chromatography
IP ₃	Inositol 1,4,5-trisphosphate

IPTG	Isopropyl β -D-1-thiogalactopyranoside
IT	Isothermal reaction buffer
ITC	Isothermal titration calorimetry
IR	Infrared
JCSG	Joint Center for Structural Genomics
JMD	Juxtamembrane domain
Kd	Equilibrium dissociation constant
kDa	Kilo-Dalton
KDR	Kinase insert domain-containing receptor
KID	Kinase insert domain
LB	Luria Bertani
LCP	Lipidic cubic phase
LED	Light-emitting diode
MAPK	Mitogen-activated protein kinase
MEK	Mitogen-activated protein kinase kinase
MMPs	Matrix metalloproteinases
MMS	Microseed matrix screening
MST	Microscale thermophoresis
mTOR	Mammalian target of rapamycin
MW	Molecular weight
NICD	Notch intracellular domain
Nrp	Neuropilin
N-terminal	Amino-terminal
PAE	Porcine aortic endothelial
PBS	Phosphate-buffered saline

PCR	Polymerase chain reaction
PDGF	Platelet-derived growth factor
PDGFR	Platelet-derived growth factor receptor
PDL	Programmed cell death ligand
PEG	Polyethylene glycol
PEI	Polyethyleneimine
PEM	Protein Expression Medium
PI-3 KINASE	Phosphatidylinositol 3'-kinase
PIP ₂	Phosphatidylinositol (4,5)-bisphosphate
PIGF	Placenta growth factor
PKC	Protein kinase C
PLC	Phospholipase C
PNGase F	Peptide: N-glycosidase F
PSF	Progression free survival
PSS	Proximal splice site
PTB	Phospho-tyrosine binding
PVDF	Polyvinylidene fluoride
RTK	Receptor tyrosine kinase
SAXS	Small angle X-ray scattering
scFv	Single chain variable fragment
SDS-PAGE	Sodium dodecylsulfate polyacryl gel electrophoresis
SEC	Size exclusion chromatography
Sf21	<i>Spodoptera frugiperda</i> cells
SH	Src-homology
SHB	Src homology-2 protein in beta-cells

SHC	Src homology 2 domain-containing transforming protein
SHP	Src-homology phosphatase
TB	Terrific Broth
TBST	Tris-buffered saline
TGF	Transforming growth factor
T _m	Melting temperature
TM	Transmembrane
TMD	Transmembrane domain
TSAd	T cell specific adapter
VD	Vapour diffusion
VEGF	Vascular endothelial growth factor
VEGFR	VEGF receptor

3. Summary

Angiogenesis is the formation of new blood vessels from pre-existing vasculature and plays an essential role in normal organ development and in specific diseases in all higher organisms. Angiogenesis is therefore required already early in embryogenesis when the new blood and lymphatic systems develop. In adult organisms angiogenesis is required in numerous processes such as in vessel formation and remodeling in the female reproductive cycle, during wound healing, or in bone formation and remodeling. Aberrant excessive vessel formation, i.e. pathological angiogenesis, plays an important role in tumor progression, in diabetic retinopathy, rheumatoid arthritis or in psoriasis. The lack of angiogenesis leads to multiple vascular failure such as coronary artery disease. It is well established that the correct balance between pro- and anti-angiogenic growth factors, cytokines, and extracellular matrix components is essential for vascular homeostasis. One of the critical regulators of both physiological and pathological angiogenesis discovered more than 30 years ago is Vascular Endothelial Growth Factor (VEGF), regulating endothelial cell (EC) proliferation, migration, and survival but also vascular topology and permeability. VEGF is a family of cysteine linked dimeric growth factors consisting of five members, VEGF-A, -B, -C, -D and Placenta Growth Factor (PlGF). These soluble or matrix associated proteins bind to three type V receptor tyrosine kinases (RTKs), VEGF-receptor (VEGFR)-1 (also known as Flt1), VEGFR-2 (KDR/Flk1), and VEGFR-3 (Flt4). VEGFRs consist of an extracellular domain (ECD) built from seven immunoglobulin (Ig)-homology domains required for ligand binding and subsequent receptor dimerization. A single transmembrane (TM) helix connects the ECD to the cytoplasmic part containing a split tyrosine kinase domain. Ligand binding to VEGFR ectodomains promotes dimerization of receptor monomers, followed by receptor autophosphorylation and kinase activation. The activated receptor contains specific tyrosine residues in the kinase domain and the carboxy-terminal (C-terminal) domain acting as docking sites for a plethora of signaling proteins involved in multiple cellular signaling pathways.

Ig-homology domains 1-3 (VEGFR-3) or 2-3 (VEGFR-1 or -2) of the ECD form the ligand binding site, while domains 4-7 are involved in homotypic receptor contacts fulfilling a regulatory function, which was the subject of this thesis. I used isothermal

titration calorimetry (ITC) in this study to determine the thermodynamic properties of ligand binding and dimer formation. The data show that the free energy of VEGF-A binding to domains 1-3 or the full-length ECD of VEGFR-2 is entropy driven and enthalpically unfavourable. Most importantly, the Gibbs free energy of VEGF-A binding to the full length ECD is 1.12 kcal/mol higher compared to the binding energy of domains 1-3. The endothermic component arising from the homotypic receptor contacts in domains 4-7 thus reduces the overall binding affinity of the full-length VEGFR-2 ECD by about 10 fold. This suggests that the homotypic interactions in domain 4-7 play a regulatory role in ligand binding and receptor activation, e.g. by promoting conformational rearrangements of receptor monomers required for active dimer formation. This mechanism might also prevent spontaneous activation of VEGFR-2 in the absence of ligand.

I also tried to crystallize the ECD of VEGFR-2 in complex with ligand. However, although I used a multitude of receptor ECD constructs, I did not obtain diffracting crystals. I therefore became involved in an accompanying project in the lab focusing on the crystal structure of the full-length VEGFR-1 ECD in complex with VEGF-A. This structure revealed distinct homotypic contacts in Ig-homology domains 5 and 7. To further characterize the contacts in domain 5 biochemically and to investigate their functional relevance in receptor activation I generated mutants disrupting specific hydrogen bonds and salt bridges involved in homotypic contact formation. The data showed a significant decrease in receptor phosphorylation activity upon stimulation with ligand. Similarly, I could show reduced receptor activity when the homologous residues were mutated in VEGFR-2. The biochemical characterization of these mutants thus document the regulatory role of domain 5 in VEGFR activation and identify domain 5 as a promising target for developing allosteric inhibitors of VEGFRs. The speciality of drugs proposed to target domain 5 lies in their ability to access the target receptor at a regulatory site in the extracellular receptor domain, which is easily accessible from the blood stream. In addition, the proposed drugs will be highly specific as compared with the currently used kinase inhibitors.

4. Zusammenfassung

Angiogenese ist die Bildung neuer Blutgefäße aus existierenden Gefäßsystemen und spielt eine essenzielle Rolle während der normalen Entwicklung und einigen Krankheiten in allen höheren Organismen. Daher findet Angiogenese schon in der frühen Embryogenese statt um neue Blut- und Lymphgefäße zu entwickeln. In erwachsenen Organismen ist Angiogenese in einigen Prozessen notwendig, wie der Bildung und dem Umbau von Gefäßen während des weiblichen Reproduktionszykluses, während der Wundheilung und dem Auf- und Umbau von Knochen. Abnormale exzessive Gefäßbildung, also pathologische Angiogenese, spielt eine wichtige Rolle in der Tumorentwicklung, der diabetischen Retinopathie, der rheumatischen Arthritis oder der Psoriasis. Der Verlust der Angiogenese wiederum führt zu mehreren Gefäßversagen wie in der koronalen Arterienerkrankung. Es ist gut etabliert, dass das richtige Gleichgewicht zwischen pro- und antiangiogenetischer Wachstumsfaktoren, Cytokinen, und extrazellulärer Matrixkomponenten essenziell ist für die Gefäßhomeostase. Ein kritischer Regulator für die physiologische wie auch pathologische Angiogenese, der vaskuläre endotheliale Wachstumsfaktor (VEGF), wurde schon vor mehr als 30 Jahren entdeckt. VEGF reguliert endotheliales Zellwachstum, -migration und -überleben, aber auch Gefäßstopologie und -permeabilität. VEGF ist ein Familie aus Cystein verbundenen dimeren Wachstumsfaktoren, die aus fünf Mitgliedern besteht: VEGF-A, -B, -C, -D und Plazenta Wachstumsfaktor (PlGF). Diese löslichen oder Matrix-assoziierten Proteine binden drei Typ V Rezeptortyrosinkinasen (RTKs), VEGF-rezeptor (VEGFR)-1 (auch Flt1 genannt), VEGF-rezeptor (VEGFR)-2 (KDR/Flk1) und VEGF-rezeptor (VEGFR)-3 (Flt4). VEGFR besteht aus einer extrazellulären Domäne (ECD) mit sieben immunoglobulin(IG)-homologen Domänen und wird für die Ligandbindung und die darauffolgende Rezeptordimerisierung benötigt. Eine einzelne transmembrane (TM) Helix verbindet die ECD mit dem cytoplasmatischen Teil, welcher eine Tyrosin Kinasendomäne beinhaltet. Die Bindung eines Liganden an der VEGFR Ectodomäne induziert die Dimerisierung des monomeren Rezeptors gefolgt von der Autophosphorylierung des Rezeptors und der Aktivierung der Kinase. Die aktive Kinase enthält spezifische Tyrosinseitenketten in der Kinasedomäne und der C-

terminalen Domäne und agiert als Andockstellen für eine Vielzahl von Signalproteinen, die in mehreren zellulären Signalwegen involviert sind.

Das Thema dieser Dissertation war die Untersuchung der Ligandenbindungsstelle, die durch Ig-homogen Domäne 1-3 (VEGFR-3) oder 2-3 (VEGFR-1) der ECD ausgebildet wird, sowie der regulatorischen Funktion der Domäne 4-7, die mit dem homotypischen Rezeptor interagiert. Es wurde isothermale Titrationskalometrie verwendet, um die thermodynamischen Eigenschaften der Ligandbindung und der Dimerisierung zu bestimmen. Die Daten zeigen, dass die Bindung von VEGF-A an die Domänen 1-3 oder die ganze ECD des VEGFR-2 entropisch, jedoch nicht enthalpisch favorisiert ist. Wichtig ist, dass die Gibbs-Energie zwischen VEGF-A und der vollen ECD 1.12 kcal/mol höher als die Bindungsenergie der Domäne 1-3 ist. Die endothermale Komponente kommt von homotypischen Rezeptorkontakten in der Domäne 4-7, die die Gesamtbindungsaffinität zwischen dem Liganden und der vollen VEGFR-2ECD um das zehnfache reduziert. Dies weist auf eine homotypische Interaktion hin, die eine regulatorische Rolle spielt, indem sie Konformationsänderungen des monomeren Rezeptors fördert, die zur Bildung eines aktiven Rezeptordimers führt. Dieser Mechanismus könnte die spontane Aktivierung von VEGFR-2 in der Abwesenheit des Liganden verhindern.

Ich habe versucht die VEGFR2-ECD zusammen mit dem Liganden zu kristallisieren. Trotz mehreren Versuchen mit verschiedenen ECD-Konstrukten wurden keine Kristalle erhalten. Dies führte dazu, dass ich mich an einem verwandten Projekt beteiligte; der Kristallisation des VEGFR1-ECD/VEGF-A Komplexes. Diese Kristallstruktur zeigt homotypische Interaktionen mit der Ig-homologen Domäne 5 und 7 auf. Um die funktionelle Relevanz festzustellen, wurden spezifische Wasserstoffbrücken und Salzbrücken, welche wichtig für die Bindung mit der homotypischen Domäne 5 sind, durch Mutationen gebrochen. Daten dieser Mutanten zeigten, dass die Phosphorylierungsaktivität dieser Rezeptoren signifikant reduziert ist, wenn sie mit Liganden stimuliert werden. In gleicher Weise wurde die Aktivität beeinträchtigt, wenn die entsprechenden Seiten der Domäne 5 der homologen VEGFR-2 mutiert wurden. Die biochemische Charakterisierung dieser Mutanten dokumentiert die regulatorische Rolle der Domäne 5 in VEGFR-Aktivierung und identifiziert sie als einen vielversprechenden Startpunkt zur Entwicklung allosterischer Inhibitoren für den

VEGF Rezeptor. Ein wichtiger Aspekt eines potenziellen Mwdikamentes wäre, dass es an die regulatorische Stelle der extrazellulären Rezeptordomäne binden könnte, welche aus dem Blut erreichbar ist. Zusätzlich wäre diese vorgeschlagene Droge hochspezifisch verglichen mit heutigen Kinaseinhibitoren.

5. Introduction

Angiogenesis is an important process, in which formation of new blood vessels takes place via extension or remodeling from the existing capillaries. It is an indispensable process required for the vertebrate development. In a developing embryo, the cardiovascular system forms in the very beginning to establish the oxygen diffusion, metabolite and nutrient exchange in rapidly expanding tissues of the embryo. Vasculogenesis is the *de novo* process of formation of the primitive network of vessels from mesoderm derived endothelial precursors (angioblasts). Pericytes and smooth muscle cells are recruited to stabilize this early network. This primary capillary plexus is progressively remodeled by the angiogenic processes to establish a mature circulatory network. Vasculogenesis, mostly known to be limited to embryonic development, can also support neovascularization from the bone marrow derived endothelial precursor cells (EPCs) in adulthood. Angiogenesis is the essential process for the maturation of the new vasculature during embryonic development. During adulthood, it is required only during the formation of new capillaries in response to injured tissue, during physical training, when physiological metabolic demand increases and during menstrual cycle of women. Therefore, ECs are considered stable, showing limited turnover in the adult vasculature (Risau, 1997). Angiogenesis can occur by two distinct mechanisms: sprouting and intussusception (Djonov *et al.*, 2002). During sprouting angiogenesis, the vascular ECs proliferate and migrate (sprout) into a proteolytically degraded extracellular matrix (ECM) guided by angiogenic signals to form a new branch derived from an existing vessel. During intussusception (non-sprouting), the vessel proliferates to extend into the lumen leading to splitting of vessel in two. Initial expansion of the capillary plexus takes place via both the processes namely sprouting and intussusception but consequent growth and remodeling is attained by intussusception.

5.1. Molecular basis of angiogenesis

Vessel formation is known to be induced by a variety of molecular players such as growth factors, cytokines, growth factor receptors and transcription factors. Out of the various models of angiogenesis, the sprouting mechanism has more thoroughly

studied molecular basis. Proangiogenic molecules such as VEGF, angiopoietin (ANG-2), fibroblast growth factors (FGFs) activate the dormant vessels. It leads to detachment of pericytes from the basement membrane by the proteolytic degradation facilitated by the matrix metalloproteinases (MMPs). VEGF plays a key role by increasing the permeability of the EC layer leading to remodeling of the preexisting matrix (Carmeliet *et al.*, 2011). One of the ECs assumes a tip cell like character in presence of VEGFRs, neuropilins (Nrp) and Notch ligands. The tip cell extends its filopodia and starts migrating towards high levels of VEGF which activates the signaling of VEGFR-2 with its co-receptor Nrp1. These cells then start expressing high levels of Notch ligand Delta-like ligand 4 (DLL-4), which interacts to Notch receptors on the adjacent ECs, releasing the cleaved Notch intracellular domain (NICD). NICD is a transcriptional regulator which down regulates the expression of *Vegfr2* and *Nrp1* on the cells adjacent to tip cells while increasing the expression of a decoy receptor, VEGFR-1 which has greater affinity for the ligand VEGF. Hence these adjacent cells acquire the characteristic of the stalk cells (Lundkvist *et al.*, 2007). Notch plays a crucial role in specification of tip and stalk cells, by acting as a negative feedback loop to VEGF signaling (Jakobsson *et al.*, 2009). The growing sprouts follow the guidance cues of a VEGF gradient and migrate towards molecules such as semaphorins and ephrins. Behind the tip cells the stalk cells proliferate for sprout elongation and lumen formation. Macrophages support the fusing of two tip cells (anastomosis) by interacting with the filopodia from the two tip cells. A connected lumen is formed after fusing of tip cells to allow blood flow which delivers nutrient and oxygen and consequently subsides the angiogenic signals. ECs become quiescent and acquire a phalanx phenotype which regulates blood flow and tissue perfusion. The ECs express platelet-derived growth factor (PDGF) and attract the pericyte precursors which differentiate in response to transforming growth factor (TGF- β) into mural cells. This brings stabilization in the newly formed vessel by reducing EC proliferation, migration and vessel leakage. Levels of angiogenic signal are reduced, whereas paracrine and autocrine signals including VEGF, FGF, Ang1 and Notch from ECs and support cells maintain ECs in quiescence. The vessel is further matured by recreating cell-cell junctions and deposition of basement membrane (BM) to promote vessel stabilization (Eichmann *et al.*, 2012) (Figure 1).

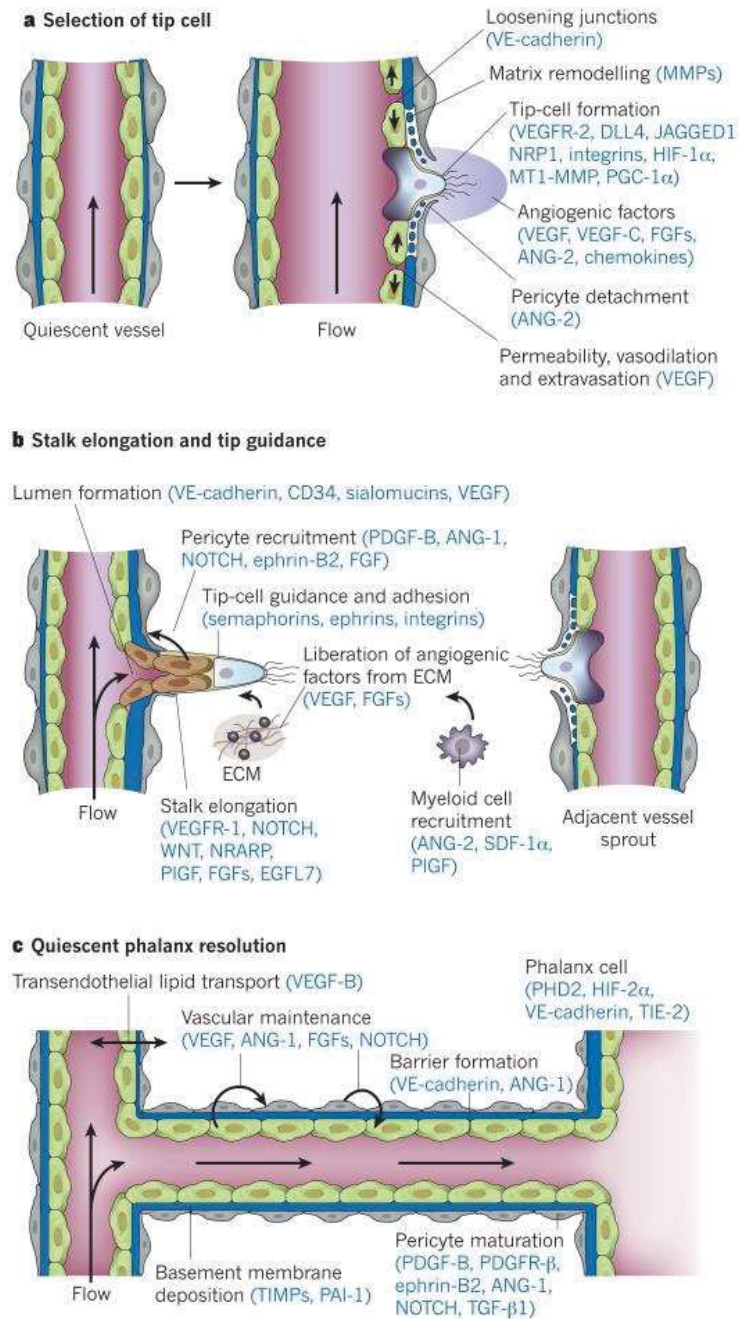


Figure 1: Molecular mechanism of vessel formation. (a) Quiescent vessel is activated by angiogenic factors and tip cell is selected for branch formation. (b) Tip cells are directed by guidance signals for migration. Stalk cells proliferate, elongate and form lumen after fusion. Stalk cells attract pericytes and basement membrane deposition for attaining stabilization. (c) Neovessels are perfused with lumen formation. Quiescent phenotype is attained by re-establishing junctions, pericyte maturation and release of vascular maintenance signals. adapted from (Carmeliet *et al.*, 2011)

This complex process of angiogenesis, has crucial involvement of VEGF family members. It is evident from the studies of knockout mice. Homozygous gene deletion of either VEGF-A or VEGFRs in mice leads to embryonic death in utero between embryonic day 8.5 and 10.5, due to abnormal vascular development. Even deletion of a single VEGF-A allele is sufficient to lead to lethality at embryonic day 11-12 (Carmeliet *et al.*, 1996; Ferrara *et al.*, 1996). Subcellular localization also plays a crucial role in VEGFR-2 signaling. Signaling of VEGFR-2 from intracellular compartments induces arterial morphogenesis (Lanahan *et al.*, 2010). Matrix bound isoforms of VEGF are known to stimulate branching, whereas soluble isoforms lead to enlargement of vessels. Autocrine VEGF produced by ECs contributes to the attainment of blood homeostasis whereas paracrine VEGF produced by tumor and stromal cells leads to increase in vessel branching (Lee *et al.*, 2007).

Vessel perfusion into different areas of the body also involves defining the ECs of an arterial or venous specification. Ephrin (Eph) receptor tyrosine kinase family is involved in this event. Eph receptors and their ligands (Ephrin) are both TM proteins and require cell to cell contact for their signaling. EphrinB2 is preferentially expressed in arterial ECs while its receptor EphB4 is mainly expressed in venous ECs (Wang *et al.*, 1998).

5.2. Pathological angiogenesis

The imbalance of pro- and anti-angiogenic factors (known as 'angiogenic switch') can lead to pathological angiogenesis. Pathologies hallmarked by excessive vessel growth include cancers, retinopathies induced by age (age-related macular degeneration, AMD), psoriasis, arthritis or diabetes. Moreover, insufficient vessel growth and abnormal vessel regression can lead to neurodegeneration, hypertension, heart and brain ischemia and pre-eclampsia and osteoporosis (Carmeliet, 2003).

Cancers have several modes of vessel formation and they can switch in between these modes: (1) Avascular tumors can induce vessel formation by angiogenic sprouting, (2) pre-existing vessels can split by a process known as intussusception, (3) tumor cells can grow around preexisting vessels known as vessel cooption, (4) tumor cells can line along vessels, acting as replacement cells for ECs (vascular mimicry), (5) due to cytogenetic abnormalities in chromosomes, putative cancer stem cells are allowed to

differentiate into ECs (6) EPCs recruited from bone marrow also contribute to tumor angiogenesis (Carmeliet *et al.*, 2011).

The tumor can tip the balance towards an angiogenic phenotype in presence of several factors such as metabolic and mechanical stress, mutation of oncogenes and inflammation (Carmeliet *et al.*, 2000). The demand for oxygen and nutrients in a tumor of size around 2 mm in diameter exceeds the local supply, making it hypoxic. Hypoxia initiates the upregulation of the transcription factor hypoxia-inducible factor 1 (HIF-1) which induces the expression of proangiogenic molecules such as VEGF, PlGF, FGFs and interleukin-8 (Baish *et al.*, 2000). The tumor vasculature due to imbalance of VEGF family ligands, form disorganized structural alterations such as unequal distribution of vessel branches, form chaotic networks of leaky vessels and frequent lack of pericytes (Nagy *et al.*, 2010). Some tumors begin with well vascularized tumors due to co-option on existing vessels. In defense against co-option, the host vessels start to express high autocrine levels of Ang2, consequently leading to vessel regression. As the vessels undergo apoptosis, the tumor becomes secondarily avascular and hypoxic. The tumor rescues itself by secreting high levels of VEGF, to initiate new angiogenic sprouting from these vessels for its further survival and growth (Holash *et al.*, 1999).

Clearly, tumor growth and metastasis depends solely on angiogenesis. The late Judah Folkman, in 1971, performed pioneering work in the field. He proposed to block the nourishment of tumors by cutting its blood supply as a new anticancer strategy. (Folkman, 1971).

The proliferative retinopathies such as diabetic retinopathy and wet AMD are leading cause of vision loss worldwide. Both the disorders are characterized by extensive proliferation of new blood vessels, triggered mainly by angiogenic factor VEGF (Caldwell *et al.*, 2003; Gariano *et al.*, 2005). The new leaky vessels formed leads to retinal edema and sub-retinal fluid accumulation, subsequently resulting in impaired vision. Hence, inhibition of VEGF is the strategy used clinically for treating ischemia-related retinopathies (Kim *et al.*, 2012).

5.3. Therapeutic approaches

Since VEGF family members are the crucial regulators of both developmental and pathological angiogenesis, many therapeutic approaches target the VEGF/VEGFR

signaling system. One of the strategies utilized by the antiangiogenic therapies is to prevent VEGF ligand binding to the receptor by blocking either of the binding sites. Bevacizumab (Avastin), a humanized monoclonal anti-VEGF antibody has been approved by the US Food and Drug Administration in combination with chemotherapy or cytokine therapy for many advanced metastatic cancers, including non-squamous non-small cell lung cancer, colorectal cancer, renal cell cancer and breast cancer. Anti-VEGF fragment antigen-binding antibody (Fab) ranibizumab (Lucentis) and a VEGF aptamer pegaptanib (Macugen) are used to treat leaky neovessels in patients suffering from wet AMD (Biswas *et al.*, 2011; Carmeliet *et al.*, 2011; Carneiro *et al.*, 2011).

Another approach applied for the clinical treatment is use of small molecule inhibitors. These bind to the intracellular domain of the receptor and inhibit the catalytic activity of the tyrosine kinase domain, by interfering with the ATP binding pocket (Type I), or preventing the kinase domain from attaining the active conformation (Type II). Sunitinib (Sutent) and Pazopanib (Votrient) are used to treat renal cell carcinoma, Sorafenib (Nexavar) for metastatic renal cell carcinoma and hepatocellular carcinoma, and Vandetanib (Zactima) for medullary thyroid cancer. Also aflibercept (Regeneron), the “VEGF Trap” which is a soluble chimeric protein constituting Ig-homology domain 2 of VEGFR-1 and Ig-homology domain 3 of VEGFR-2, predimerized by a constant region (Fc-region) of human IgG1, is used to neutralize the ligands VEGF-A, VEGF-B and PlGF in patients with metastatic colorectal cancer as well as wet macular degeneration (Holash *et al.*, 2002). To block VEGFR-2 signaling, a fully humanized monoclonal antibody targeting the ligand binding site on the receptor ECD called ramucirumab, is used for treating advanced gastric or gastro-esophageal adenocarcinoma (Krupitskaya *et al.*, 2009). Alitalo and colleagues generated monoclonal antibody against VEGFR-3 that inhibits homodimer and heterodimer formation but does not block ligand binding (Tvorogov *et al.*, 2010). They showed inhibition in sprouting, migration and signal transduction of microvascular ECs.

A new approach in therapeutics which should theoretically result in effective tumor growth inhibition, is to use combination of anti-VEGF agents with other angiogenic inhibitors or inhibitors from non-related pathways. Since, VEGF-A inhibition studies show considerable increase in the number of tumor-infiltrating lymphocytes. Hence clinical trials are being performed which use a combination of anti VEGF-A treatment

with immune checkpoint inhibitors eg. Cytotoxic T lymphocyte protein 4 (CTLA4) or programmed cell death ligand (PDL1) (Shrimali *et al.*, 2010). Also the sequential treatments with VEGF-A inhibitors and inhibitors of mammalian target of rapamycin (mTOR) such as everolimus (Afinitor Disperz; Novartis) have resulted in increased progression free survival (PSF) in patients with metastatic renal cell carcinoma (Motzer *et al.*, 2015) .

Despite of many clinical benefits of these anti-angiogenic therapies, there are several more challenges and concerns to be solved. Problem is the development of resistance to the treatment. Some tumors become unresponsive during treatment and produce other proangiogenic factors and induce angiogenesis independent of the VEGF pathway. Vessel pruning by VEGF blockade sometimes aggravates hypoxia, leading to recruitment of various immune cell subsets, and release of angiogenic factors such as PlGF, FGFs, chemokines and ephrins (Bergers *et al.*, 2008). Depriving a tumor of blood vessels, switches it to become more invasive by selecting “hypoxia” resistant clones and making it more metastatic. Tumors also adopt other modes of vascularization besides sprouting, such as vessel co-option or vascular mimicry and recruitment of bone-marrow derived progenitor cells which are less sensitive to VEGFR inhibition.

Hence, there is urgent need for the development of predictive biomarkers which can differentiate between responders and non-responders, refining molecular targeting, development of appropriate combinatorial therapies and finally more bench to bedside studies, to improve the efficacy of the antiangiogenic therapies.

5.4. VEGFs/VEGFR signaling cascade

The VEGF family comprises 5 mammalian dimeric glycoproteins designated VEGF-A, VEGF-B, VEGF-C, VEGF-D and PlGF. In addition VEGF E, found in parapox viruses and VEGF-F, found in snake venoms are highly related structurally to mammalian VEGFs (Shibuya, 2003; Yamazaki *et al.*, 2009). VEGFs undergo either proteolytic processing (VEGF-C and VEGF-D) and/or alternative splicing (VEGF-A, VEGF-B and PlGF), to give rise to distinct isoforms, leading to diverse signaling functions. VEGFs bind with high affinity in an overlapping pattern to type V RTKs namely VEGFR-1, VEGFR-2 and VEGFR-3, to exert their biological effects (Takahashi *et al.*, 2005). The

receptors are dimerized upon ligand binding leading to activation of the tyrosine kinase and autophosphorylation of tyrosine residues to initiate multiple signal transduction pathways. Signaling output is further modified by binding of co-receptors, such as Nrp, heparin sulfate proteoglycans (HSPG) and integrins (Koch *et al.*, 2011).

VEGFRs have a similar structural arrangement comprising of seven Ig-homology domains in the extracellular region, a single TM helix, a juxtamembrane domain (JMD), a split tyrosine-kinase and a long tail at C-terminal. The Ig-homology domains 1-3 present in the ECD are involved in ligand binding to different extents in distinct ligand receptor interactions. And the membrane proximal Ig-homology domains 4-7 are involved in proper positioning of receptor dimers.

5.4.1. The ligands

VEGF-A

VEGF-A plays a crucial role in vascular development during embryo formation, maintenance of proper vessel function in adults and also in disease. It is produced in vascular ECs and immune cells. Alternatively spliced variants of human VEGF-A encodes eleven different isoforms with distinct biological properties: VEGF-A₁₂₁, VEGF-A₁₄₅, VEGF-A₁₄₈, VEGF-A₁₆₂, VEGF-A₁₆₅, VEGF-A_{165b}, VEGF-A₁₈₃, VEGF-A₁₈₉, VEGF-A₂₀₆ (Bates *et al.*, 2002; Lange *et al.*, 2003), newly discovered VEGF-A₁₁₁ and VEGF-A_{111b} (Gu *et al.*, 2013).

The gene of VEGF consists of eight exons: where exon 1, and four residues of exon 2, encode for the signal peptide; exon 3 and exon 4 encodes for VEGFR-1 and 2 binding sites; exon 5 encodes a sequence which is recognized for cleavage by plasmin and metalloproteinases; exon 6 and 7 respectively encode for the heparin binding site and the Nrp binding site; and exon 8 encodes for a unique sequence (Claffey *et al.*, 1995; Keyt *et al.*, 1996; Lee *et al.*, 2005). On the basis of the presence of sub-exon 8a or sub-exon 8b, the VEGF isoforms are classified in two different subfamilies: full agonists (VEGF-xxx) and partial agonists (VEGF-xxxb) (Gu *et al.*, 2013) (Figure 2). Based on the ability to bind to heparin sulfate or Nrp co-receptors, the isoforms are further categorized as cell bound isoforms (VEGF-A₁₈₉, VEGF-A₂₀₆), isoforms which

have both the soluble and cell bounded properties (VEGF-A₁₆₅), and soluble isoforms which lack the binding domains (VEGF-A₁₂₁, VEGF-A₁₁₁) (Houck *et al.*, 1991).

The distinct isoforms, generated from alternative splicing of VEGF-A, are indispensable for normal development. This is evident from different studies using transgenic mice. Mice embryos expressing only VEGF-A₁₂₀ show severe defects in lung vascular development, vascularization of retina, and myocardial ischemia. Due to congenital birth defects half of the embryos died in perinatal period within 2 weeks after birth (Carmeliet *et al.*, 1999; Stalmans *et al.*, 2002). Knockout of VEGF-A₁₆₄ or VEGF-A₁₈₈ in mice results in lethality after birth or death between embryonic day 9.5 and 13.5 (Carmeliet *et al.*, 1999). These studies show the importance of the presence of VEGF-A isoforms containing exon 6-8 encoding the heparin and Nrp binding domain in the normal development.

Mice expressing only VEGF-A₁₆₄ are reported to be healthy with a normal retinal angiogenesis, but mice with only VEGF-A₁₈₈ have reduced arterial development in retinas and disrupted development of secondary ossification centers and knee joint dysplasia (Maes *et al.*, 2004). These findings indicate the role of diverse VEGF isoforms having distinct functions in the vascular and arterial development with VEGF-A₁₆₅ as the central player.

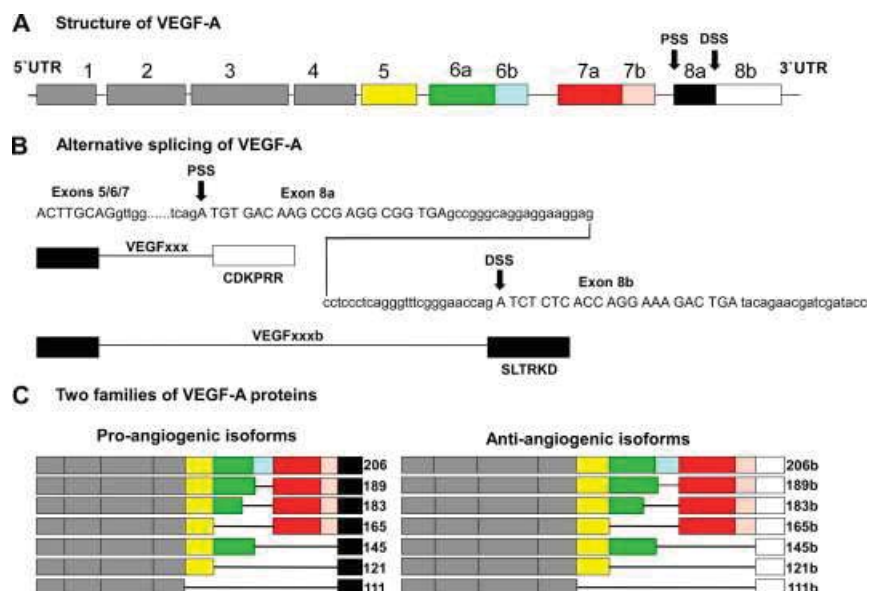


Figure 2: Schematic representation of the structure of VEGF-A isoforms. (a) VEGF-A gene containing 8 exons. (b) and (c) Alternative splicing of exon 8 at proximal splice site (PSS) leads to a full agonist (VEGFxxx) and distal splice site (DSS) creates anti-angiogenic splice variant (VEGFxxx b). (Gu *et al.*, 2013)

VEGF-B

The VEGF-B gene consists of seven exons and alternative splicing gives rise to two isoforms: VEGF-B₁₆₇ and VEGF-B₁₈₆. The isoforms differ in their C-terminal due to the presence of acceptor splice sites in exon 6 but have an identical 116 amino acid amino-terminal (N-terminal) region. VEGF-B₁₆₇ comprises a basic C-terminal which is able to tightly bind HSPGs on the cell surface and in the ECM (Olofsson *et al.*, 1996a). VEGF-B₁₈₆ is a freely diffusible isoform which consists of a hydrophobic C-terminal and undergoes O-glycosylation. But after undergoing proteolytic processing VEGF-B₁₈₆ can bind to Nrp-1 (Olofsson *et al.*, 1996b). The homodimers of the both isoforms are expressed in numerous tissues simultaneously and bind to VEGFR-1 and Nrp-1 for transducing their signal (Makinen *et al.*, 1999).

VEGF-B is highly expressed in myocardium, skeletal muscle and vascular smooth muscle, brown adipose tissue and neuronal tissue (Bry *et al.*, 2014; Enholm *et al.*, 1997). Although VEGF-B has high sequence homology and similar receptor binding patterns as of VEGF-A, reports suggest it has very weak angiogenic activity. The knockout of VEGF-B in mice seems to be viable and fertile with no noticeable vascular or developmental defects, which is contrasting to a VEGF-A knockout (Kivela *et al.*,

2014). However they show smaller hearts and impaired recovery from cardiac ischemia and dysfunctional coronary vasculature (Bellomo *et al.*, 2000).

A recent study has shown VEGF-B as a key regulator of energy metabolism. They demonstrate that VEGF-B regulates the fatty acid transport by increasing the expression of fatty acid transport proteins (FATPs) across the endothelium. The deficient mice for VEGF-B showed a decreased level of lipids in heart, muscle and brown adipose tissue while accumulation of lipids in the white adipose tissues instead (Hagberg *et al.*, 2010).

VEGF-B also plays a neuroprotective role facilitated directly by VEGFR-1 expressing neuronal cells. Mice lacking VEGF-B show degeneration of sensory neurons, while the treatment with VEGF-B, rescue neurons from apoptosis (Dhondt *et al.*, 2011). Hence VEGF-B seems to have a wide range of function and a potential molecule through which one can study the association between angiogenesis and tissue metabolism.

VEGF-C

VEGF-C is secreted as a dimeric protein comprising long N-terminal and C-terminal propeptides flanking the VEGF homology domain. This uncleaved VEGF-C undergoes two proteolytic maturation steps to yield multiple processed forms. The first proteolytic cleavage takes place at the C-terminal by furin which generates an intermediate form, having moderate affinity for VEGFR-3. The second cleavage takes place at the N-terminal and silk homology domain present at the C-terminal by A disintegrin and metalloproteinase with thrombospondin motifs 3 (ADAMTS3) resulting in fully mature form which is able to bind to VEGFR-3 with higher affinity (Joukov *et al.*, 1996; Joukov *et al.*, 1997). This fully processed form of VEGF-C also has a significant affinity for VEGFR-2. VEGF-C has a major role in lymphangiogenesis. It is also strongly expressed in various normal human tissues such as large intestine epithelium, and mammary duct epithelium, skeletal and cardiac muscle, thyroid, ovary, and the prostate and a variety of cancerous tissues (Joory *et al.*, 2006). VEGF-C is absolutely essential for development of lymphatic vessels as even loss of single allele leads to lymphedema. And VEGF-C knockout mice die as embryos due to defective lymphatic vasculature and of edema (Karkkainen *et al.*, 2003).

VEGF-D

VEGF-D is produced as a precursor protein, similar to VEGF-C. Proteolytic processing generates mature forms which are capable of binding to both VEGFR-3 and VEGFR-2 leading to growth and development of blood vessels and lymphatics. Surprisingly, VEGF-D knockout mice are viable with minimal defects (Baldwin *et al.*, 2005). Though VEGF-C and VEGF-D show similar bioactivities but recent studies indicate towards their distinct signaling mechanisms. Mature form of VEGF-D consist of distinct amino acid residues in the N-terminal α -helix which are required for binding VEGFR-3 and VEGFR-2 whereas in VEGF-C same set of residues are involved in binding to both the receptors (Davydova *et al.*, 2016). Exact role of VEGF-D is not known yet. But studies show VEGF-D influences the metastasis of cancerous cells (Stacker *et al.*, 2001).

VEGF-E

VEGF-E submembers are encoded by genome of Orf virus, a parapoxvirus known to infect sheep, goats and human (Lyttle *et al.*, 1994). Different subtypes of VEGF-E which are derived from several strains of Orf virus: VEGF-ENZ-2, VEGF-ENZ-7, VEGF-ENZ-10, VEGF-ED₁₇₀₁ and VEGF-EVR₆₃₄ (from pseudo cowpox virus strain) (Meyer *et al.*, 1999; Ogawa *et al.*, 1998; Wise *et al.*, 1999; Wise *et al.*, 2003). Their amino acid sequence is only 20% to 25% identical to VEGF-A (Lyttle *et al.*, 1994). They bind with high affinity and stimulate VEGFR-2 but not VEGFR-1 nor VEGFR-3. They vary in their ability to bind Nrp-1. VEGF-ENZ-2, VEGF-ENZ-10, and VEGF-ED₁₇₀₁ can bind Nrp-1 whereas VEGF-ENZ-7 and VEGF-EVR₆₃₄ are unable to bind Nrp-1. VEGF-E_{NZ-7} transgenic mice have shown induction of significant angiogenesis with fewer side effects, hence it is a potential target to be used as pro-angiogenic factor in the clinics (Kiba *et al.*, 2003).

PIGF

PIGF is mainly expressed in the placenta but is also found in low levels in other tissues, such as the heart, lung, thyroid, liver, skeletal muscle and bone (Persico *et al.*, 1999). Alternative splicing of the human PIGF gene generates four different isoforms exhibiting different binding properties: PIGF-1 and PIGF-3 are freely diffusible whereas, PIGF-2 and PIGF-4 comprise a C-terminal domain encoding the heparin binding

domain and hence are cell membrane associated isoforms (Maglione *et al.*, 1993; Yang *et al.*, 2003). PIGF binds to VEGFR-1 and sVEGFR-1 (soluble receptor lacking TM and intracellular domains) (Kendall *et al.*, 1993). PIGF-2 can also bind to Nrp-1 and Nrp-2 due to the presence of additional 21 basic amino acids at the C-terminal (Gluzman-Poltorak *et al.*, 2000).

VEGFR-1 activation by PIGF leads to transphosphorylation and activation of VEGFR-2 and hence amplifies VEGF-A signaling (Autiero *et al.*, 2003). Though PIGF is very similar to VEGF-B in many respects, PIGF is able to induce stronger VEGFR-1 tyrosine phosphorylation compared to VEGF-B (Anisimov *et al.*, 2013). Similar to VEGF-B, the deletion of PIGF in mice does not affect the development of vessels in the embryo (Carmeliet *et al.*, 2001). However PIGF is able to stimulate angiogenesis in pathological conditions such as heart and lung ischemia, as efficiently as VEGF-A (Luttun *et al.*, 2002). PIGF, apart from being expressed in vascular cells, is also found in pathological conditions in fibroblasts, leucocytes, hepatocytes, bone marrow derived cells, neurons, epithelial cells and tumor cells. Hence PIGF has been a target molecule for being clinically exploited posing no severe side effects to normal physiology. But there has been conflicting data between pharmacological PIGF blockade studies, which use several anti-PIGF antibodies and PIGF knockout studies (Dewerchin *et al.*, 2012). Hence, more studies are required to be conducted to know the exact function and therapeutic potential of PIGF.

5.4.2. VEGFRs

VEGFR-1

VEGFR-1 is encoded by the Flt-1 (Fms-like tyrosine kinase 1) gene in humans. Alternative splicing of this gene gives rise to two isoforms: membrane bound VEGFR-1 and sVEGFR-1 (Kendall *et al.*, 1993). VEGFR-1 binds with high affinity to VEGF-A, VEGF-B, PIGF and some VEGFs in snake venom. VEGF-A binds with more than 10 fold higher affinity to Ig-homology domains 2 and 3 of VEGFR-1 when compared to VEGFR-2 (Wiesmann *et al.*, 1997). However, the kinase domain of VEGFR-1 shows weak tyrosine autophosphorylation activity and poorer signal transduction than VEGFR-2 (Seetharam *et al.*, 1995; Waltenberger *et al.*, 1994). Study on chimeric

VEGFR-1/2 molecules reveal the presence of negative regulatory sequence in the juxtamembrane region responsible for attenuation of kinase activity and phosphatidylinositol 3'-kinase (PI-3 KINASE) activation (Gille *et al.*, 2000). Furthermore, mutation of the amino acid N1050 to D in the activation loop of kinase domain of VEGFR-1, lead to increase in its activity (Meyer *et al.*, 2006). Tyrosine phosphorylation pattern depends on the type of ligand binding to VEGFR-1 and hence resulting in a distinct signaling output (Cunningham *et al.*, 1997; Sawano *et al.*, 1997). It is evident from a study showing binding of the ligand VEGF-A to VEGFR-1 that leads to phosphorylation of Y1213, whereas PlGF binding phosphorylates Y1309 (Autiero *et al.*, 2003). Distinct conformational arrangements arising in the extracellular region of VEGFR-1 due to binding of different ligands may be attributed as a reason for different signaling outcomes. Several molecules interacting with the phosphorylated tyrosine residues in the intracellular kinase domain of VEGFR-1 have been identified, such as p85/PI-3 KINASE, phospholipase C (PLC γ 1), Src-homology (SH) phosphatase-2 (SHP2 or Nck), and growth factor receptor bound-2 (Grb2) protein (Matsumoto *et al.*, 2001). Due to the weak kinase activity and modest signaling output of the VEGFR-1, the characterization of its signaling network has been very challenging and much more needs to be explored.

VEGFR-1 is expressed in various cell types, including vascular ECs, dendritic cells, pericytes, macrophages, monocytes and hematopoietic stem cells (Hattori *et al.*, 2002; Sawano *et al.*, 2001). VEGFR-1 knock out mice embryos die at embryonic day 8.5-9 due to increased proliferation of EPCs and disorganized vessel formation (Fong *et al.*, 1995). However, mice expressing kinase domain deleted VEGFR-1 have normal vasculature and are viable (Hiratsuka *et al.*, 1998). Thus, VEGFR-1 has been suggested to act as a decoy receptor during embryonic development by sequestering excess VEGF-A and preventing over activation of VEGFR-2. Moreover, the membrane localization of the receptor plays a crucial role, since 50% of mice expressing sVEGFR-1 die at embryonic day 8.5 to 9.0 due to disorganized vasculature (Hiratsuka *et al.*, 2005). Further the occurrence of sVEGFR-1 consisting of the first six Ig-homology domains, acting as a ligand scavenger was demonstrated from the study of Shibuya *et al.* (Shibuya *et al.*, 1990). sVEGFR-1 is known to be expressed in the human placenta and its overexpression has pathological implications such as causing pre-eclampsia. (Fan *et al.*, 2014; Maynard *et al.*, 2003). The negative regulatory role of VEGFR-1 is

also evident from a study which shows the existence of VEGFR-1/2 heterodimers, involved in blocking of VEGF-A induced extracellular-signal-regulated kinase (ERK1/2) activation and Ca^{2+} entry (Cudmore *et al.*, 2012). Apart from being able to negatively regulate the homodimer activity of VEGFR-2, the phosphorylated VEGFR-1 is also involved in transphosphorylation of VEGFR-2 (Autiero *et al.*, 2003). Though the underlying mechanisms by which VEGFR-1 and VEGFR-2 regulate each other remains to be revealed.

VEGFR-2

The human VEGFR-2 (also called KDR, Kinase insert domain-containing receptor) gene was cloned in 1991 and was found to be located at chromosome 4 (Terman *et al.*, 1991). The canonical activation of VEGFR-2 occurs by binding to alternatively spliced variants of VEGF-A, VEGF-E and proteolytically processed forms of VEGF-C and VEGF-D. Ig-homology domains 2 and 3 are involved in ligand binding. Moreover, there is a study showing in cultured cells, existence of pre-formed receptor dimers with certain kinase activity (Sarabipour *et al.*, 2016). VEGFR-2 also exists as a soluble isoform (sVEGFR-2) in various tissues such as the skin, heart, spleen, kidney, ovary, and in plasma. It is believed to act as a scavenger for VEGF-C and hence negatively regulates VEGFR-3 induced lymphangiogenesis (Albuquerque *et al.*, 2009; Ebos *et al.*, 2004).

VEGFR-2 is the major player involved in angiogenesis and vasculogenesis. It mediates migration, proliferation, cell survival and permeability in ECs by binding to VEGF-A ligand. VEGFR-2 knockout mice die at embryonic day 8 to 9 due to lack of a functional vasculature similar to mice deficient for VEGF-A (Shalaby *et al.*, 1995). Apart from being expressed in vascular and lymphatic ECs, VEGFR-2 is also found in neuronal cells, hematopoietic stem cells and retinal cells (Kabrun *et al.*, 1997; Shiote *et al.*, 2005; Yang *et al.*, 1996). Although VEGFR-2 has lower binding affinity to ligand VEGF-A compared to VEGFR-1, astonishingly VEGFR-2 exhibits strong kinase activity upon ligand binding. The dimerization of VEGFR-2 leads to conformational changes and activation by autophosphorylation of multiple intracellular tyrosine residues. Each phosphotyrosine residue serves as a binding site for regulatory proteins via their SH or phospho-tyrosine binding (PTB) domains, leading to distinct downstream signaling.

The chief autophosphorylation sites in human VEGFR-2 bound to VEGF-A are: Y801 in the JMD, Y951 in the kinase insert domain (KID), Y1054 and Y1059 in the activation loop and Y1175 and Y1214 in the C-terminal (Kendall *et al.*, 1999; Matsumoto *et al.*, 2005; Takahashi *et al.*, 2001). Phosphorylation of Y951 residue leads to binding of T cell specific adapter (TSA_d) protein via its SH2 and PTB domains (Matsumoto *et al.*, 2005). TSA_d then further interacts with cytoplasmic tyrosine kinase c-Src via its SH3 domain to regulate cytoskeleton components such as actin, cell-cell adhesion molecules and matrix components. Src additionally phosphorylates focal adhesion kinase (FAK) at cell-cell junctions which then regulates cell shape, adhesion and vessel permeability (Claesson-Welsh, 2016; Matsumoto *et al.*, 2005). Phosphorylation sites Y1054 and 1059 are required by the receptor for acquiring complete kinase activation and catalytic activity (Dougher *et al.*, 1999; Kendall *et al.*, 1999; Manni *et al.*, 2014a). Tyrosine 1175 is the chief phosphorylation site which interacts with PLC- γ via its SH2-domain and leads to its activation. Phosphorylated PLC- γ then hydrolyses the membrane phospholipid phosphatidylinositol (4,5)-bisphosphate (PIP₂) releasing 1,2-diacylglycerol (DAG) and inositol 1,4,5-trisphosphate (IP₃). IP₃ triggers the release of intracellular calcium and DAG activates protein kinase C (PKC). PKC in turn then activates the Ras-independent mitogen-activated protein kinase (MAPK) pathway (Raf-MEK-ERK) leading to changes in gene transcription and thereby cell migration, proliferation and cell fate specification (Cunningham *et al.*, 1997; Koch *et al.*, 2012; Xia *et al.*, 1996). PLC- γ signaling plays a crucial role in vasculogenesis. A study with mice shows, both *plc- γ* gene deletion and mutation of site Y1173 (in humans Y1175) leads to death of embryo in 9.0 days due to decreased vasculogenesis and erythropoiesis (Sakurai *et al.*, 2005). Phosphorylation at site Y1175 initiates multiple downstream signaling cascades. The same site also binds to other adaptor proteins, SHB (Src homology-2 protein in beta-cells) and Src homology 2 domain-containing transforming protein (SHC2 or SCK) (Koch *et al.*, 2011). Phosphorylated SHB binds to FAK which regulates cell migration and cell attachment (Abedi *et al.*, 1997). The inactivation of genes of adaptor proteins in mice leads to impaired vessel function and tumor growth (Koch *et al.*, 2012). Activated SHB also stimulates lipid kinase PI-3 KINASE, which further activates Protein kinase B (Akt) and endothelial nitric oxide synthase (eNOS). This leads to increased cell survival and nitric oxide-induced vascular permeability (Roskoski, 2007). Phosphorylated Y1214 recruits Nck and proto-oncogene tyrosine-

protein kinase (Fyn), and subsequently activates the p38MAPK pathway which stimulates migration in ECs (Lamallice *et al.*, 2004) Figure 3.

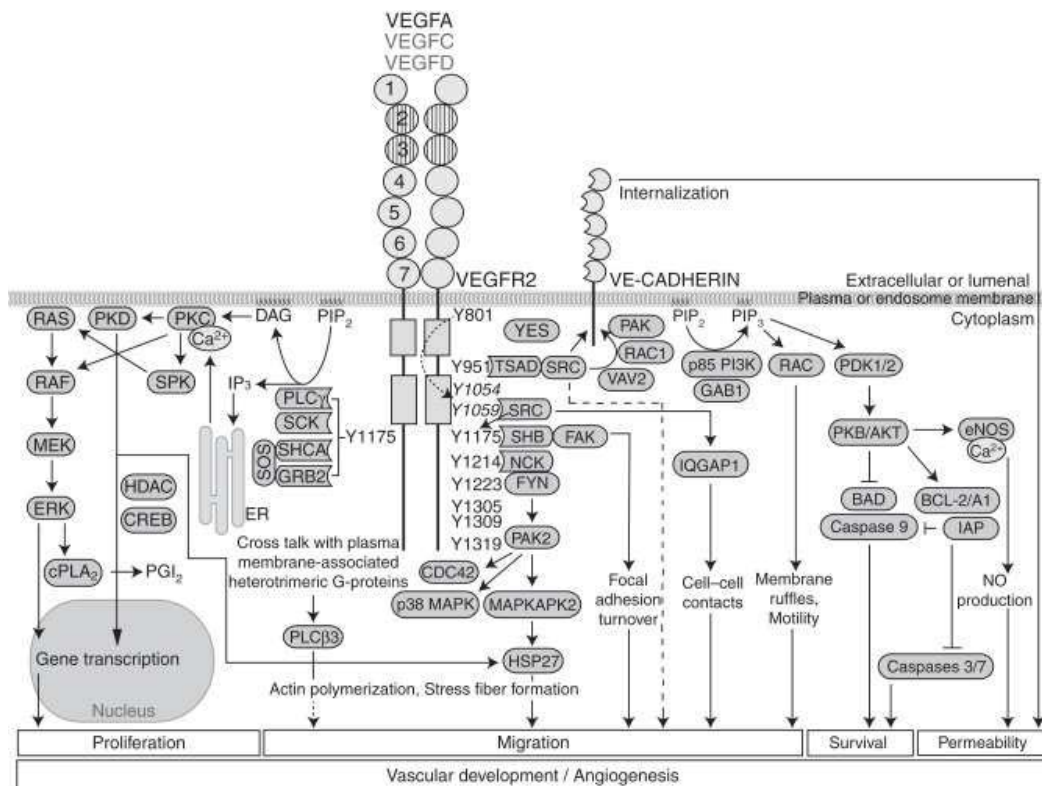


Figure 3: VEGF-A₁₆₅ mediated signal transduction of VEGFR-2 (Koch *et al.*, 2012)

VEGFR-3

VEGFR-3 (also called Flt-4) binds to ligands VEGF-C and VEGF-D with its Ig-homology domains 1 and 2 present in the ECD (Jeltsch *et al.*, 2006; Leppänen *et al.*, 2011). VEGFR-3 is synthesized as a precursor molecule and proteolytically processed at the fifth Ig-homology domain in the ECD. The two split ECD domains are bound by a disulfide bridge (Pajusola *et al.*, 1994). VEGFR-3 is mainly known for its requirement in lymphatic endothelial development but is also cited for its mechanistic role in early vessel development. Tip cells also express VEGFR-3, in blood vascular cells during early embryonic development (Nilsson *et al.*, 2010). VEGFR-3 knockout mice die at embryonic day 10 to 11 due to defective vascular development (Dumont *et al.*, 1998).

VEGFR-3 binding to ligands VEGF-C and VEGF-D leads to phosphorylation of residues at C-terminal: Y1230, Y1213, Y1265, Y1337 and Y1363 (Dixelius *et al.*, 2003). Upon phosphorylation, site Y1337 recruits SHC and Grb2, leading to activation of Ras and mitogenic signaling (Fournier *et al.*, 1995). Akt activation via PI-3 KINASE and p42/p44 MAPK activation via PKC are other known downstream signaling cascades of phosphorylated VEGFR-3 (Makinen *et al.*, 2001). VEGFR-2 and VEGFR-3 can form heterodimers upon binding to ligand VEGF-C. Interestingly a change in autophosphorylation pattern of VEGFR-3 present in the heterodimers is observed, which might also lead to distinct downstream signaling as compared to the homodimeric form. The two residues Y1337 and Y1363 present at the C-terminal do not get phosphorylated of the above five autophosphorylation sites (Dixelius *et al.*, 2003). VEGFR-2/3 heterodimers regulate migration and proliferation of lymphatic ECs and are found to be present on tip cell filopodia of developing blood vessels and immature lymphatic sprouts (Nilsson *et al.*, 2010). VEGFR-3 can also be activated independent of ligands by c-Src activation via integrins leading to vessel expansion in lymphatic system and regulating interstitial fluid uptake (Galvagni *et al.*, 2010).

5.5. Aims of the thesis

The establishment of the blood and lymphatic vascular system are crucial requirements for the development of an embryo (Karkkainen *et al.*, 2003). In addition, dysregulated vasculogenesis and angiogenesis in adults has implications in numerous pathological conditions (Shibuya, 2011). The members of the VEGF family are known to be key regulators in both the physiological and pathological vessel development (Shibuya, 2014; Smith *et al.*, 2015). The five VEGF ligands interact with three type V RTKs, VEGFR-1, VEGFR-2 and VEGFR-3 with overlapping specificity (Koch *et al.*, 2011). The ECD of VEGFRs comprises seven Ig-homology domains. The first 3 domains mediate ligand binding, whereas the membrane proximal domains 4-7 are involved in ligand-induced receptor dimerization. Ligand binding allows dimerization of the ECD in a precise conformation, followed by exact positioning of the TM and intracellular domains for initiating autophosphorylation of the kinase domain and subsequent activation of downstream signaling. Our previous low resolution single particle electron microscopy (EM) and small angle solution scattering (SAXS) data

suggested homotypic contacts in domains 4-7 (Kisko *et al.*, 2011; Ruch *et al.*, 2007). To gain information on the molecular details of the homotypic interactions occurring in VEGFR-2 required for activation of the receptor, we applied several strategies for crystallization of VEGFR-2 ECD complexes. In order to study the function of individual Ig-domains in receptor activation we investigated the interaction of VEGFR-2 ECD with ligand using various biophysical techniques.

We and others have shown that homotypic interactions occurring between receptor dimerization upon ligand binding are indispensable for VEGFR-2 and -3 activation (Hyde *et al.*, 2012; Leppänen *et al.*, 2013; Yang *et al.*, 2010). Domains 4-7 of VEGFRs thus represent novel allosteric receptor-regulatory sites.

Our aim was to investigate the structure of ligand induced homotypic contacts in full length ECD/ligand complexes of VEGFR-1. We validated the biological relevance of the molecular details found in the structural study by carrying out functional studies in cell culture. This will provide an insight for the future development of highly specific inhibitory drugs.

6. Materials and Methods

6.1. Cloning, expression and purification of VEGFR-2 ECD subdomains for crystallization experiments

6.1.1. Cloning of a VEGFR-2 ECD subdomain construct for insect cell expression

The construct VEGFR-2 domains 2-5 was polymerase chain reaction (PCR) amplified and cloned into the insect cell expression vector pFL by PCR subcloning (Geiser *et al.*, 2001) using the following primers.

Fwd 5'-
 CTGCGTGGAGACCAGAGCCGCATCTGTTCAAGATTACAGATCTCCATTTATTGC
 TTCT -3'

Rev 5'- GTGATGGTGATGGTGATGTCTGCCCTCGATACCCCTGGTCACGTGG -3'.

6.1.2. Cloning of VEGFR-2 constructs for baculovirus mediated transduction in mammalian (HEK293S GnTi-) cells

The cDNA of VEGFR-2 ECD subdomains 1-7, 2-7 and 1-3 were PCR amplified from their respective pcDNA3 plasmids using Phusion High-Fidelity DNA polymerase (Finnzymes) and the following primers.

Fwd 5'-
 GCTGGCTAGCGTTTAACTTAAGCTTGGTACCATGGAGAGCAAGGTGCTGCT -3'

Rev 5'-
 CGGGCCCTCTAGACTCGAGCGGCCGCTTATCAGTGATGGTGATGGTGATG -3'.

Following incubation at 72°C for 10 min with Taq Plus Precision polymerase (Stratagene), the amplicons were ligated to the pGEM-T vector (Promega). The inserts were cut from these vectors with NheI and XhoI (Fermentas), purified from TAE agarose gels with the Qiaquick gel extraction kit (Qiagen) and ligated to pFL plasmids. The VSV-G cDNA was PCR amplified using Phusion High-Fidelity DNA polymerase (Finnzymes) and the following primers:

Fwd 5'- AGCACGTGGGATCCGAATTCAAC-3'

Rev 5'- CTGCACTCTAGAGGGGTGAATTCCATA-3'

The PCR amplicons and pUCDM (Fitzgerald *et al.*, 2006) were digested with BamHI and XbaI (Fermentas), purified from TAE agarose gels with the Qiaquick gel extraction kit (Qiagen) and ligated using T4-ligase (Fermentas).

The *Cre/LoxP* recombination reaction between the acceptor plasmid pFL carrying the VEGFR-2 ECD subdomains and the donor plasmid pUCDM carrying VSV-G was performed at 37°C for 60 min (New England BioLabs). *Escherichia coli* (*E. coli*) DH10 β cells were transformed with the reaction mixture by electroporation and incubated for 1 h at 37°C. Then they were plated on agar plates containing ampicillin and chloramphenicol. The colonies were picked and plasmid DNA was extracted with a Miniprep kit (Qiagen). The constructs were verified by sequencing the plasmid-DNA (Microsynth AG).

6.1.3. Cloning of mouse mVEGFR-2 ECD constructs for expression in mammalian (HEK293 EBNA) cells

The mouse VEGFR-2 ECD subdomain constructs were PCR amplified from an artificially synthesized sequence (Genewiz) encoding the mouse VEGFR-2 ECD cDNA using the primers shown in Table 1.

mVEGFR-2 Construct	5'-3' Primer Sequence
Domains 1-7	Fwd 5'- CTCGTCTCTAGACGCCTCTGTGGGTTTGCCTGG -3' Rev 5'- TGCTTAGCGGCCGCTCATCAGTGATGGTGATGGTGATGGGGGCCCTGG AACAGCACCTCCAGCAAGTTGGTCTTTTCCTGGGCAC-3'
Domains 2-7	Fwd 5'- CTCGTCTCTAGACCGAGATTACAGATCACCATTTCATCGC -3' Rev 5'- TGCTTAGCGGCCGCTCATCAGTGATGGTGATGGTGATGGGGGCCCTGG AACAGCACCTCCAGCAAGTTGGTCTTTTCCTGGGCAC-3'
Domains 1-6	Fwd 5'- CTCGTCTCTAGACGCCTCTGTGGGTTTGCCTGG -3' Rev 5'- TGCTTAGCGGCCGCTCATCAGTGATGGTGATGGTGATGGGGGCCCTGG AACAGCACCTCCAGTAGGATGATGAGCTGTTTGACCAGG-3'
Domains 2-5	Fwd 5'- CTCGTCTCTAGACCGAGATTACAGATCACCATTTCATCGC -3' Rev 5'- TGCTTAGCGGCCGCTCATCAGTGATGGTGATGGTGATGGGGGCCCTGG AACAGCACCTCCAGCCTGATCACATGGAAGGAGATGACC -3'
Domains 1-3	Fwd 5'- CTCGTCTCTAGACGCCTCTGTGGGTTTGCCTGG -3' Rev 5'- TGCTTAGCGGCCGCTCATCAGTGATGGTGATGGTGATGGGGGCCCTGG AACAGCACCTCCAGAGGCTTTGTGTGAACTCGGACAAAT-3'
Domains 4-7	Fwd 5'- CTCGTCTCTAGAC ACAAAGCCTTTTATTGCTTTCGGTAGTG-3' Rev 5'- TGCTTAGCGGCCGCTCATCAGTGATGGTGATGGTGATGGGGGCCCTGG AACAGCACCTCCAGCAAGTTGGTCTTTTCCTGGGCAC-3'
Domains 5-7	Fwd 5'- CTCGTCTCTAGACGTCCCACCCAGATCGGTGAG-3' Rev 5'- TGCTTAGCGGCCGCTCATCAGTGATGGTGATGGTGATGGGGGCCCTGG AACAGCACCTCCAGCAAGTTGGTCTTTTCCTGGGCAC-3'

Table 1: Primers used for cloning mouse VEGFR-2 ECD subdomains in the pCEP4-Pu vector for expression in mammalian (HEK293 EBNA) cells.

The PCR products and the backbone of the pCEP4-Pu plasmid (obtained from Dr. Richard Kammerer) were digested with the NheI and NotI restriction enzymes prior to ligation using T4-ligase (Fermentas).

6.1.4. Cloning of glycosylation lacking VEGFR-2 constructs for mammalian (HEK293 EBNA) cell expression

An artificially synthesized sequence (Genewiz) for human VEGFR-2 ECD with all asparagine residues substituted with glutamine residues was used as a template for PCR amplification of ECD subdomains using Phusion high-fidelity DNA polymerase (Finnzymes) and the primer shown in Table 2.

Construct	5'-3' Primer Sequence
Domains 1-3 mutant	Fwd 5'- CTC GTC GCT AGC CTC CGT GGG ACT CCC TTC -3' Rev 5'- TGCTTAGCGGCCGCTCATCAGTGATGGTGATGGTGATGGGGGCCCTGGA ACAGCACCTCCAGGTGCACCCTCACGAAGGTGCTCTG-3'
Domains 2-5 mutant	Fwd 5'- CTCGTCGCTAGCC GACTACAGGAGCCCCTTTATCGCCTCC -3' Rev 5'- TGCTTAGCGGCCGCTCATCAGTGATGGTGATGGTGATGGGGGCCCTGGA ACAGCACCTCCAGTCTTGTGACGTGGAAGGAGATCACCTC -3'
Domains 1-3 wild-type	Fwd 5'-CTCGTCGCTAGCC GGTTTGCCTAGTGTTTCTCTTGATCTGCC -3' Rev 5'- TGCTTAGCGGCCGCTCATCAGTGATGGTGATGGTGATGGGGGCCCTGGA ACAGCACCTCCAGATGGACCCTGACAAATGTGCTGTTCTTC -3'
Domains 2-5 wild-type	Fwd 5'- CTCGTCGCTAGCCGATTACAGATCTCCATTTATTGCTTCTGTTAGTGACC - 3' Rev 5'- TGCTTAGCGGCCGCTCATCAGTGATGGTGATGGTGATGGGGGCCCTGGA ACAGCACCTCCAGGGTCACGTGGAAGGAGATCACCTCTC -3'
Domains 1-7 wild-type	Fwd 5'-CTCGTCGCTAGCC GGTTTGCCTAGTGTTTCTCTTGATCTGCC -3' Rev 5'- TGCTTAGCGGCCGCTCATCAGTGATGGTGATGGTGATGGGGGCCCTGGA ACAGCACCTCCAGCTCCAAGTTCGTCTTTTCTGGGCAC-3'

Table 2: Primers used for cloning of wild-type and glycosylation-lacking mutant (asparagines mutated to glutamines) human VEGFR-2 ECD subdomains in the pCEP4-Pu vector used for expression in mammalian (HEK293 EBNA) cells.

The amplified inserts were cloned into the HEK293 EBNA expression plasmid pCEP4-Pu following a classic restriction digestion/ligation method, using the NheI and NotI restriction enzymes.

6.1.5. Protein production of ligands

Human VEGF-A₁₂₁ and pox virus VEGF-E NZ2 with an N-terminal 6xhistidine tag were produced in *Pichia pastoris* by Thomas Schleier as described before (Scheidegger *et al.*, 1999).

6.1.6. Production and purification of human VEGFR-2 ECD subdomain proteins in insect cells

All human VEGFR-2 ECD variants were expressed in *Spodoptera frugiperda* (Sf)21 insect cells, which were maintained in suspension in serum-free InsectXpress medium (Lonza) at 27°C with agitation at 90 rpm. Recombinant baculovirus was produced in Sf21 cells in serum-free Insect-XPRESS medium (Lonza) at 27°C. Large scale protein expression of ECD and dimeric Ig homology domains 2-7 (VEGFR-2 domains 2-7 GCN4) was carried out in a 5-l benchtop fermenter sparged with an air/oxygen mix on demand to maintain a 36% O₂ saturation. The culture in the vessel was agitated at 140 rpm impeller speed and maintained at 27°C and pH 6.2. All other ECD variants were expressed in baffled Erlenmeyer flasks. Sf21 cell cultures were infected with recombinant baculovirus when they had reached a density of 1x10⁶ cells/ml. The supernatant was harvested 72 h after infection by centrifugation at 1000xg, concentrated using a tangential flow ultrafiltration device with a 10 kDa cut-off membrane (for the VEGFR-2 domains 2-4 construct a 3 kDa cut-off membrane was used instead) to a 500 ml volume and buffer exchanged with 50 mM HEPES pH 7.5, 300 mM NaCl. The proteins were purified by immobilized metal ion affinity chromatography (IMAC) using 5 ml His-Trap HP columns (GE Healthcare). Non-specifically bound proteins on the resin were washed away with buffer (50 mM HEPES pH 7.5, 300 mM NaCl) supplemented with 40 mM imidazole. The strongly bound proteins were then step eluted with high (400 mM) amounts of imidazole. VEGFR-2 ECD and VEGFR-2 domains 1-3 were eluted with a 0-500 mM imidazole gradient in Tris buffered saline (50 mM Tris, 300mM NaCl) at pH 8.0. The proteins were further

purified by size exclusion chromatography (SEC) on a Superdex 200 HR 16/600 column (GE Healthcare) equilibrated with 50 mM HEPES pH 7.5, 150 mM NaCl. Complexes for crystallization were formed by mixing VEGFR-2 ECD variants with ligands in 1:2 molar ratio and purified by SEC on Superdex 200.

6.1.7. Production and purification of mouse VEGFR-2 ECD subdomains in mammalian cells

The HEK293 EBNA cell line (R620-07, Invitrogen) was maintained in Dulbecco's modified Eagle's medium (DMEM) High Glucose supplemented with L-Glutamine (1-26F03-I, Bioconcept), 10% fetal bovine serum (FBS) and 250 µg/ml of G418 (108321-42-2, InvivoGen). Four µg of plasmid pCEP4-Pu containing the mVEGFR-2 ECD subdomain cDNA were dissolved in 0.4 ml serum-free medium and were mixed with 8 µl of PEI (Polyethyleneimine, stock 1mg/ml, Aldrich 408727, 25 kDa branched). The mixture was incubated for 10 min at room temperature to allow for DNA-PEI complex formation. The mixture was then added to HEK293 EBNA cells grown in a 6-cm culture dish, in which the medium was replaced with 1.2 ml DMEM containing 0.5% FBS, and was incubated for 3 h. Then, 0.8 ml of DMEM with 2% FBS was added to the culture and the cells were incubated for 20 h. Finally, the medium was exchanged with DMEM containing 10% FBS, 250 µg/ml G418 (108321-42-2, InvivoGen) and 1 µg/ml puromycin (A11138-30, Gibco) for selection of transfected cells. The cells were maintained under selection pressure for 7 days. Positive clones of transfected cells were selected and expanded to scale-up the production of mVEGFR-2 ECD subdomains. Briefly, two 15-cm culture dishes, each with a confluent monolayer of selected cells that had been gradually adapted in DMEM with 1% FBS were transferred to a sterile baffled Erlenmeyer shaking flask containing 50 ml Protein Expression Medium (PEM) without L-glutamine (12661-013, Gibco) supplemented with 2 mM Glutamax (35050-038, Gibco), 250 µg/ml G418 (108321-42-2, InvivoGen) and 1 µg/ml puromycin. The suspension cultures were grown at 37°C, 5% CO₂ with agitation at 100 rpm. The cell density of the cultures were maintained below 3x10⁶cells/ml and scaled up to a volume of approximately 2 l. This expanded culture was centrifuged at 1000xg in a fixed-angle rotor for 30 min at 4°C. The culture supernatant was passed through a 0.45-µm filter and, concentrated with a 10 kDa molecular weight (MW) cut-off tangential flow concentrator to an approximate volume of 500 ml. The sample was

buffer exchanged twice with 500 ml of buffer containing 50 mM HEPES pH 7.5, 300 mM NaCl and further concentrated to 250 ml. It was then loaded on a 5 ml His-Trap HP column (GE Healthcare) and washed with 50 mM HEPES pH 7.5, 300 mM NaCl, 20 mM imidazole. The protein was eluted with a gradient of 40-500 mM imidazole and concentrated to 5 ml using a 10 kDa MW cut-off centrifugal concentrator. The sample was filtered with a 0.45- μ m syringe filter and passed over a Superdex 200 16/60 column (GE Healthcare). VEGFR-2 ECD variants were mixed with human VEGF-A₁₂₁ for complex formation and purified by SEC as described in section 6.1.6.

6.1.8. Cloning, expression and purification of soluble Fab

Previous members of the group (Thomas Schleier and Dr. Sandra Markovic-Mueller) had selected a single chain variable fragment (scFv) from the ETH2-Gold phage-display library that could bind to VEGFR-2 domain 1 (Silacci *et al.*, 2005). Initially, the scFv antibody fragment bearing a flexible polypeptide linker Gly₄SerGly₄SerGly₄ was cloned into the phagemid vector pHEN followed by reformatting into a Fab (termed ADH9) by subcloning into the pMX9 vector. Then, Mach1 *E. coli* competent cells were transformed with this construct (Fab ADH9 in the pMX9 vector) by electroporation. The cells were subsequently grown in Terrific Broth (TB) medium supplemented with 0.1% glucose plus chloramphenicol (17 μ g/ml) at 37°C and induced with 1 mM isopropyl β -D-1-thiogalactopyranoside (IPTG) when the culture reached an OD 600 of 0.8. After induction, the culture was grown at 30°C for 12 h, centrifuged at 2500xg at 4°C for 15 min and the pellet was resuspended in lysis buffer containing 50 mM Tris pH 7.5, 150 mM NaCl, 1 mg/ml lysozyme, 20 μ g/ml DNase and 2 complete protease inhibitor tablets (11836170001 Merck). The cells were homogenized with a Turrax disperser (IKA) and lysed in a high-pressure Emulsiflex C-3 homogenizer (Avestin®) at 15000 psi. Non-lysed cells, cell debris, and aggregates were removed by centrifugation at 13000xg for 45 min. The Fab was purified from the filtered supernatant by IMAC on a 1 ml His-Trap HP column (GE Healthcare), equilibrated with 5 ml binding buffer: 50 mM Tris pH 7.5, 150 mM NaCl, 10 mM imidazole. Samples were eluted with elution buffer: 50 mM Tris pH 7.5, 150 mM NaCl, 500 mM imidazole. The proteins were further purified by SEC on a Superdex 200 HR 16/600 column (GE Healthcare) equilibrated with 20 mM HEPES pH 7.5, 150 mM

NaCl. Eluted fractions, containing the Fab were collected, concentrated, frozen in liquid nitrogen and stored at -80°C.

6.2. Biochemical and biophysical characterization of recombinant proteins

6.2.1. Limited proteolysis

Five microliter of VEGFR-2 domains 1-7/VEGF-A₁₂₁ complex at a concentration of 10 mg/ml was digested with 5 µl of several proteases namely Glu-C, trypsin, papain, α-chymotrypsin and subtilisin (Sigma-Aldrich) at various ratios (1:10, 1:100 and 1:1000 of the 1 mg/ml of stock solutions) in buffer containing 50 mM HEPES pH 7.5 and 150 mM NaCl. The mixture was incubated for 90 min or 16 hr at room temperature and 4°C respectively. The reaction was stopped by boiling for 1 min at 90°C in Laemmli buffer (0.25 M Tris-HCl pH 6.8, 0.5 M DTT, 10% SDS, 50% glycerol, 0.5% Bromophenol Blue). Samples were stored at -20°C prior to analysis by sodium dodecylsulfate polyacryl gel electrophoresis (SDS-PAGE).

6.2.2. Differential scanning fluorimetry

The extent of protein unfolding was measured for the purified VEGFR-2 domains 1-7, 2-7 and 1-3 proteins in their monomeric form as well as in complex with VEGF-A₁₂₁ in one of the following buffers: (1) phosphate-buffered saline (PBS) containing 137 mM NaCl, 2.7 mM KCl, 10 mM Na₂HPO₄, 1.8 mM KH₂PO₄, (2) 10 mM HEPES pH 7.5, 100 mM NaCl, and (3) 25 mM HEPES pH 7.5, 500 mM NaCl, at a final concentration of 20 µM. Next, SYPRO Orange dye (5000x, Invitrogen) was added to the protein solutions to a final dilution of 10x. Melting curves were measured by heating the samples from 25°C to 95°C at 1°C increments with a 5 sec incubation at each increment using a Rotor-Gene Q real time PCR machine (Rotor disc 72, Qiagen). Fluorescence intensity was measured using excitation/emission wavelengths of 485 nm/575 nm. Data analysis was performed with the Rotor-Gene Q series software 2.0.2.

6.2.3. Isothermal titration microcalorimetry

VEGFR-2 ECD and VEGFR-2 domains 1-3 were purified by SEC using a Superdex 200 column (GE Healthcare) equilibrated with 20 mM HEPES pH 7.5 buffer, containing 150 mM NaCl before being used for ITC. The relevant fractions were pooled, concentrated. All samples were filtered and degassed prior to analysis. VEGF-A₁₂₁ ITC titrations against VEGFR-2 ECD and VEGFR-2 domains 1-3 were carried out at 4°C using an iTC200 calorimeter (MicroCal; GE Healthcare). VEGFR-2 constructs were used in the calorimeter cell at a concentration of 10-30 µM and the VEGF ligands in the syringe at 150-250 µM. To increase the signal-to-noise ratio, the following parameters were used: one initial injection of 0.6 µl followed by 14 more injections of 2.6 µl at an injection speed of 1 µl/s, with data filter of 1 s and 500 s recovery time between each peak. The data were concatenated using the ConCat program (MicroCal) and processed and analyzed using Origin Version 7.0 software (OriginLab) supplemented with the ITC plug-in provided by the instrument manufacturer.

6.2.4. Microscale thermophoresis (MST)

VEGF-A₁₂₁ was labeled using the Monolith NT Protein Labeling kit BLUE-NHS (MO-L003, NanoTemper Technologies) by optimizing the manufacturer's guidelines. The concentration of labeled VEGF-A₁₂₁ was maintained constant at 100 nM. The corresponding unlabeled binding partner (VEGFR-2 domains 1-7 and 1-3) was titrated in 2:1 dilutions, with the highest final concentration chosen about 20-fold above the K_d expected from previously published ITC results (Brozzo *et al.*, 2012). Thus, the highest final concentrations were 25 µM for VEGFR-2 domains 1-7 and 0.98 µM for VEGFR-2 domains 1-3. The measurements were performed at 4°C in 20 mM HEPES buffer, pH 7.5 containing 150 mM NaCl. Hydrophilic capillaries (NanoTemper Technologies) were used for the measurements on a Monolith NT.115 system (Nano Temper Technologies) using 100% LED and 20% IR-laser power. Laser on and off times were set at 30 s and 5 s respectively. Domains 1-7 quantification was carried out by fitting the three data sets that had the same concentration range using the Prism software. Since the three datasets overlapped very well with no systematic offset in the Y-axis, the fitting was done without normalisation. All points were fitted as a single data set, rather than taking the mean and weighting the fit by the error on the mean, as the

former method makes no assumptions about the sampling error in the three experiments.

6.3. Functional analysis of Ig-homology domain 5 mutants of VEGFR-1 and 2

6.3.1. Cloning of VEGFR-1 mutants for functional analysis

VEGFR-1 was PCR amplified and cloned into the mammalian expression vector pcDNA3.1+ (Invitrogen) by PCR subcloning (Geiser *et al.*, 2001) using the following primers:

Fwd 5'-TTTTTGGTACCGCCACCATGGTCAGCTACTGGG-3'

Rev 5'-TTTTTGCGGCCGCTTATCAAGCGTAGTCTGGGACGTCGTATGGGTAAC-3'.

TM mutations (TM_ANGG and TM_ΔSSS) were introduced into pcDNA3.1+ VEGFR-1 wild-type construct by PCR subcloning (Geiser *et al.*, 2001) using appropriate primers (Table 3). We applied site-directed mutagenesis for generating the domain 5 interaction mutations on wild-type and TM activated constructs. For introducing the third mutation we used the mutated constructs as a template for subsequent site-directed mutagenesis.

Mutations	5'-3' Primer Sequence
Domain 5_E513A/K517A	Fwd 5'- GGCAATAATAAAGGGAAAGAATGCCATGGCTAGC ACCTTGGTTGTGGCTGACTCTAGAATTTCTGG-3' Rev 5'- GCTAGCCATGGCATTCTTTCCCTTTATTATTGCCATGCG CTGAGTGATGCTCTCAATTCTGTTTC-3'
Domain 5_T455W/E513K/ K517A	Fwd 5'- CTGACTTGTGGGCATATGGTATCCCTCAACCTACAATC AAGTGGTTC-3' Rev 5'- GTTGAGGGATACCATATGCCCAACAAGTCAGGATTTGTC TGCTGCCAGTGG-3'

<p>Domain 5_T455E /K517A</p>	<p>Fwd 5'- CATCACTCAGCGCATGGCAATAATAGAAGGAAAGAATGC CATGGCTAGCACCTTG-3'</p> <p>Rev 5'- CTAGCCATGGCATTCTTTCCCTTCTATTATTGCCATGCGCT GAGTGATGCTCTC-3'</p>
<p>Domain 5_T455E / E513A /K517A</p>	<p>Fwd 5'- CAGCAGACAAATCCTGACTTGTTGGGCATATGGTATCCC TCAACCTACAATC-3'</p> <p>Rev 5'- GTTGAGGGATAACCATATGCCCAACAAGTCAGGATTTGTC TGCTGCCCAGTGGGTAG-3'</p>
<p>TM_ANGG</p>	<p>Fwd 5'- GAAAAGGGCCAACGGCGGTGAAATAAAGACTGACTACC TATCAATTATAATGGAC-3'</p> <p>Rev 5'- AGTCTTTATTTACCCGCCGTTGGCCCTTTTCATTTTTCGG ATAAAGAGGGTTAATAGGAG-3'</p>
<p>TM_ANGG_ Domain 5_ E513K /K517A</p>	<p>Fwd 5'- GGCAATAATAAAGGGAAAGAATGCCATGGCTAGCACCTT GGTTGTGGCTGACTCTAGAATTTCTGG-3'</p> <p>Rev 5'- GCTAGCCATGGCATTCTTTCCCTTTATTATTGCCATGCG CTGAGTGATGCTCTCAATTCTGTTTC-3'</p>
<p>TM_ANGG_ Domain 5_T455W/E513K/ K517A</p>	<p>Fwd 5'- CTGACTTGTTGGGCATATGGTATCCCTCAACCTACAATC AAGTGGTTC-3'</p> <p>Rev 5'- GTTGAGGGATAACCATATGCCCAACAAGTCAGGATTTGTC TGCTGCCCAGTGG-3'</p>
<p>TM_ΔSSS</p>	<p>Fwd 5'- CCGAAAAATGAAAAGGGAAATAAAGACTGACTACCTATC AATTATAATGGAC-3'</p> <p>Rev 5'- GTAGTCAGTCTTTATTTCCCTTTTCATTTTTCGGATAAAG AGGGTTAATAGGAG-3'</p>
<p>TM_ΔSSS_ Domain 5_ E513K /K517A</p>	<p>Fwd 5'- GGCAATAATAAAGGGAAAGAATGCCATGGCTAGCACCTT GGTTGTGGCTGACTCTAGAATTTCTGG-3'</p> <p>Rev 5'- GCTAGCCATGGCATTCTTTCCCTTTATTATTGCCATGCG CTGAGTGATGCTCTCAATTCTGTTTC-3'</p>

<p>TM_ΔSSS_ Domain 5_ T455W/E513K/ K517A</p>	<p>Fwd 5'- CTGACTTGTGGGCATATGGTATCCCTCAACCTACAATC AAGTGGTTC-3' Rev 5'- GTTGAGGGATACCATATGCCCAACAAGTCAGGATTTGTC TGCTGCCAGTGG-3'</p>
--	--

Table 3: Primers used for cloning VEGFR-1 mutants for functional analysis.

The constructs were amplified by PCR using Phusion High-Fidelity DNA polymerase (Finnzymes). Template DNA was digested by adding 1 µl of DpnI (Fermentas) to the PCR product mixture and incubating for 8 h at 37°C. Subsequently, electrocompetent *E. Coli* DH10β were transformed with 0.5 µl of the digested PCR mixture and plated on Luria Bertani (LB)-Ampicilin agar plates. Positive colonies were picked after 16 h incubation at 37°C and inoculated in 5 ml overnight cultures. Plasmid DNA was then extracted with a Miniprep kit (Qiagen). The mutations were verified by sequencing plasmid DNA (Microsynth AG).

6.3.2. Cloning of VEGFR-2 mutants for functional analysis

Our starting material was wild-type VEGFR-2 cloned in the pBE vector (a modified pEGFP-N1 vector; Takara Bio Europe/Clontech), suitable for mammalian expression. We also subcloned VEGFR-2 domain 7 R726A from the expression vector pcDNA5/FRT (Invitrogen) into the pBE vector. The pBE vector was PCR amplified using the following primers: Fwd 5'-GAAAAGACGAACTTGGAAATCATTATTCTAGTAGGCACGGCGGTG-3' and Rev 5'-CATCGCTGCTCCCCGAAGAGCTCGCTCCGGCTC-3'. The homology regions needed for integration are underlined. The insert VEGFR-2 domain 7 R726A was amplified with the following primers: Fwd 5'-CTTCGGGGAGCAGCGATGGAGAGCAAGGTGCTGCTGGCCGTC - 3' and Rev 5'-GATTTCCAAGTTCGTCTTTTCTGGGCACCTTTATTATGAAAAATGCCTC-3'. The underlined non-annealing 5' tails were complementary to the homology regions of the 5' ends of the primers used above for the vector linearization. PCR amplified plasmid and insert were assembled *in vitro* using the Gibson assembly (Gibson *et al.*, 2009). (Figure 4).

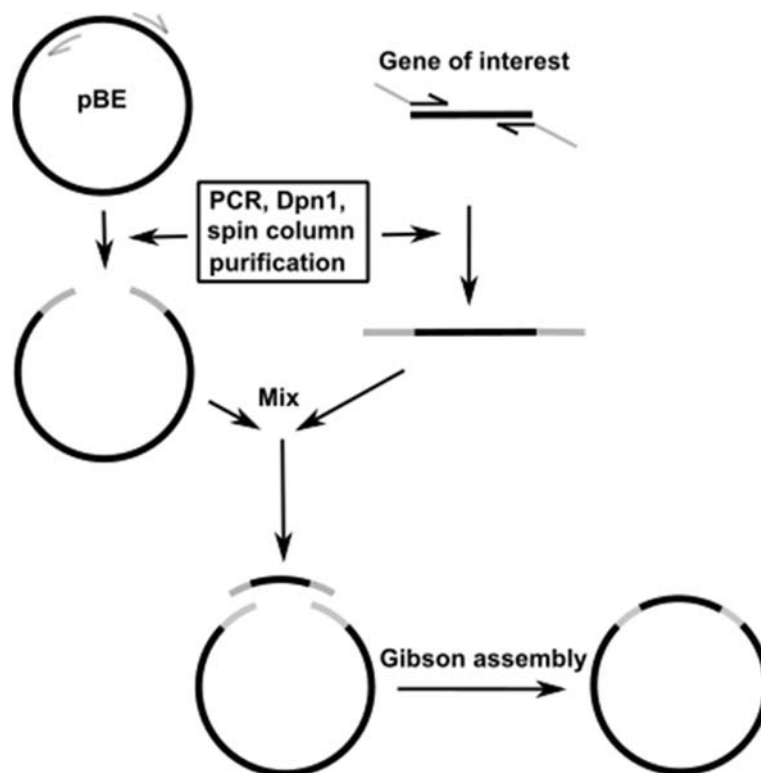


Figure 4: Schematic representation of Gibson assembly using PCR-linearized plasmids.

The VEGFR-2 domain 5 T446E/K512A and T446E/ E508K/K512A mutations were introduced into the pBE VEGFR-2 construct by cloning two overlapping fragments of the gene harbouring mutations into the vector backbone in a single Gibson assembly (Gibson *et al.*, 2009) reaction using the primers shown in Table 4.

Mutations	5'-3' Primer Sequence
Domain 5_E508K/K512A	Fwd 5'- AAAGGAAAAAACGCAACTGTAAGTACCCTTGTTATCCAAG CGGCAAATG-3' Rev 5'- CTTACAGTTGCGTTTTTTCCTTTAATTAGAGCAAATTGATTT TTATTA ACTTC-3'
Domain 5_T446E/K512A	Fwd 5'- TCAATTTGCTCTAATTGAAGGAAAAAACGCAACTGTAAGTA CCCTTGTTATCCAAGCGGCAAATG-3' Rev 5'- CTTACAGTTGCGTTTTTTCCTTCAATTAGAGCAAATTGATT TTTATTA ACTTC-3'
Domain 5_T446E/ E508K/K512A	Fwd 5'- CAAACGCTGACATGTGAAGTCTATGCCATTCTCCCCCGC ATC-3' Rev 5'- GAATGGCATAGACTTCACATGTCAGCGTTTGAGTGGTGCC GTAC-3'
Domain 7_R726A_Domain 5_T446E/K512A	Fwd 5'- TCAATTTGCTCTAATTGAAGGAAAAAACGCAACTGTAAGTA CCCTTGTTATCCAAGCGGCAAATG-3' Rev 5'- CTTACAGTTGCGTTTTTTCCTTCAATTAGAGCAAATTGATT TTTATTA ACTTC-3'
Domain 7_R726A_Domain 5_T446E/ E508K/K512A	Fwd 5'- CAAACGCTGACATGTGAAGTCTATGCCATTCTCCCCCGC ATC-3' Rev 5'- GAATGGCATAGACTTCACATGTCAGCGTTTGAGTGGTGCC GTAC-3'

Table 4: Primers used for cloning VEGFR-2 mutants for functional analysis.

The PCR products were digested with 1 µl DpnI ((New England Biolabs) in the presence of NEB4 buffer for 8 h at 37°C, and then purified using the MiniElute PCR purification kit (Qiagen). An insert-plasmid mastermix was prepared such that each Gibson assembly reaction consisted of 2.7 µl 5x isothermal reaction buffer (5x IT buffer), 2 µl insert-plasmid mastermix (containing 75 ng plasmid and an 8-fold molar excess of insert), 5.3 µl 1:1000 diluted T5 exonuclease (New England Biolabs, 10'000

U/ml), 1.6 μ l of 1:10 diluted Phusion HF DNA polymerase (NEB, 2'000 U/ml), 1.3 μ l Taq DNA ligase (NEB M0208L, 40'000 U/ml, undiluted) and H₂O to a final volume of 13.5 μ l. The 5x IT buffer consisted of 25% PEG 8000 (Sigma-Aldrich), 500 mM Tris HCl pH 7.5, 50 mM MgCl₂, 50 mM DTT, 1 mM of each dNTP (New England Biolabs) and 5 mM NAD⁺ (New England Biolabs). The reactions were incubated in the PCR machine at 50°C for 1 h. Chemically competent *E.Coli* Mach1 cells were transformed with 2 μ l of the above assembly mixture and plated on LB-Kanamycin agar plates. Cell colonies were picked after an incubation of 16 h at 37°C and inoculated in 5 ml overnight cultures. Plasmid DNA was extracted with a Miniprep kit (Qiagen). The mutations were verified by sequencing the plasmid DNA (Microsynth AG).

6.3.3. Cloning of VEGFR-1/2 chimeric constructs for functional analysis

For cloning the chimeric VEGFR-1/2 constructs, consisting of VEGFR-1 ECD (residues 1-752) and the intracellular domain of VEGFR-2 (residues 759-1356) we PCR-amplified wild-type, domain 5_E513K/K517A and domain 5_T455W/E513K/K517A VEGFR-1 ECD from their respective constructs in the pcDNA 3.1+ vector using the following primers:

Fwd- 5'CTTCGGGGAGCAGCGATGGTCAGCTACTGGGACACCGGGGTCCTGCTGTG-3'
 and Rev-5' GATTTCCAAGTTCGTCTTTTCCGAGGTTCTTGAACAGTGAGGTATGCTGAAC-3'

The DNA fragments were integrated into the wild-type VEGFR-2 pBE plasmid by replacing VEGFR-2 ECD using the Gibson assembly as described in section 6.3.2. For this, the pBE VEGFR-2 plasmid was linearized using the following primers: Fwd 5'-TAAAGGTTTTACTGCTTTAAAAAACTCCCACATCCCCCTGAACTGAAAC-3' and Rev 5'-CATCGCTGCTCCCCGAGCTCGCTCCGGCTC-3'.

6.3.4. Cloning of VEGFR-1 for lenti viral expression

In order to stably transfect PAE cell lines expressing domain 5 mutants using lenti viruses, we PCR-amplified wild-type, domain 5_E513K/K517A and domain 5_T455W/E513K/K517A VEGFR-1 from their respective constructs in the pcDNA 3.1+ vector using the following primers:

Fwd 5'-
ATCCACCGGTCCGCCACCATGATGGTCAGCTACTGGGACACCGGGGTCC-3' and

Rev 5'-
GATTGTGACGCGGCCGCTTTATATCAAGCGTAGTCTGGGACGTCGTATGG-3'

and subcloned them into the transfer vector plasmid pRRLSIN.cPPT.PGK-GFP.WPRE (Addgene) by Gibson assembly as described in section 6.3.2. For this, the pRRLSIN.cPPT.PGK-GFP.WPRE plasmid was linearized and amplified using the following primers:

Fwd 5'
GGACCCCGGTGTCCCAGTAGCTGACCATCATGGTGGCGACCGGTGGAT-3' and

Rev 5'-
CCATACGACGTCCCAGACTACGCTTGATATAAAGCGGCCGCGTCGACAATC-3'

Chemically competent *E. Coli* Mach1 cells were transformed with the above assembly mixture and plated on LB-Ampicillin agar plates. Cell colonies were picked after overnight incubation at 37°C and inoculated in 5 ml overnight cultures. Plasmid DNA was extracted with a Miniprep kit (Qiagen). The mutations were verified by sequencing the plasmid DNA (Microsynth AG).

6.3.5. Cell Culture

Porcine aortic endothelial cells (PAE), human embryonic kidney epithelial 293 cells (HEK293), HEK293T and NIH3T3 cells were grown in DMEM supplemented with 10% FBS and 1% penicillin–streptomycin. Cells were cultured in a humidified atmosphere at 37°C and 5% CO₂.

6.3.6. Transient transfections

NIH3T3 cells were seeded in 3.5-cm dishes and allowed to reach 60% confluence, at which point their medium was replaced with 1.6 ml fresh DMEM containing 0.5% FBS. Four µg plasmid DNA carrying either the VEGFR-1/2 or VEGFR-2 cDNA was dissolved in 0.4 ml serum-free culture medium and mixed with 8 µl PEI. After 10 min incubation at room temperature, allowing for the successful formation of a DNA-PEI complex, the

mixture was added to the cells. Following 5 h incubation at 37°C, an additional 2 ml DMEM containing 10% FBS was added and the cells were incubated for 20 h prior to analysis.

Alternatively, HEK293 and NIH3T3 cells, grown to 60% confluence in 3.5-cm dishes, were transfected with plasmid DNA containing the VEGFR-1 or VEGFR-2 cDNA using either FuGENE (Promega) or Lipofectamine 2000 or 3000 (Invitrogen) according to the manufacturer's instructions.

6.3.7. Generation of stably transfected PAE cells by chemical transfections

PAE cells were plated 6-9 h prior transfection in 10-cm dishes. Cells were 40-50% confluent prior to transfection. Twenty µg linearized plasmid DNA containing the VEGFR-1 cDNA dissolved in 2 ml serum-free DMEM were mixed with 40 µl PEI. The mixture was incubated for 10 min at room temperature. The medium in the culture dishes was replaced with 6 ml DMEM containing 0.5% FBS and the DNA/PEI complex was added for 5 h. Cells were passed into ten 10-cm plates 40 h after transfection in different dilutions (1:5, 1:10, 1:50, 1:100, 1:200, 1:400, 1:600, 1:800, 1:1000, 1:2000) and selection was applied by adding 500 µg/ml G418 (Geneticine) to the medium. Single cell colonies were picked with clone rings with grease after 14 days and transferred to 1-cm wells to grow in the presence of selection drug. Once cells were 90% confluent they were passed in 6-cm plates and frozen into aliquots.

6.3.8. Generation of stably transfected PAE cells by lentiviral transductions

HEK293T cells plated at 85-90% confluence in 10-cm culture dishes were used for transfections. Twelve µg of transfer vector containing the VEGFR-1 cDNA was mixed with 4 µg each of the packaging plasmids pMDLg/pRRE and pREV, and 4 µg of the envelope plasmid pVSVg-PMD2.G in 2 ml serum-free medium (Opti-MEM; Life technologies). Seventy two µg PEI was added to this mixture and incubated at room temperature for 10 min. Subsequently, 5 ml fresh DMEM was added to it. The plated cells were incubated for 3 h with the above mixture. Afterwards, 5 ml DMEM containing 5% FBS was added and the cells were incubated for 72 h at 37°C. The supernatants

were collected and centrifuged for 5 min at 180xg to remove cell debris, and stored at 4°C. Prior to transfection, they were concentrated by ultracentrifugation at 80,000xg (24,000 rpm on a SW-28 ultracentrifuge rotor) for 1.5 h at 4°C and resuspended in 100 µl PBS. The concentrated virus solution was added to PAE cells grown in 3.5-cm dishes at 60% confluence for 24 h. To increase the efficiency of infection, polybrene (Hexadimethrine bromide, Sigma H9268) was added to a final concentration of 4 µg/ml. After 24 h, the medium was changed to 2 ml DMEM containing 10% FBS, and the cells were incubated for 72 h at 37°C prior to VEGFR-1 expression analysis.

6.3.9. Immunocytochemistry

PAE cells stably expressing VEGFR-1 were grown on glass coverslips coated with Poly-L-Lysine (P4707, Sigma) to 60% confluence. Cells were fixed with 3.7% formaldehyde in PBS for 20 min at 37°C, permeabilized for 10 min with 0.1% (wt/vol) NP-40 in PBS, and blocked for 20 min in 5% (wt/vol) bovine serum albumin (BSA) in PBS at room temperature. The samples were sequentially exposed to primary (1:400) and fluorescently labelled secondary (1:1000) antibodies in PBS containing 1% BSA, and embedded in Gelvatol (15% Gelvatol [Celanese Corporation, Lanaken, Belgium], 33% glycerol, 0.1% sodium azide). The coverslips were washed thrice with PBS after each step. Images were acquired with an Olympus IX8 equipped with an Andor iXonEM camera and with a Leica SP5 laser scanning confocal microscope at 60X magnification.

6.3.10. VEGF receptor activity assay

PAE, HEK293, or NIH3T3 cells were serum starved in DMEM supplemented with 1% BSA and stimulated with VEGF or PIGF for 10 and 5 min respectively, at 37°C. Cell lysates were prepared in lysis buffer (50 mM Tris pH 7.5, 100 mM NaCl, 0.5% [wt/vol] Triton X-100) supplemented with a protease inhibitor cocktail (Complete Mini EDTA-free, Roche Diagnostics), phosphatase inhibitors (200 µM Na₃VO₄, 10 mM NaF, 10 mM sodium pyrophosphate, 30 mM p-nitrophenly-phosphate, 80 mM glycerophosphate, and 20 µM phenylarsine oxide) and 10% glycerol. The Bicinchoninic Acid (BCA) assay (Pierce BCA Protein assay kit; Thermo Fischer Scientific) was used to determine the total amount of protein in the lysates. Lysates

were diluted with Laemmli buffer (0.25M Tris-HCl pH 6.8, 0.5M DTT, 10% SDS, 50% Glycerol, 0.5% Bromophenol Blue), incubated at 95°C for 1 min, resolved on 8% SDS polyacrylamide gels, transferred to polyvinylidene (PVDF, GE Healthcare) membranes, and immunoblotted with primary antibodies (dilution 1:1000) followed by secondary alkaline phosphatase-coupled antibodies (dilution 1:10000), and developed with the Novex AP Chemiluminescent Substrate (Invitrogen). The signal was detected on a GE Healthcare ImageQuant RT ECL scanner and densitometrically quantified using the ImageJ gel analysis plugin.

The antibodies used were as follows: pY1175-VEGFR-2 (2478, Cell Signaling), tVEGFR-2 (2479, Cell Signaling), α -tubulin (T5168 Sigma-Aldrich), anti-rabbit IgG HRP-linked (7074S, Cell Signaling), anti-mouse IgG HRP-linked (7076S, Cell Signaling). Alkaline phosphatase (AP) conjugated secondary antibodies were obtained from Jackson ImmunoResearch. The fluorescently labeled Dylight 488 secondary antibody was purchased from Abcam. The protein marker used for all SDS-PAGE and western blot experiments was PageRuler™ Plus Prestained Protein Ladder, 10 to 250 kDa (26619, ThermoFisher).

7. Results

7.1. Structural characterization of VEGFR-2 ECD complexes

7.1.1. Expression and purification in insect cells

A great motivation for this project was the limited structural information available on the ECD of VEGFR-2. Our main aim was to perform biophysical and structural studies in order to understand the regulatory role of the various extracellular Ig-homology domains in VEGFR-2 activation. To achieve this goal, we engineered several multi-domain fragments of VEGFR-2 ECD for high-level expression in insect cells. We also included VEGFR-2 domains 2-7 GCN4 in our study, which contains the two-stranded coiled-coil domain of the yeast transcription activator GCN4 at the C-terminal followed by the membrane proximal end of VEGFR-2 ECD (Table 5). Such design may mimic the stability provided to the ECD by the transmembrane domains (TMD) in the native form of the receptor, present in the cell membrane.

For expression in insect cells, we used the Multibac baculovirus expression vector pFL (Berger *et al.*, 2004) or the commercially available pFASTBAC-1 vector (Invitrogen). The constructs VEGFR-2 domains 1-7, 2-7 and 2-7 GCN4 in pFL and VEGFR-2 domains 1-3 in pFASTBAC-1 were already present in the laboratory. The construct VEGFR-2 domains 2-5 was cloned during this work into one of the two multiple cloning sites of pFL. All constructs contained the endogenous VEGFR-2 signal sequence to trigger protein secretion and a C-terminal 8xhistidine tag with a preceding factor Xa cleavage site for removal of the tag. The pFL and pFASTBAC plasmids with the various ECD constructs were used to generate baculovirus for Sf21 insect cell infection and consequent recombinant protein expression. Several types of media were tested for the growth of Sf21 cells in suspension. We found that the medium from Lonza promoted cell growth, while reducing cell clumping of Sf21 cells in suspension (Figure 5). To further minimize cell clumping, we also assessed the growth of cells in suspension in different vessels, including square bottles, flat-bottom and baffled Erlenmeyer flasks and a small-scale bioreactor. We found that the small-scale bioreactor minimized cell clumping and promoted cell growth. VEGFR-2 domains 1-7 and 2-7 GCN4 were expressed in a 4 l Sf21 culture in a small-scale bioreactor,

whereas all other proteins were expressed in 4 l cultures in baffled Erlenmeyer flasks. Due to technical difficulties we were able to optimize expression of only two constructs in the bioreactor. The optimal purification protocol involved a first step of IMAC to remove most of the impurities, followed by a second step of SEC for removing remaining aggregates. The cultures in Erlenmeyer flasks gave yields ranging from 0.5–1.6 mg per l of cultured cells, whereas protein expression in the bioreactor resulted in a final yield of 10-13 mg/l due to better aeration than in shaker cultures. This gave sufficient material for carrying out initial characterization and crystallization experiments.

The elution profiles of the purified proteins from a calibrated Superdex 200 column is shown in Figure 6. The elution profiles of constructs VEGFR-2 domains 1-7, 2-7, 2-7 GCN4 and 2-5 indicates a homogenous receptor preparation. On the other hand, the elution profile of the VEGFR-2 domains 1-3 construct shows clear signs of polydispersity. The first two peaks, at 48 ml and 64 ml respectively, correspond to the aggregates and oligomers eluted at the void volume (45 ml), whereas the monomeric protein was eluted at a retention volume of 84 ml, as shown in Figure 6d. The protein purity of all the constructs judged from SDS-PAGE was found to be 95%. However, SDS-PAGE of the eluted fractions showed diffuse bands and the proteins were detected at higher MW than expected (calculated MW are as follows: domains 1-7: 88 kDa, domains 2-7: 78 kDa, domains 2-7GCN4: 80.2 kDa, domains 1-3: 39.4 kDa, domains 2-5: 51.5 kDa). This can be attributed to heterogeneous glycosylation of the proteins expressed in insect cells (potential N-glycosylation sites are shown in Table 5). To improve this, we designed new constructs for expression in mammalian cells.

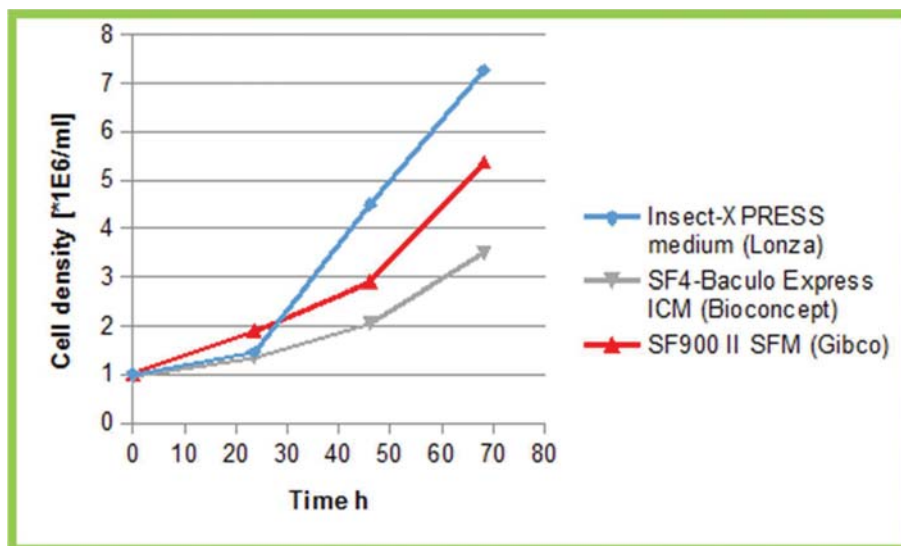


Figure 5: Test of different media for their suitability for suspension culture of Sf21 cells. Growth curves of Sf21 cells in suspension were monitored for three different culture media: Insect-XPRESS (Lonza), SF4-Baculo Express ICM (Bioconcept) and SF900 II SFM (Gibco). Cells cultured in the Insect-XPRESS medium achieved maximum cell density, while showing the least clumping.

Domain boundaries	Amino acids	Diagram
Domains 1-7	20-764	
Domains 2-7	118-756	
Domains 2-7GCN4	118-756	
Domains 1-3	20-335	
Domains 2-5	118-550	



Table 5: VEGFR-2 ECD recombinant proteins expressed in insect cells.

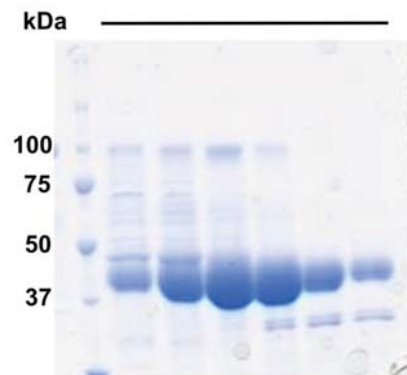
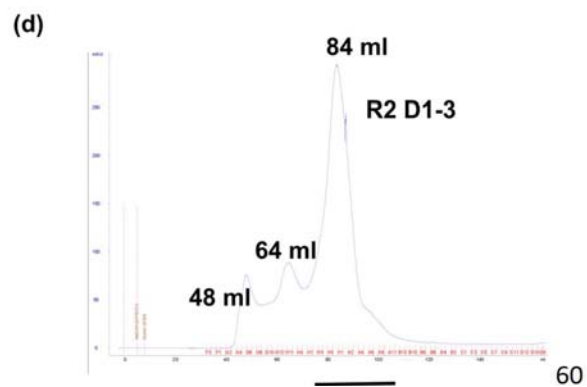
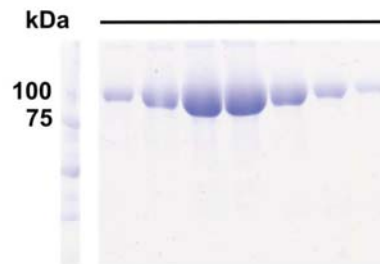
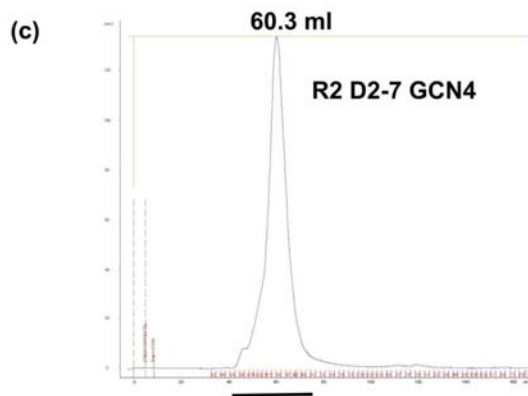
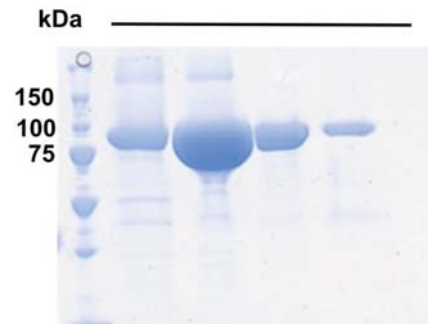
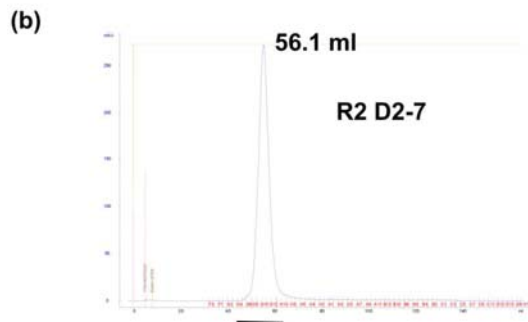
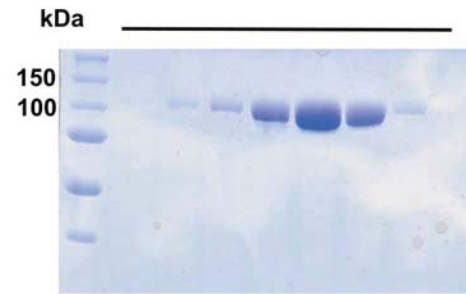
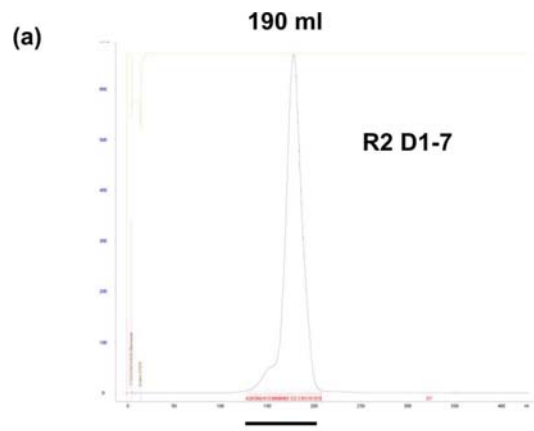




Figure 6: SEC profiles of VEGFR-2 ECD subdomains expressed in insect cells. Soluble proteins were produced in Sf21 cells and purified from the culture supernatant by IMAC and SEC. The Superdex S200 elution profiles (left panel) with their corresponding SDS-PAGE analysis (right panel) are shown. (a) VEGFR-2 domains 1-7 (b) VEGFR-2 domains 2-7 (c) VEGFR-2 domains 2-7 GCN4 (d) VEGFR-2 domains 1-3 (e) VEGFR-2 domains 2-5. Black bars indicate the fractions that were loaded for SDS-PAGE.

7.1.2. Expression and purification in mammalian cells

VEGFR-2 has 18 potential N-glycosylation sites within the extracellular domain. As insect cells are unable to produce sialylated complex glycans, we expressed VEGFR-2 ECD subdomains in mammalian cells in order to obtain near native-like post-translational modifications in the secreted proteins. Since complex glycans could interfere with protein crystallization, we used HEK293S GnTi⁻ cells which lack the capability to process N-linked glycans on glycoproteins from the high mannose to the complex mature form resulting in more homogeneously glycosylated protein. Furthermore, these proteins greatly facilitate enzymatic removal of the bulk of the attached N-linked glycans via Endoglycosidase F (EndoF) (Reeves *et al.*, 2002).

7.1.2.1. Baculovirus mediated gene expression of VEGFR-2 ECD subdomains in mammalian cells

We expressed VEGFR-2 ECD subdomains by adapting the baculovirus mediated gene transduction of mammalian cells (BacMam) system as shown in Figure 7. In contrast to other commonly used viral vectors, baculoviruses are insect cell viruses that can be modified to express proteins in mammalian cells without initiating a replication cycle.

The viruses can be manipulated to accommodate large inserts of foreign DNA and have a good biosafety profile.

Three different constructs were made having different genes of interest: VEGFR-2 domains 1-7 (residues 20-764), 2-7 (residues 118-756) and 1-3 (residues 20-335) containing the factor Xa cleavage site and an 8xhistidine tag. VEGFR-2 domains 1-7 would provide insights for the full extracellular domain. VEGFR-2 domains 2-7 was also cloned to remove the flexible domain 1, which might cause difficulty in crystal formation. VEGFR-2 domains 1-3 was cloned to get more insight into the contribution of domain 1 in ligand binding to domains 2 and 3. The acceptor vector was reengineered from the pFL vector (Fitzgerald *et al.*, 2006), and carried the gene of interest, a mammalian promoter (CMV), mammalian transcriptional regulatory elements and a poly A signal. The acceptor vector was recombined by cre-loxP recombination to a donor vector containing a VSV-G gene under an insect cell promoter (polh). The VSV-G gene was incorporated for enhancing virus titer. *E.Coli* DH10EMBacYFP were transformed with the donor-acceptor plasmid pairs, and the resulting bacmid DNA was used to transfect Sf21 and produce the baculoviruses. The resultant baculovirus was concentrated 400 times by ultracentrifugation through a sucrose cushion (25% w/w sucrose, 5 mM NaCl and 10 mM EDTA), and 100 μ l of this concentrated virus was used to infect HEK293S GnTi- cells in 6-well plates. However, the protein yields from BacMam transductions in HEK293S GnTi- cells were not significantly higher when compared to PEI transfections in HEK293T cells, even when concentrated baculovirus was used (Figure 8). In addition, the protein yield (~50 μ g/100 ml of culture) did not meet our requirements for milligram quantities of soluble proteins produced in a relatively short time for crystallization trials.

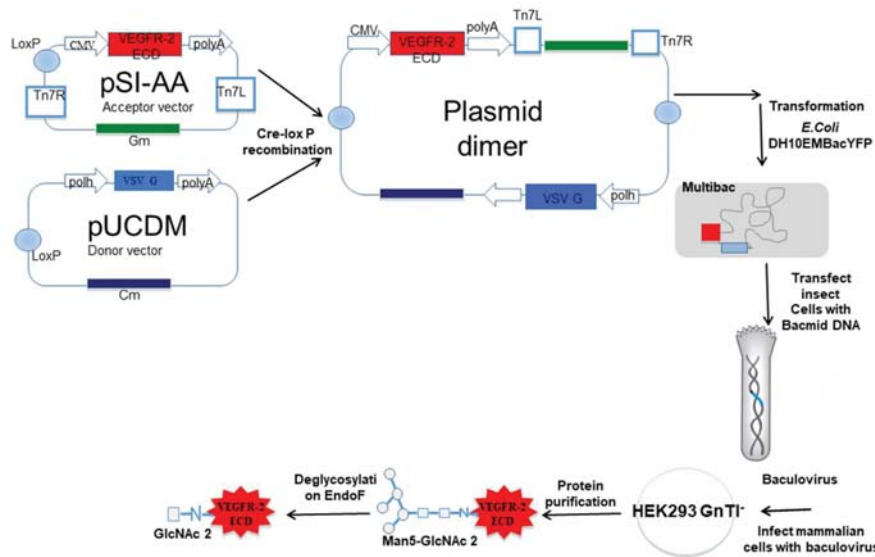


Figure 7. Strategy for VEGFR-2 ECD subdomain expression by baculovirus mediated gene transduction in mammalian cells. The ECD variant gene is inserted into an acceptor vector (pSI-AA), which is recombined to a VSV-G bearing donor vector (pUCDM) to generate the dimeric expression vector. *E. coli* DH10EMBacYFP cells are then transformed with the dimeric expression vector to generate the bacmid DNA, which is used for infecting Sf21 cells for baculovirus production. The baculovirus is in turn used for transducing HEK293S GnTi-cells for protein production. The purified proteins can be enzymatically deglycosylated by EndoF.

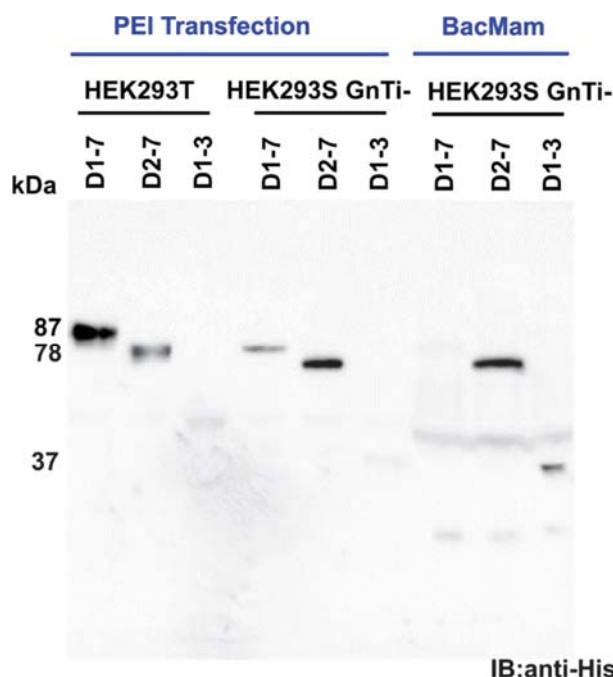
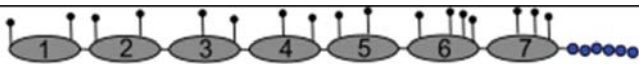
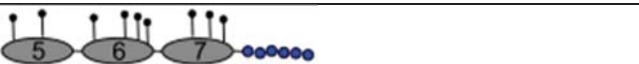


Figure 8: Comparison of different expression systems for the production of VEGFR-2 ECD subdomains. The various VEGFR-2 ECD subdomains (D1-7, D1-2 and D1-3) were expressed in HEK293T and HEK293S GnTi- cells by either chemical transfection or using the BacMam strategy. The expression levels of the various VEGFR-2 ECD subdomains was probed in the culture supernatants by western blotting using an anti-His antibody, which recognizes the histidine tag of all three recombinant proteins.

7.1.2.2. Expression and purification of mouse VEGFR-2 ECD subdomains in HEK293 EBNA cells

In order to achieve protein expression in sufficient quantities to carry out structural analysis experiments, we assessed stable gene expression in mammalian cells. In these studies, we used the mouse homologue of VEGFR-2. The human and mouse VEGFR-2 ECD have high degree of sequence identity (80% by CLUSTALW). Stable cell lines expressing mouse VEGFR-2 ECD subdomains (Table 6) were generated in HEK293 EBNA cells, which express the Epstein-Barr nuclear antigen 1 (EBNA-1). The product of the EBNA-1 gene drives the episomal amplification of expression plasmids carrying the origin of replication derived from the Epstein-Barr virus (EBV). Thus, these cells under selection pressure (Puromycin) are expected to increase recombinant protein expression levels by permitting more plasmid copies to persist in the transfected cells throughout the production phase.

All the constructs were cloned in the pCEP4-Pu vector and carried a 6xhistidine tag and a C-terminal precision protease cleavage site to allow tag removal. The stable HEK293 EBNA cells expressing VEGFR-2 domains 2-5, 1-3 and 4-7 were not expanded due to very weak expression. On the other hand, stable cells expressing VEGFR-2 domains 1-7, 2-7, 1-6 and 5-7 could be upscaled to 4 l cultures in Erlenmeyer flasks. The recombinant proteins were purified by IMAC followed by a second purification step of SEC. The SEC profiles show VEGFR-2 domains 1-7, 1-6 and 5-7 eluting with a predominantly monodisperse peak, whereas VEGFR-2 domains 2-7 gave a broad polydisperse peak indicating oligomerization (Figure 9). The eluted fractions were analyzed by SDS-PAGE. Due to N-glycosylation, the proteins ran at a higher MW (domains 1-7: 120 kDa, domains 2-7: 110 kDa, domains 1-6: 100 kDa and domains 2-5: 70 kDa) than their theoretical MW (domains 1-7: 86.5 kDa, domains 2-7: 75.4 kDa, domains 1-6: 75 kDa and domains 5-7: 39.3 kDa). High protein yields were obtained upon purification, in the range of 2.5-4.2 mg/l. All recombinant proteins, either glycosylated or deglycosylated with Peptide: N-glycosidase F (PNGase F) and Endo F were used for crystallization experiments.

Domain boundaries	Amino acids	
Domains 1-7	20-762	
Domains 2-7	123-762	
Domains 1-6	20-661	
Domains 5-7	421-762	



Iq-like domain
 6X-his tag
 N-glycosylation site

Table 6: Mouse VEGFR-2 ECD subdomain recombinant proteins expressed in HEK293 EBNA cells.

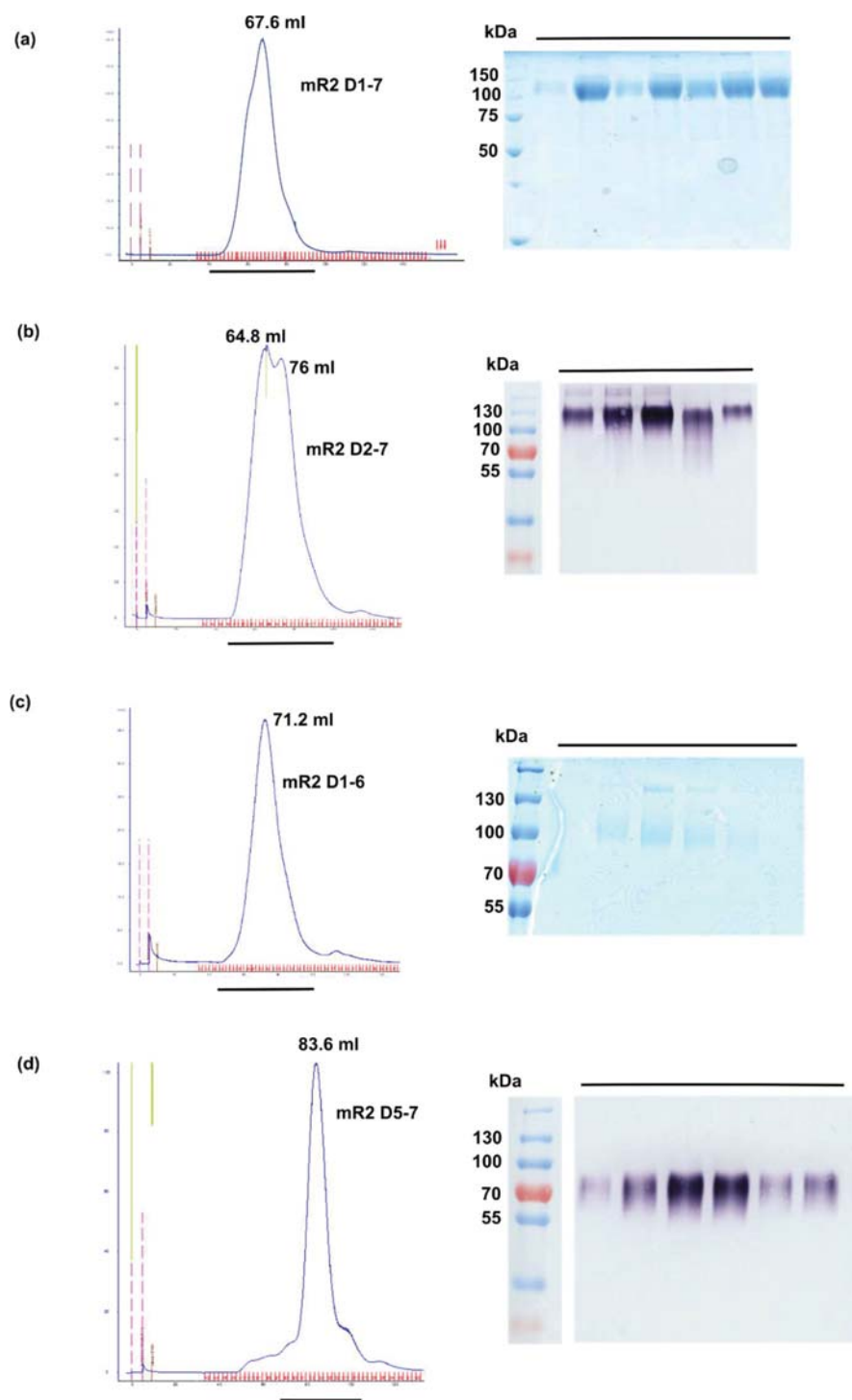


Figure 9: SEC profiles of mouse VEGFR-2 ECD subdomains expressed in mammalian cells. Soluble proteins were produced in HEK293 EBNA cells and purified from the culture supernatant by IMAC and SEC. The Superdex S200 elution profiles (left panel) with their corresponding SDS-PAGE (right panel) are shown. (a) mVEGFR-2 domains 1-7 (b) mVEGFR-2 domains 2-7 (c) mVEGFR-2 domains 1-6 (d) mVEGFR-2 domains 5-7. Black bars indicate the fractions that were loaded for SDS-PAGE.

Since we achieved higher expression with the mouse VEGFR-2 ECD constructs in HEK293 EBNA cells than with the human VEGFR-2 ECD constructs in insect cells (section 7.1.2.1), we decided to use this expression system for human VEGFR-2 ECD subdomains as well. Additionally, mammalian cells should provide a more physiologically relevant environment for VEGFR-2. However, glycosylation may be a bottleneck for obtaining crystals. Thus, we cloned constructs of human VEGFR-2 ECD subdomains (domains 1-7, 2-5 and 1-3) in the pCEP4-Pu vector, with all asparagine residues replaced with glutamine residues, leading to proteins lacking any N-glycosylation. However, the transfected HEK293 EBNA cells did not survive, possibly due to accumulation of glycosylation-lacking misfolded proteins. This suggests that at least some of the N-glycosylation sites are absolutely essential for proper protein folding.

7.1.3. Crystallization of VEGFR-2 ECD complexes

Recombinantly produced proteins underwent extensive crystallization screening using commercial 96-well screens (Table 7), both at 4°C and 20°C. Complexes of VEGFR-2 ECD subdomains with different ligands (VEGF-A₁₂₁ or VEGF-E) were either preformed and purified by SEC or formed *in situ* in the crystallization drop. Co-crystallization of receptor with ligand was preferred to crystallization of monomeric receptor for two reasons: (a) the receptor-ligand complex is the more biologically relevant form of the receptor, and (b) complex formation may substantially stabilize the receptor and increase the chances of crystallization. Additionally, multiprotein complexes containing ligand, antibody fragments (scFV and Fab) and recombinant VEGFR-2 ECD proteins were also subjected to crystallization screening. Hanging-drop and sitting-drop methods for vapour diffusion (VD), or in lipidic cubic phase (LCP) in batch, were used with two different drop ratios per reservoir (1:1 and 1:2 protein:reservoir volume) for crystallization trials. Furthermore, we used seeding with crystals of VEGFR-1, a VEGFR-2 homologue, for initiating crystal growth or inducing nucleation and growth at a lower level of supersaturation than might otherwise spontaneously occur. The crystals of VEGFR-1 domains 1-6 and 2-7 were crushed and used as seed stock to be dispensed into all the conditions of the screen, following

the random microseed matrix screening (MMS) technique. *In situ* limited proteolysis was also performed by adding either α -chymotrypsin or subtilisin in a 1:100 (w/w) ratio to the complexes just before crystallization (Table 8).

Commercial Screens	Supplier
Joint Center for Structural Genomics (JCSG) core screen I-IV suites	Qiagen
pH clear I-II	Qiagen
Additive screen HT	Molecular dimension
PEG suite	Qiagen
Morpheus	Molecular dimension
Proplex	Molecular dimension
saltRX	Hampton research
Stura footprint screen	Molecular dimension
PACT premier screen	Molecular dimension

Table 7: Commercial screens used for crystallization trials.

7.1.3.1. Co-crystallization of VEGFR-2 ECD subdomains with ligands

For co-crystallization experiments, VEGFR-2 ECD subdomains and ligands VEGF-A₁₂₁ and VEGF-E were expressed and purified separately. SEC-purified and concentrated proteins were mixed in a 1:2 molar ratio and subjected to another round of SEC to isolate the complex. The SEC profiles of human and mouse VEGFR-2 ECD variants in complex with either VEGF-A₁₂₁ or VEGF-E from a Superdex 200 column are shown in Figure 10 and Figure 11 respectively. The two separate peaks correspond to the VEGFR-2 ECD subdomain-ligand complex and to unbound ligand, as confirmed by SDS-PAGE: both receptor and ligand were present in the peak corresponding to the complex. The peak corresponding to the complex was collected, concentrated to 2-6 mg/ml and used for crystallization screening.

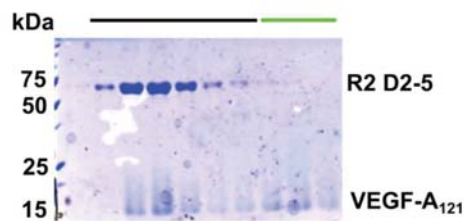
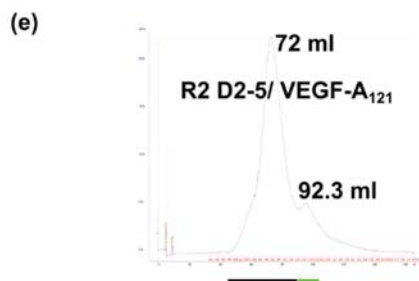
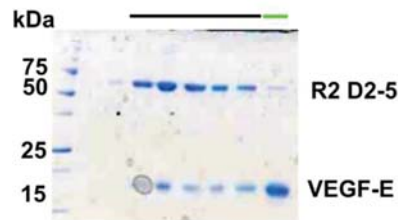
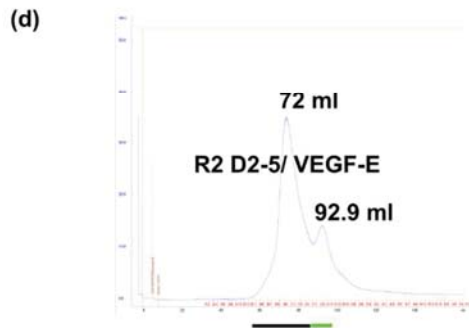
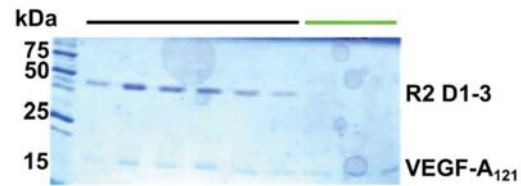
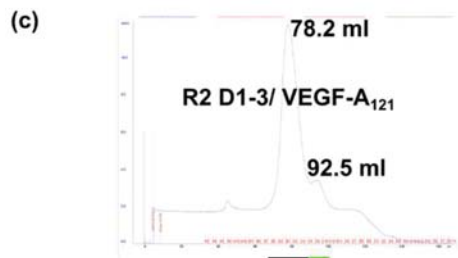
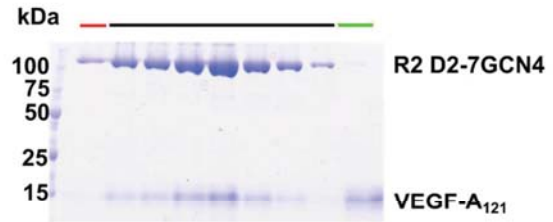
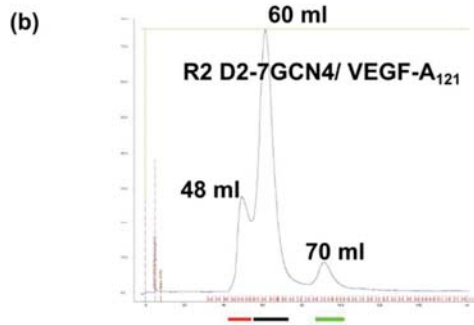
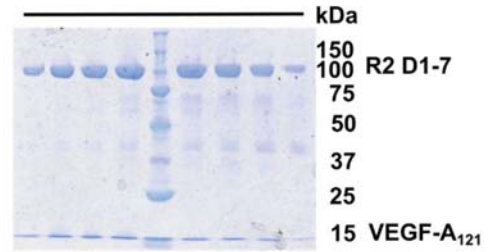
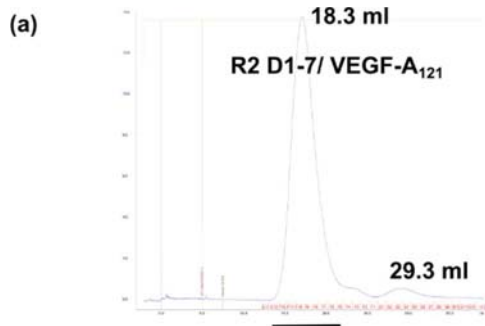


Figure 10: SEC profiles of human VEGFR-2 ECD subdomains complexed with ligands.

The receptor subdomains and ligands were mixed in 1:2 molar ratio and purified over a Superdex 200 column. (a) VEGFR-2 domains 1-7 co-eluting with VEGF-A₁₂₁ in a peak with retention volume 18.3 ml. The excess VEGF-A₁₂₁ elutes at 29.3 ml. (b) VEGFR-2 domains 2-7GCN4 co-eluting with VEGF-A₁₂₁ in a peak with retention volume 60 ml. The excess VEGF-A₁₂₁ elutes at 70 ml. (c) VEGFR-2 domains 1-3 co-eluting with VEGF-A₁₂₁ in a peak with retention volume 78.2 ml. The excess VEGF-A₁₂₁ elutes at 92.5 ml. (d) VEGFR-2 domains 2-5 co-eluting with VEGF-E in a peak with retention volume 72 ml. The excess VEGF-E elutes at 92.9 ml. (e) VEGFR-2 domains 2-5 co-eluting with VEGF-A₁₂₁ in a peak with retention volume 72 ml. The excess VEGF-A₁₂₁ elutes at 92.3 ml. The results of SDS-PAGE analysis of the various SEC fractions under reducing conditions are shown in the right panel. The coloured bars indicate the fractions from the corresponding SEC peaks that were loaded for SDS-PAGE.

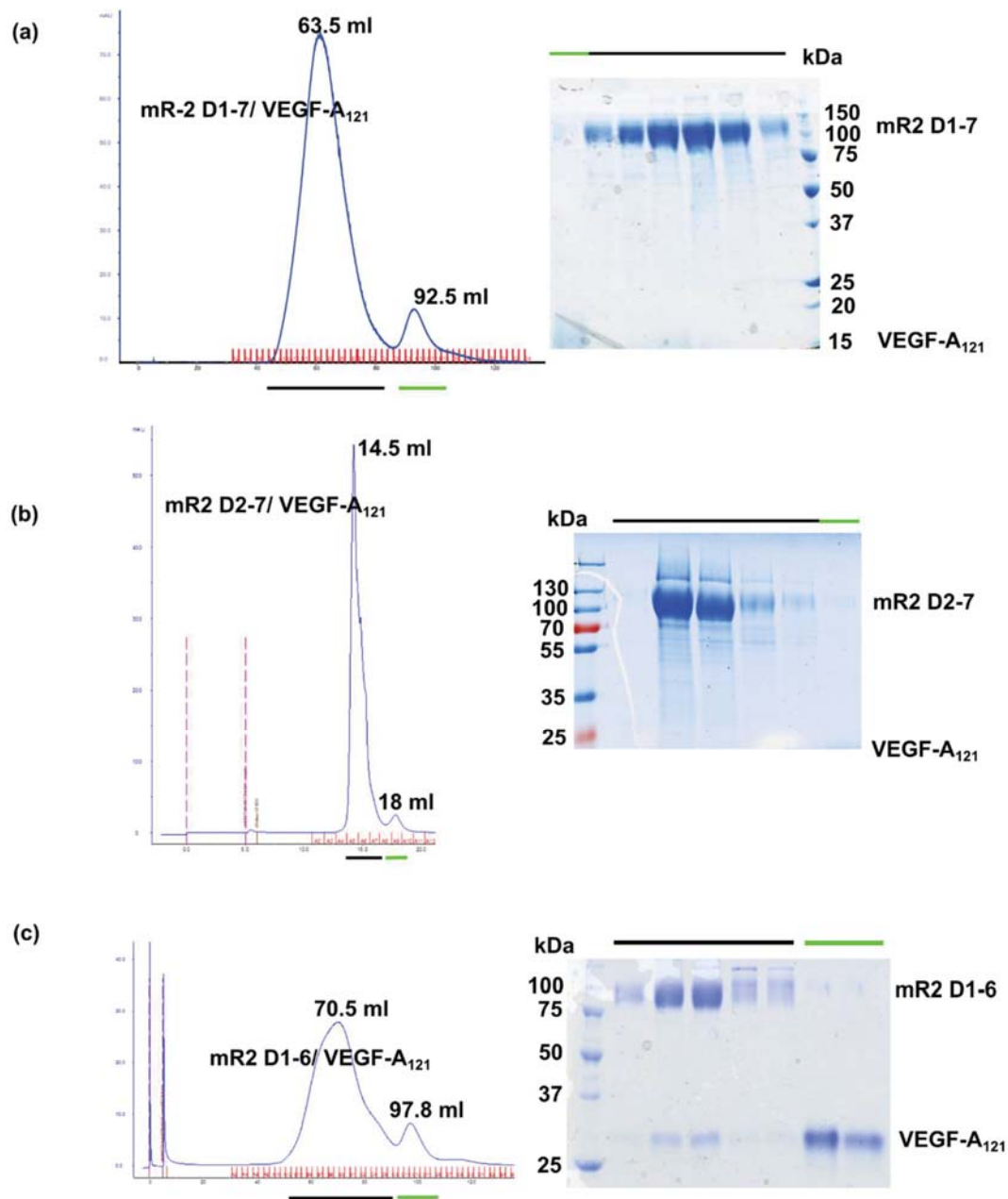


Figure 11: SEC profiles of mouse VEGFR-2 ECD variants complexed with ligand. The mouse receptor subdomains were mixed with human ligands in 1:2 molar ratio and purified over a Superdex 200 column. (a) mVEGFR-2 domains 1-7 co-eluting with VEGF-A₁₂₁ in a peak with retention volume 63.5 ml. The excess VEGF-A₁₂₁ elutes at 92.5 ml. (b) mVEGFR-2 domains 2-7 co-eluting with VEGF-A₁₂₁ in a peak with retention volume 14.5 ml. The excess VEGF-A₁₂₁ elutes at 18 ml. (c) mVEGFR-2 domains 1-6 co-eluting with VEGF-A₁₂₁ in a peak with retention volume 70.5 ml. The excess VEGF-A₁₂₁ elutes at 97.8 ml. The coloured bars indicate the fractions from the corresponding SEC peaks that were loaded for SDS-PAGE.

7.1.3.2. Co-crystallization of VEGFR-2 ECD/VEGF-E with scFV

Since we did not obtain any crystals from the experiments described in section 7.1.3.1, we used scFv A7 as a chaperone to facilitate the crystallization of VEGFR-2 ECD-ligand complexes. ScFv A7 targets the ligand binding domains 2-3 without interfering with VEGFR-2 ECD/VEGF-A complex formation. The antibody was isolated from the ETH-2 Gold library, expressed in *E.coli* Mach 1 cells, and characterized by Dr. Dragana Avramovic, as previously described (Ballmer-Hofer *et al.*, 2018). For carrying out co-crystallization trials, VEGFR-2 ECD, VEGF-E and scFv A7 were mixed in a molar ratio of 1:2:3, and purified by SEC (Figure 12). The chromatograph shows a main peak at 25 ml, expected to correspond to the trimeric complex, with a shoulder that could be due to the binding of oligomeric scFvs. The eluted fractions were subjected to SDS-PAGE analysis, which confirmed the co-elution of all three proteins; the fractions from the shoulder showed the presence of scFvs with a MW between 25 and 37 kDa. The unbound scFv A7 and VEGF-E, which were present in excess, eluted at higher retention volumes of 42 ml and 38 ml respectively. The fractions comprising the complex were concentrated and used for crystallization trials.

Despite screening a broad range of crystallization conditions no crystals were obtained. The co-crystallization of scFv A7 with VEGFR-2 ECD and VEGF-E was possibly impaired because the flexible GS-linker connecting the heavy and light segments of the binding protein may interfere with the formation of crystal contacts.

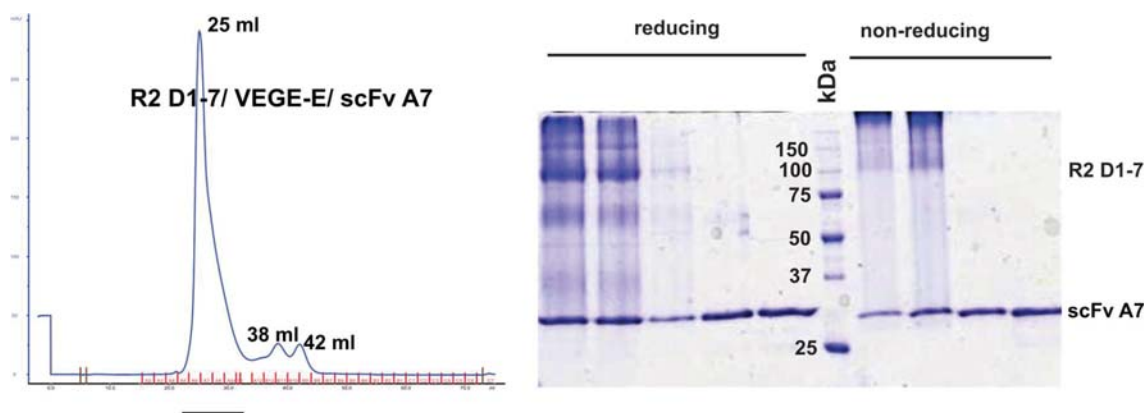


Figure 12: SEC profile of the VEGFR-2 domains 1-7/VEGF-E/scFv A7 complex. Recombinant VEGFR-2 domains 1-7, VEGF-E and scFv A7 were mixed in 1:2:3 molar ratio and purified over a Superdex S200 column. The left panel shows the SEC profile of VEGFR-2 domains 1-7 co-eluting with VEGF-E and scFv A7 at a retention volume of 25 ml. Excess scFv

A7 and VEGF-E elute at higher retention volumes, i.e 42 ml and 38 ml respectively. The right panel shows SDS-PAGE analysis of the eluates under reducing and non-reducing conditions. The black bars indicate the fractions from the corresponding SEC peak that were loaded for SDS-PAGE.

7.1.3.3. Co-crystallization of VEGFR-2 ECD/VEGF-A₁₂₁ with Fab

To overcome potential problems with the flexible linker present in the scFv we used a Fab fragment that contains the variable and one of the constant regions of the light and heavy antibody chains for co-crystallization trials. Additionally, the Fab offers a larger hydrophilic surface that may support the formation of additional crystal contacts.

We used a Fab antibody fragment that binds to the flexible domain 1 of VEGFR-2 ECD. This could provide more stability to ECD when complexed with ligand and hence increase the likelihood of crystallization. The Fab ADH9 fragment was expressed by IPTG induction using the Mach1 *E. coli* strain. The recombinant Fab was extracted from the periplasm and the lysate was purified by IMAC. Subsequently, the Fab was subjected to SEC and the elution profile shows two major peaks (Figure 13). The first peak of aggregates eluted near the void volume (Peak1: 49.6 ml); the second polydisperse peak (Peak2: 86.6 ml) shows the presence of Fab oligomers. The protein yield after purification was in the range of 0.5-1.5 mg/l. The Fab fractions under SDS-PAGE conditions showed a MW of approximately 50 kDa.

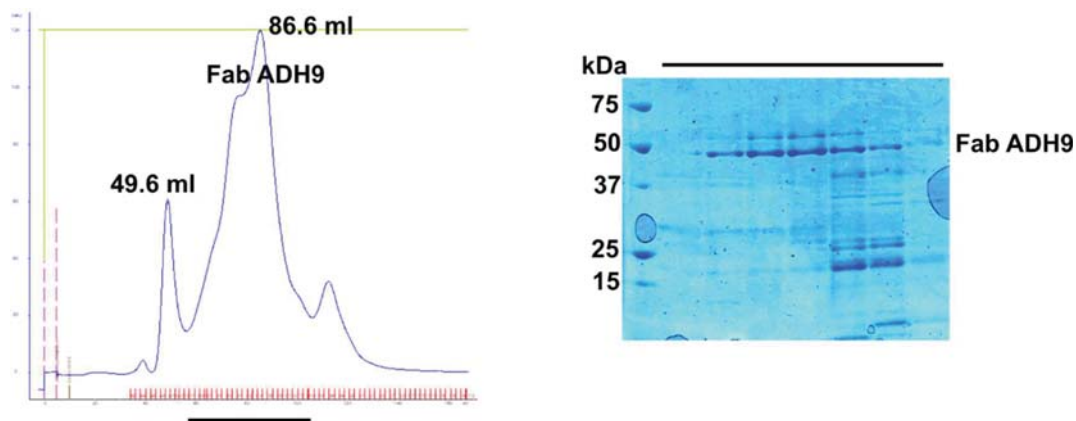


Figure 13: SEC profile of the Fab fragment. IMAC-purified Fab ADH9 was further purified over a Superdex S200 column, resulting in a broad elution peak at a retention volume of 86.6 ml (left panel). The right panel shows the SDS-PAGE analysis of the eluted fractions. The black bar indicates the fractions from the corresponding SEC peak that were loaded for SDS-PAGE. The band corresponding to Fab ADH9 ran at approximately 50 kDa.

For co-crystallization experiments, VEGFR-2 ECD was mixed with VEGF-A₁₂₁ and ADH9 Fab in a 1:2:3 molar ratio and purified by SEC using a Superdex S200 column. Co-elution was confirmed by a shift in the elution volume towards higher molecular weight, from 18.3 ml corresponding to the VEGFR-2 domains 1-7/VEGF-A₁₂₁ complex (Figure 10a) to 18 ml (Figure 14). Also the presence of all three components with appropriate MW of VEGFR-2 domains 1-7 (~86.5 kDa), Fab ADH9 (~50 kDa) and VEGF-A₁₂₁ (~30kDa) in the eluted fractions, as shown by SDS-PAGE under non-reducing conditions, confirmed the formation of a triple complex between Fab ADH9, VEGFR-2 domains 1-7 and VEGF-A₁₂₁. However, the peak corresponding to unbound Fab fragment at 23.9 ml did not resolve completely from the major peak of the complex. Nonetheless, the fractions corresponding to the complex were collected, concentrated to 2-6 mg/ml and used for crystallization trials, which however were unsuccessful. Since the complex did not elute as a single monodisperse peak but had a small shoulder, which indicates possible dissociation or heterogeneity, VEGFR-2 domains 1-7/VEGF-A₁₂₁ complexes and ADH9 Fab were purified individually and mixed prior to crystallization in a lower (1:2) molar ratio. Still, none of these experiments yielded any crystals.

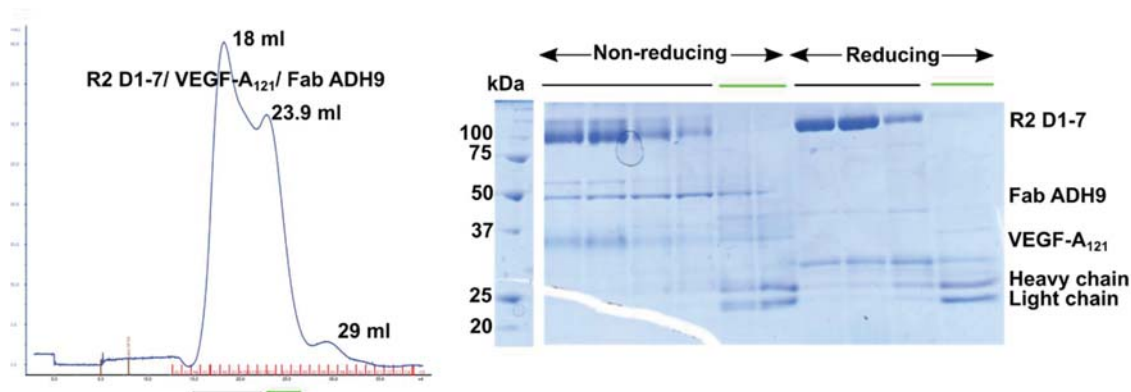


Figure 14: SEC profile of the VEGFR-2 domains 1-7/VEGF-A₁₂₁/Fab ADH9 complexes. VEGFR-2 domains 1-7, VEGF-A₁₂₁ and Fab ADH9 were mixed in 1:2:3 molar ratio and purified over a Superdex S200 column. The trimeric complex eluted at a retention volume of 18 ml. The excess Fab ADH9 and VEGF-A₁₂₁ eluted at 23.9 ml and 29 ml respectively. The right panel shows SDS-PAGE analysis of the eluates under reducing and non-reducing conditions. Fractions from the first peak (black bar) show a band around 100 kDa, corresponding to VEGFR-2 domains 1-7 (Expected MW: 86.5 kDa). The band at around 50 kDa corresponds to Fab ADH9 and the band between 37 kDa and 25 kDa to VEGF-A₁₂₁ (Expected MW: 30kDa). The fractions corresponding to excess Fab ADH9 are indicated with a green bar.

Construct	Method of crystallization	Temperature of incubation of plates (°C)	Concentrations used for crystallization
hVEGFR-2 domains 2-5 /VEGF-A ₁₂₁	VD	20 and 4	2-5 mg/ml
hVEGFR-2 domains 2-5 /VEGF-E	VD	20 and 4	2-5 mg/ml
hVEGFR-2 domains 1-3/VEGF-A ₁₂₁	VD	20 and 4	2-6 mg/ml
hVEGFR-2 domains 2-7GCN4/ VEGF-A ₁₂₁	VD	20 and 4	2-5 mg/ml
hVEGFR-2 ECD/ VEGF-A ₁₂₁ / Fab ADH9	VD, MMS, α -chymotrypsin to the drop	20 and 4	2-6 mg/ml
hVEGFR-2 ECD/VEGF-E/ scFV A7	VD	20	2-6 mg/ml
hVEGFR-2 ECD/VEGF-A ₁₂₁	VD, MMS, LCP, α -chymotrypsin and subtilisin to the drop	20 and 4	2-6 mg/ml
hVEGFR-2 ECD/VEGF-E	VD	20	3-6 mg/ml
mVEGFR-2 ECD/VEGF-A ₁₂₁	VD, MMS, LCP, α - chymotrypsin to the drop	20 and 4	2-6mg/ml
mVEGFR-2 domains 2-7/ VEGF-A ₁₂₁	VD	20 and 4	2-6mg/ml
mVEGFR-2 domains 1-6/VEGF-A ₁₂₁	VD	20 and 4	2-6mg/ml

mVEGFR-2 domains 5-7	VD	20 and 4	2-6mg/ml
-------------------------	----	----------	----------

Table 8: Summary of crystallization trials of VEGFR-2 ECD complexes.

7.2. Biochemical and biophysical characterization of VEGFR-2 ECD complexes

7.2.1. Analysis of unstructured regions in VEGFR-2 ECD

Although we were able to express and purify many VEGFR-2 ECD variants (section 7.1.1 and 7.1.2), we failed to obtain crystals from any of them. This could be due to long stretches of disordered regions within protein domains, which may hinder crystallization. In these cases, more sophisticated protein engineering might become necessary to displace these disordered residues. One approach would be to replace these regions with equivalent residues of homologue proteins that are known or predicted to be less flexible. Alternatively, the predicted disordered residues can be cut out and the ends joined by short flexible linkers. We investigated intrinsic disordered regions in VEGFR-2 ECD computationally using a prediction algorithm called FoldIndex (Prilusky *et al.*, 2005). This is an *ab initio* method, which predicts the inherently unstructured regions in the protein taking into account a balance between attractive and repulsive forces. Figure 15 shows that VEGFR-2 ECD is predicted to have 5 disordered regions. Two of these disordered segments are quite long consisting of 35-40 residues. One of them corresponds to Ig-homology domain 3 and the other lies in Ig-homology domain 5. The smaller (5-7 residues) unstructured segments are in Ig-homology domain 6 and 7, and the linker region connecting Ig-homology domains 4 and 5.

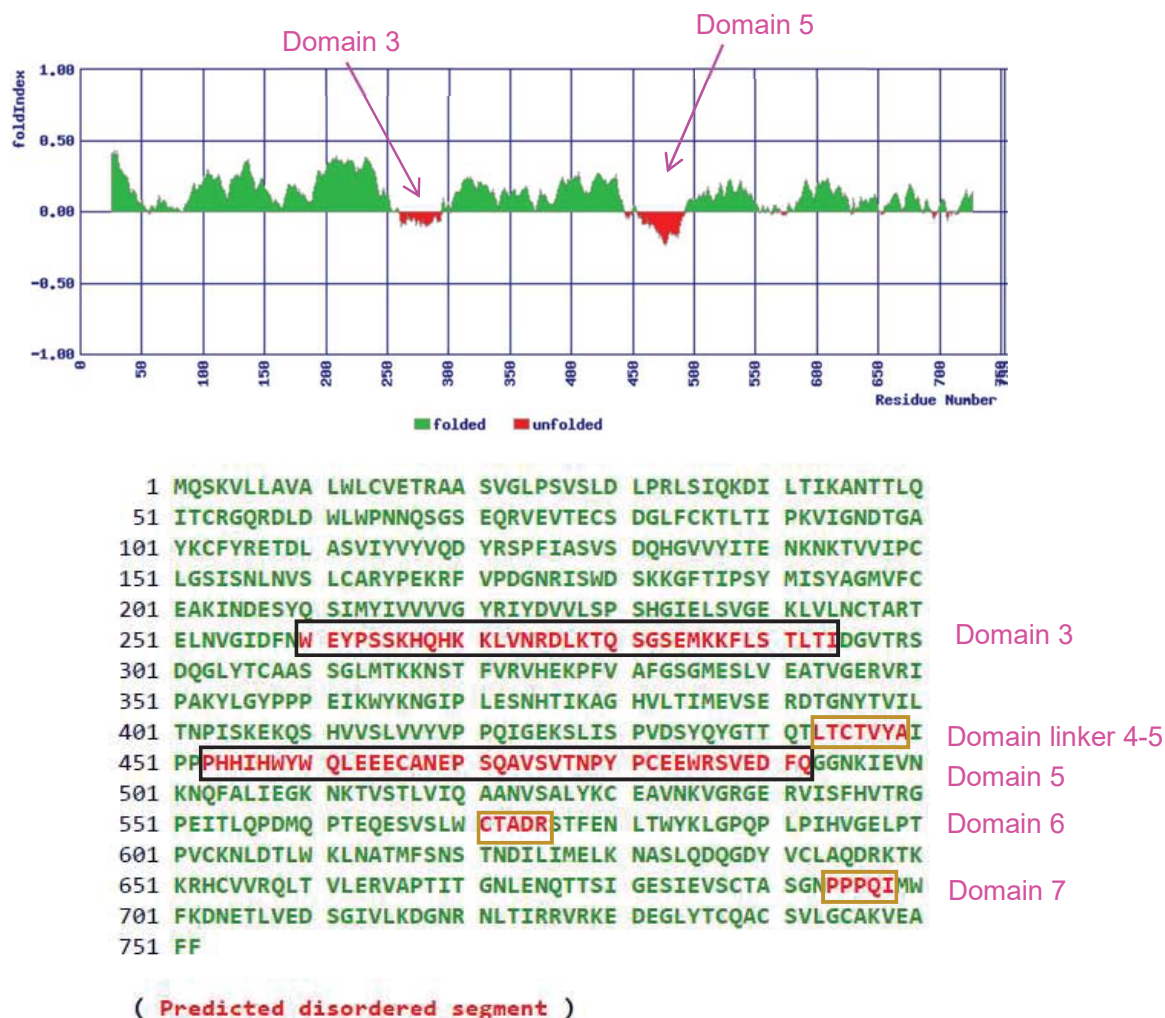


Figure 15: Schematic representation of probability of disorder in human VEGFR-2 ECD protein predicted by the FoldIndex algorithm. FoldIndex plot for VEGFR-2 ECD. Positive and negative numbers represent ordered and disordered protein, respectively. Amino acid sequences suggested as being ordered are shown in green, whereas disordered sequences are shown in red.

7.2.1.1. Limited proteolysis

Limited proteolysis was attempted on the VEGFR-2 ECD/VEGF-A₁₂₁ complex with a series of dilutions of proteases to find conditions leading to the digestion of the unstructured parts while leaving the rest of the protein intact. Comparing the limited proteolysis experiments from shorter to longer incubation times also helped in identifying the protease that yielded a more stable fragment upon digestion. Figure 16 shows that digestion with 1:10 and 1:100 GluC and papain and 1:1000 α-chymotrypsin

did not have any effect on the protein. On the other hand, incubation with 1:10 trypsin, and 1:100 α -chymotrypsin and subtilisin gave much smaller fragments in the range of 50-37 kDa. Higher concentrations (1:10) of α -chymotrypsin and subtilisin resulted in a very fast (within 90 min) and complete proteolysis. Treatment with 1:1000 subtilisin gave bigger stable fragments in the range of 100-50 kDa. Figure 16d shows the results of limited proteolysis with subtilisin of deglycosylated VEGFR-2 ECD/VEGF-A₁₂₁ complex: the fragments generated by 1:1000 subtilisin appeared sharper in SDS-PAGE. Based on these results, we carried out in-situ proteolysis by adding α -chymotrypsin and subtilisin to complexes right before setting up crystallization experiments. However, no crystals were obtained. Future experiments to identify the stable region boundaries of the proteolytic fragments by mass spectrometry may help designing new constructs more suitable for crystallization.

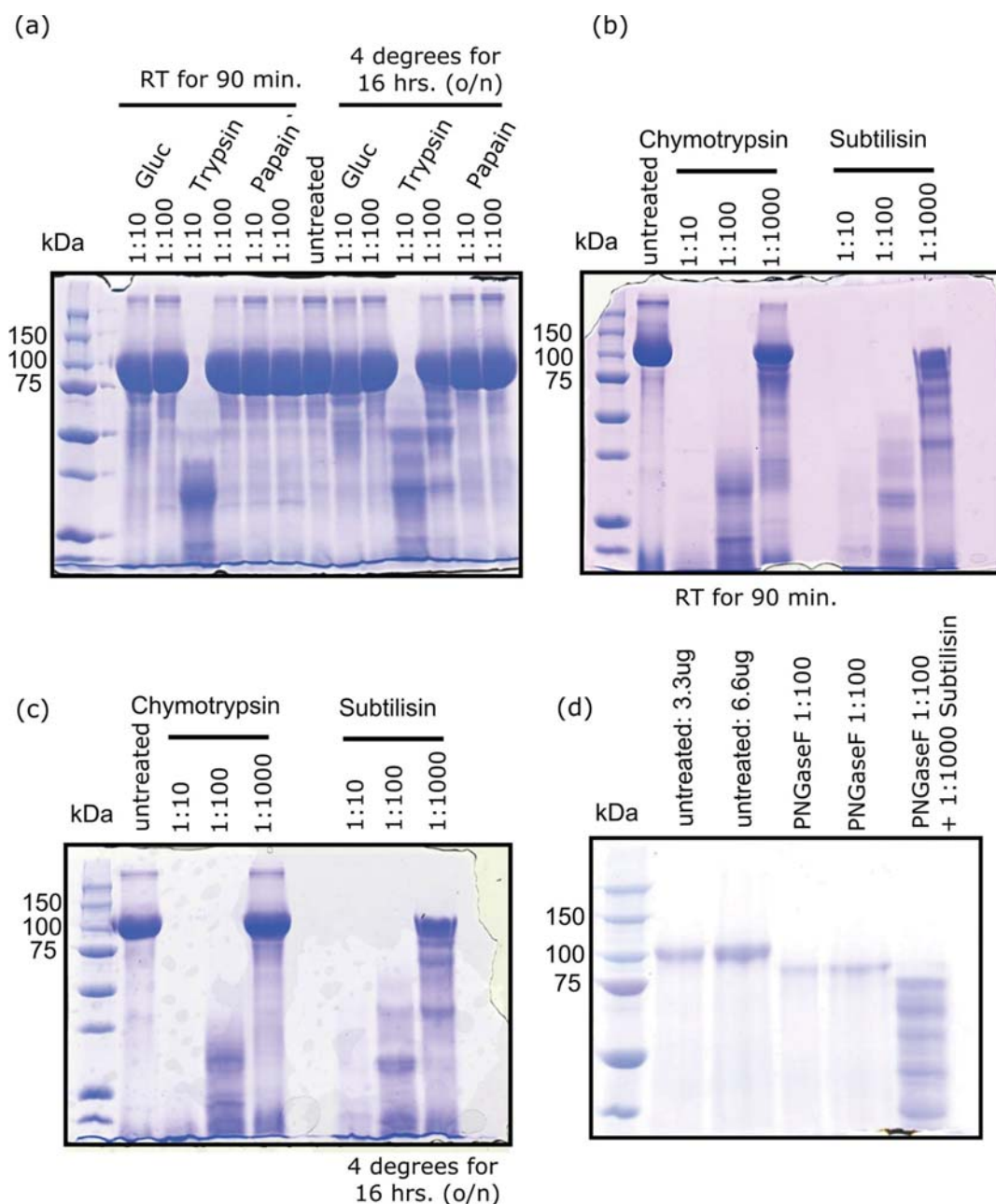


Figure 16: Limited proteolysis analysis of the VEGFR-2 ECD/VEGF-A complex. (a), (b) and (c) SDS-PAGE analysis of VEGFR-2 ECD/VEGF-A complex digested with proteases (Gluc, trypsin, papain, α -chymotrypsin, subtilisin) at dilutions 1:10, 1:100 and 1:1000 for 90 min at room temperature (RT) and overnight (o/n) at 4°C. (d) SDS-PAGE analysis of deglycosylated VEGFR-2 ECD/VEGF-A complex with PNGase F (1:100) and digested with 1:1000 subtilisin.

7.2.2. Thermal stability assay

In order to investigate the thermal stability of human VEGFR-2 subdomains 1-7, 2-7 and 1-3 upon binding of ligand VEGF-A₁₂₁ in different buffers, we performed a fluorescence-based thermal shift assay using an environmentally sensitive dye, Sypro Orange. Melting curves were obtained in the following buffers: (1) PBS, (2) 10 mM HEPES pH 7.5, 100 mM NaCl, and (3) 25 mM HEPES pH 7.5, 500 mM NaCl. Unfolding of monomeric proteins showed high melting temperature (T_m) values ranging from 54°C to 63°C (Figure 17). VEGFR-2 domains 2-7 and 1-3 complexed with ligand showed a shift towards higher T_m values compared to their corresponding monomers, indicating a stabilization effect due to ligand binding in all three buffers. However, ligand binding to VEGFR-2 domains 1-7 showed a slight decrease in the T_m value suggesting destabilization. Although in all the buffers the proteins were highly stable, we chose the low ionic strength buffer for carrying out further biophysical experiments.

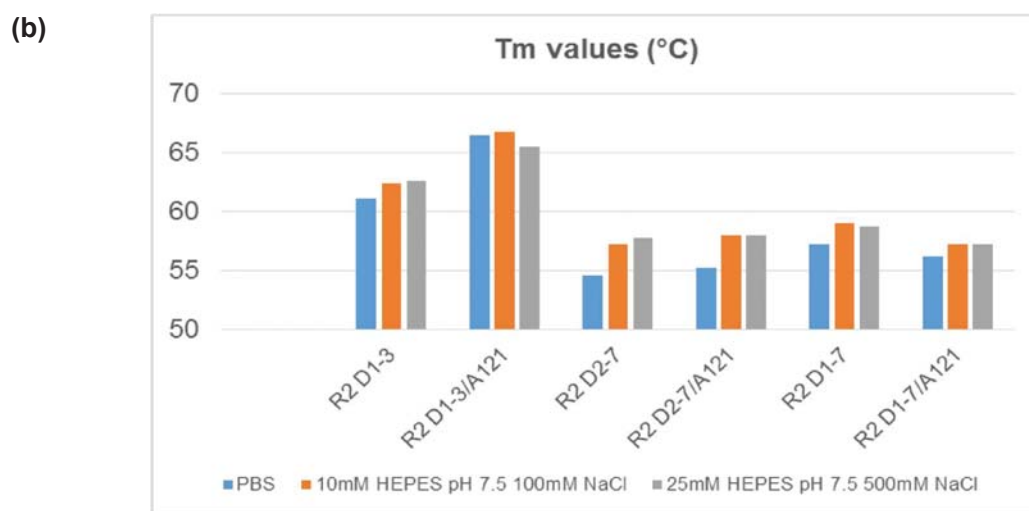
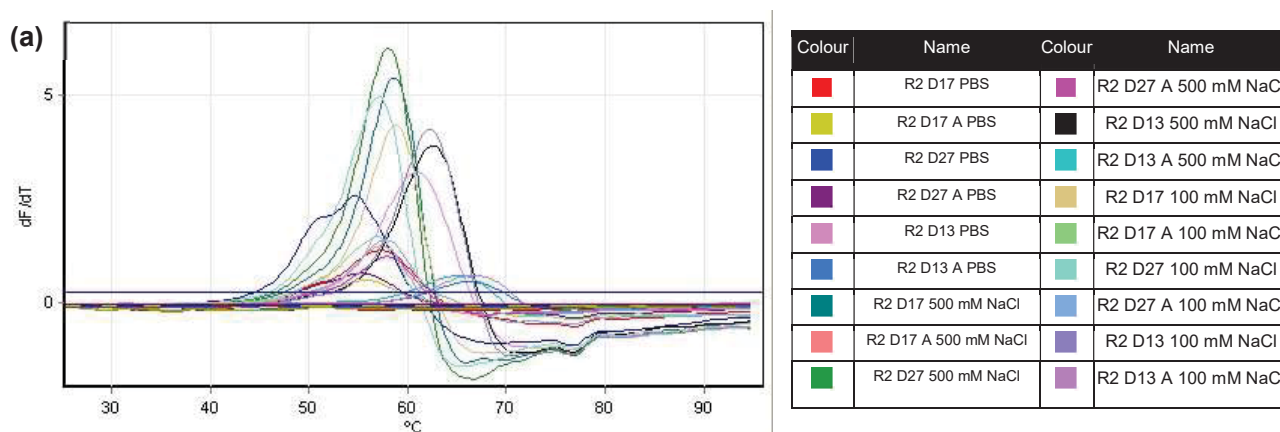


Figure 17: Effect of buffers on thermal stability of VEGFR-2 ECD subdomains and their complexes. (a) First derivative curves of thermal denaturation (“melting”) of VEGFR-2 domains 1-7, 2-7 and 1-3, monomeric or complexed with VEGF-A₁₂₁, in buffers (1) PBS, (2) 10 mM HEPES pH 7.5, 100 mM NaCl, and (3) 25 mM HEPES pH 7.5, 500 mM NaCl. The protein solution was heated in the presence of a hydrophobic dye (SYPRO Orange). (b) Bar graph showing the T_m in degree Celsius, calculated from the melting curves shown in (a), for the different constructs and buffers.

7.2.3. Thermodynamic analysis of VEGFR-2 ECD complexes

To assess the contributions of the membrane proximal Ig-domains 4-7 to the binding of full-length ECD (domains 1-7) to the ligand, we investigated the heat energies associated with complex formation by ITC. We compared the thermodynamic parameters for VEGF-A₁₂₁ binding to VEGFR-2 full-length ECD with that to the minimal ligand-binding domains 1-3. The recombinant receptor proteins used were produced in insect cells and purified as described in section 7.1.1. The obtained isotherms (Figure 18) indicate that binding of VEGF-A₁₂₁ to VEGFR-2 ECD is entropically driven and enthalpy disfavoured. The derived binding constant for domains 1-7 was 0.9 μ M, while the binding constant for domains 1-3 was only 0.14 μ M. Surprisingly, the presence of the membrane proximal Ig-homology domains in the full-length construct reduces the binding affinity.

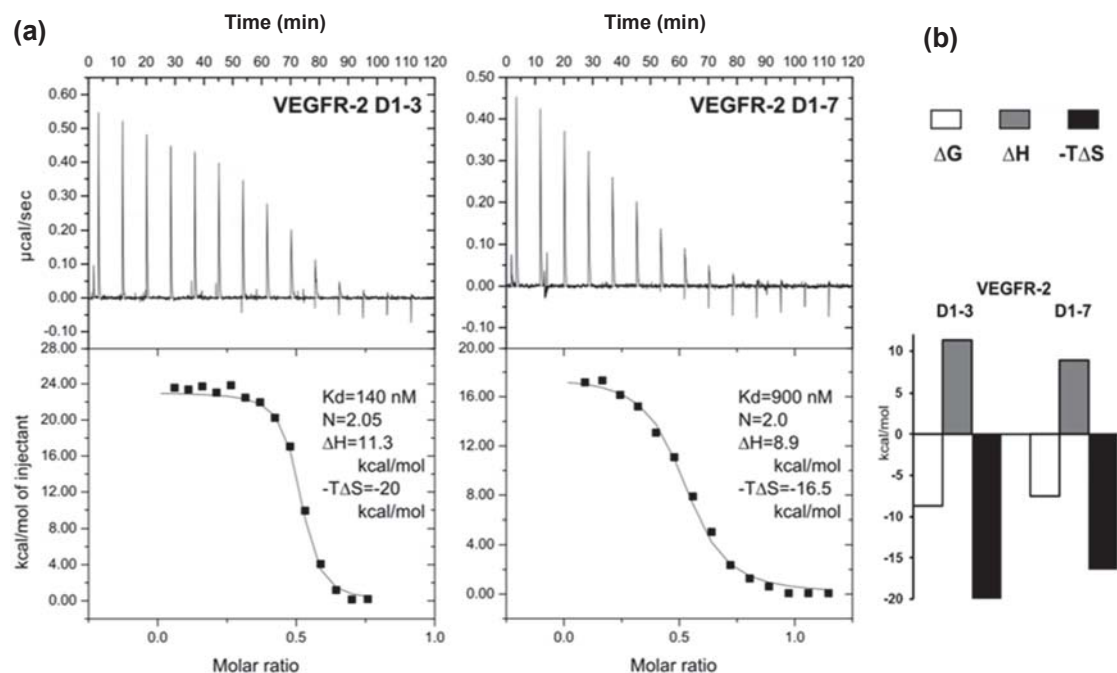


Figure 18. Quantification of VEGFR-2 ECD/VEGF-A interaction by ITC. (a) Raw titration data (upper panel) and integrated and concentration normalized isothermograms (lower panel) of VEGF-A₁₂₁ binding to the VEGFR-2 domains 1-3 (left) and domains 1-7 (right) constructs. Solid lines in the isothermograms represent the best fit according to the “One Set of Sites” model. (b) Thermodynamic signature of complex formation, showing the Gibbs free energy (ΔG), enthalpy (ΔH), and entropy ($-T\Delta S$) associated with receptor-ligand binding.

These results were also confirmed by another biophysical technique, MST. MST is a technique used to study binding affinities of interacting biomolecules in solution, resembling their natural environment (Jerabek-Willemsen *et al.*, 2011). An infrared laser is used for local heating and the molecule mobility in the resulting temperature gradient is analyzed by fluorescence. MST allows quantitative analysis of protein interactions from low amounts of sample without requiring an immobilization step. However, it fails to provide any kinetic information (i.e association and dissociation rates) of the reaction. For the measurements, the ligand VEGF-A₁₂₁ was fluorescently labelled using an optimized primary amine labelling kit protocol (section 6.2.4). The studies were conducted by titrating the unlabelled binding partner VEGFR-2 domains 1-7 or 1-3, to a fixed concentration of labelled VEGF-A₁₂₁. The binding constant for the full-length ECD construct was measured to be between 0.77 and 1.24 μ M (95% confidence interval) (Figure 19a), which is in agreement with the binding affinity value for the same construct obtained by ITC. The binding affinity of VEGFR-2 domains 1-3 for VEGF-A₁₂₁, however, could not be precisely determined, and it was estimated by

simulation to be approximately 10 nM (Figure 19b). One should bear in mind that MST works poorly for affinities higher than the low nano-molar range. The binding data obtained from both techniques corroborate the hypothesis that the membrane proximal domains (domains 4-7) reduce the receptor affinity for the ligand by approximately 10 fold.

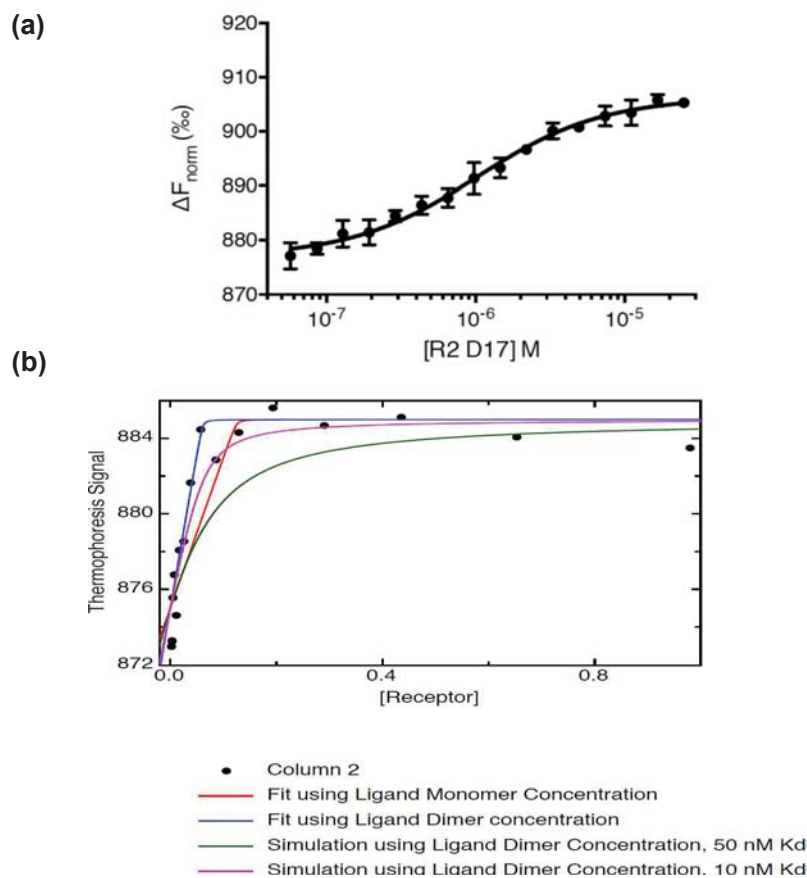


Figure 19. Quantification of VEGFR-2 ECD/VEGF-A₁₂₁ interaction by MST. (a) Unlabeled VEGFR-2 domains 1-7 was titrated into a fixed concentration of labeled VEGF-A₁₂₁. The K_d value calculated from the fit is in the range of 0.7662 to 1.244 μ M (95% confidence interval). Measurements were performed in triplicates. (b) Unlabeled VEGFR-2 domains 1-3 was titrated into a fixed concentration of labeled VEGF-A₁₂₁. The K_d value based on fits and simulations was estimated to be in the low nanomolar range.

7.3. Functional analysis of ligand binding and activation of VEGFR-1

7.3.1. Functional analysis of VEGFR-1 domain 5 mutants

The crystal structure of the VEGFR-1 dimer complexed with VEGF-A supports the hypothesis that homotypic contacts between the two receptor monomers occur in domain 5 (Section 7.4). In particular, the highly conserved amino acids T455 (β strand B), K517 (β strand E) and E513 in the D-E loop of domain 5 are involved in inter-chain hydrogen bonds and salt bridges. In order to investigate the functional significance of the domain 5 interface in the receptor dimer, we generated mutant constructs unable to form these non-covalent interactions and studied their ability to respond to VEGF-A activation.

Several mutants were generated in which charged residues were replaced with neutral amino acids (E513A, K517A) or vice versa (T455E). Also, the T455W mutation was introduced to substitute a polar amino acid (T) with a non-polar bulky residue (W). However, these single mutants were not used in our study because, their individual effect on receptor activation might have been too small to lead to any gain or loss of function. Instead, the double mutant T455E/K517A was used based on a previous study by Leppänen *et al.*, which used the equivalent VEGFR-3 T446/E/K516A mutant to validate the importance of domain 5 interface in VEGF-C-induced VEGFR-3 activation (Leppänen *et al.*, 2013). Furthermore, the double mutant E513A/K517A was generated to study the effect of loss of charge in the domain 5 interface in receptor activation.

However, before we could investigate the effect of domain 5 homotypic interactions in VEGFR-1 activation, a suitable activity assay had to be established. Although VEGFR-1 contains a classical tyrosine kinase domain, it shows poor kinase activity even in overexpressing ECs, and therefore, its signaling activity remains elusive (Waltenberger *et al.*, 1994). On the other hand, the homologous protein VEGFR-2 shows strong kinase activity upon ligand binding (Shibuya, 2006). The structural basis for the strikingly different kinase activity between these highly conserved proteins can be attributed to a set of amino acid residues present in the juxtamembrane regions of VEGFR-1, leading to the inhibition of its phosphorylation activity (Gille *et al.*, 2000).

These non-conserved amino acids are three serine residues in VEGFR-1, which are replaced by the sequence ANGG in VEGFR-2 (Figure 20). In order to enhance the activity of VEGFR-1, we designed juxtamembrane mutant constructs that either lacked the three serine residues or contained the ANGG sequence from VEGFR-2 instead. Initially, the mutants were transiently expressed in HEK293 cells. However, the inability to specifically detect total VEGFR-1 present in these cells due to the lack of a suitable antibody led to non-conclusive results and prevented us from using these constructs for further experiments.

```

VEGFR-2  RTVKRANGGELKTGYLSIVMDPDELPLDEH
VEGFR-1  RKMKRSS SEIKTDYLSIIMDPDEVPLDEQ

```

Figure 20: Alignment of juxtamembrane regions of VEGFR-1 and VEGFR-2. Adapted from Gille *et al.*

We henceforth set to optimize the functional assay by using stably transfected PAE cell lines as an alternative expression system, which also offers a more physiological environment for functional studies of VEGFR-1. A series of control experiments were performed on stable PAE cell lines expressing wild-type VEGFR-1, where several commercial antibodies were tested for their ability to specifically detect the total levels of VEGFR-1 by western blot. Antibodies from Abcam (ab32152) and Santa Cruz Biotechnology (sc-31173) were not suitable since they gave false positive results in the non-transfected cells, and the antibody available from R&D systems (AF321) did not show any band at the expected molecular weight (150 kDa). We obtained the best results with the antibody offered from Cell Signaling (2893S), which was both specific and selective in detecting VEGFR-1 in whole cell lysates (Figure 21a). However, the antibody from Santa Cruz Biotechnology (sc-31173) worked well in immunocytochemical staining of PAE cell lines stably expressing wild-type VEGFR-1, confirming its correct localization at the plasma membrane (Figure 21b; VEGFR-1 staining in green). A summary of our experiments with various VEGFR-1 antibodies, showing their different applicability, is shown in Table 9.

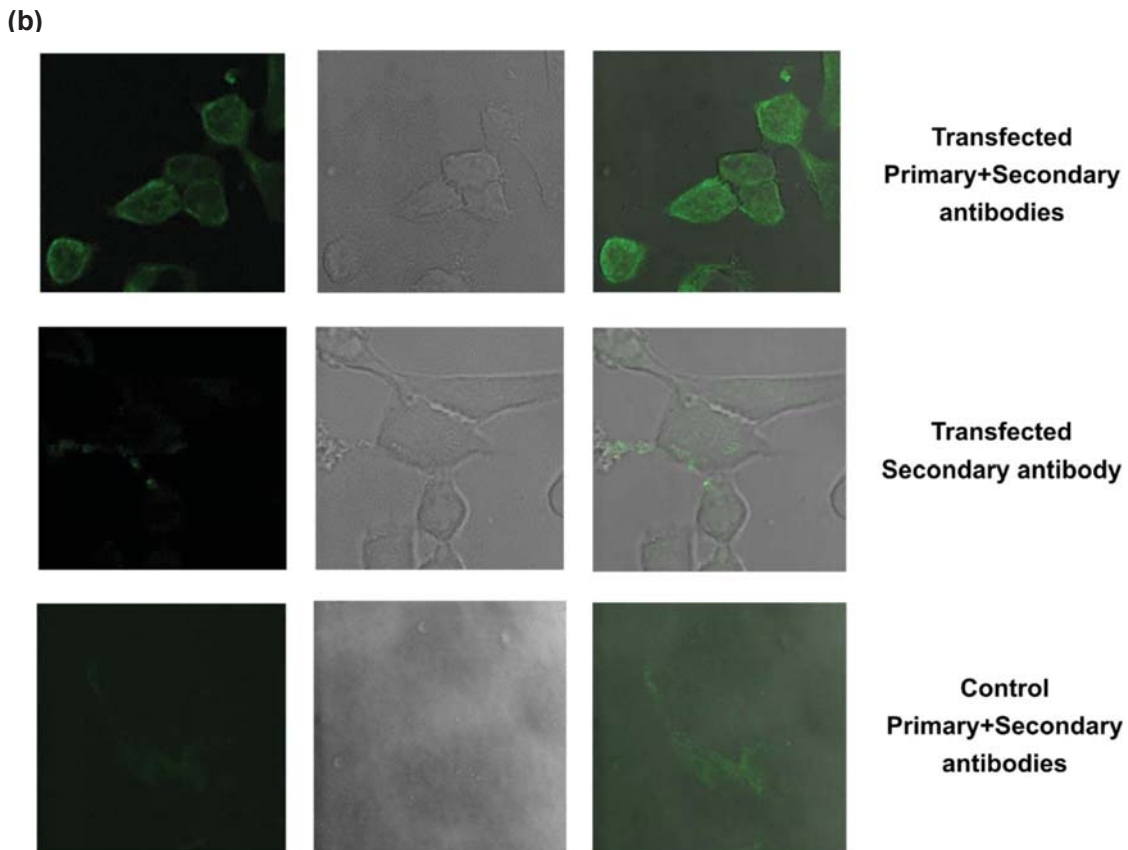
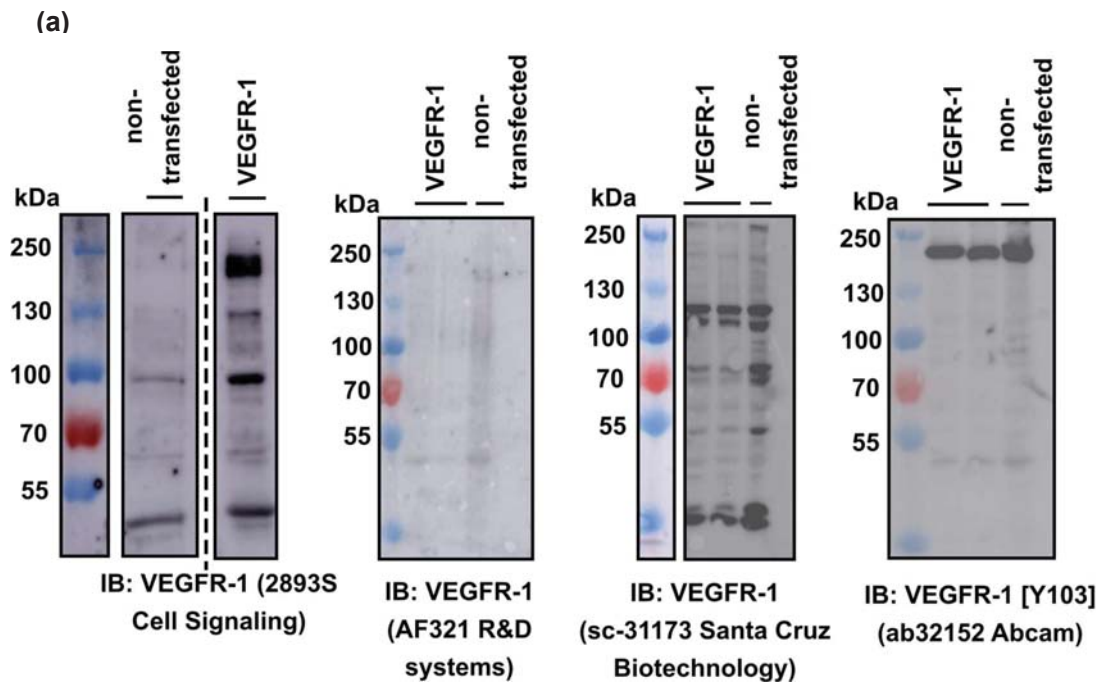


Figure 21: Antibodies used for VEGFR-1 detection. (a) Immunoblot analysis on cell lysates from non-transfected or VEGFR-1-expressing PAE cell lines using several antibodies against VEGFR-1. Samples from equal cell numbers were loaded in each gel. (b) Immunostaining of non-transfected or VEGFR-1-expressing PAE cells using the Santa Cruz anti-VEGFR-1 antibody and a Dylight 488-labeled secondary antibody. Left panel: Dylight 488 fluorescence image; middle panel: phase contrast image; right panel: overlay.

Antibodies	Dilution	Blocking/ dilution buffer	Incubation Time/temperature	Immuno- flore- scent	Western blot
Flt-1 (C17) (sc-31173 Santa Cruz Biotechnolog y, Inc.)	1:400	1% BSA in PBS	One hour at room temperature	Good	×
VEGF Receptor 1 Antibody (2893S Cell Signaling)	1:1000	5% BSA in TBST	Overnight at 4°C	×	Good
Anti Flt-1 (AF321 R&D systems)	1:200	5% BSA in TBST	One hour at room temperature	–	×
Anti-VEGF Receptor 1 [Y103] (ab32152 Abcam)	1:1000	5% BSA in TBST	Overnight at 4°C	×	–
Anti- phospho-Flt- 1 (Tyr1213) (07-758 Millipore)	1:1000	3% milk in TBST with washes in water	Overnight at 4°C	–	Good
Anti-Phospho Flt-1 (Tyr1213) (AF4170 R&D systems)	1:1000	5% milk for blocking and 2% milk for antibody in TBST	One hour at room temperature	–	×

Table 9: Antibodies tested for detection of VEGFR-1 expression in PAE cells. TBST: Tris-buffered Saline, 0.1 % Tween-20.

Next, we studied the parameters regulating ligand-induced VEGFR-1 activation in stable PAE cell lines. We tested two VEGFR-1 ligands, PIGF and VEGF-A₁₆₅, at different concentrations and with different stimulation times, and assessed VEGFR-1

activation by detecting Y1213 phosphorylation by western blot (Figure 22). We chose Y1213 based on studies of VEGFR-1-associated proteins, which revealed that phosphorylated Y1213 within VEGFR-1 is a major binding site for PI-3 KINASE and Nck (Igarashi *et al.*, 1998). VEGF-A₁₆₅ was recombinantly produced in our laboratory, whereas PIGF was obtained from three different sources: Reliatech (PIGF-2, 300-020), R&D systems (264-PG-010) and Peprotech (100-06). We detected VEGFR-1 phosphorylation only upon stimulation with PIGF from Peprotech and VEGF-A₁₆₅. PIGF was able to stimulate VEGFR-1 phosphorylation when used at 0.25 nM or 1.5 nM for 5 min, whereas VEGF-A₁₆₅ required 10 min of stimulation to give comparable results (Figure 22a). Maximal receptor activation was achieved after stimulation with 0.25 nM PIGF from Peprotech for 5 min (Figure 22b).

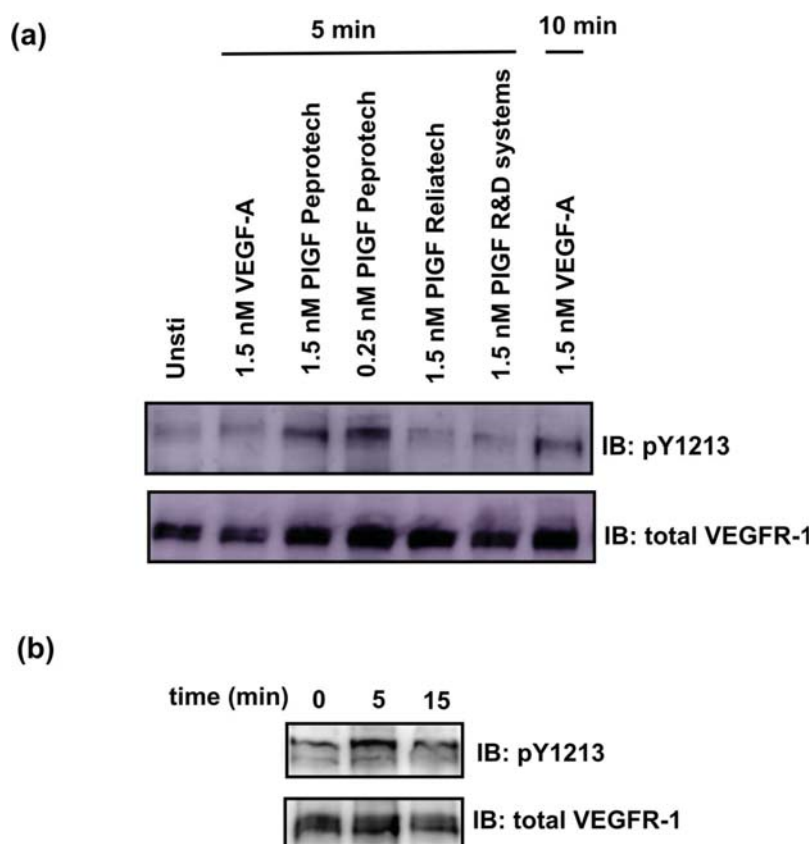


Figure 22: Ligand-induced VEGFR-1 activation. (a) PAE cells stably expressing VEGFR-1 were stimulated with various concentrations of VEGF-A₁₂₁ or PIGF from different sources, for different time points. The levels of Y1213 phosphorylated and total VEGFR-1 were assessed in whole cell lysates by western blotting. (b) Western blot analysis of time-course of VEGFR-1 phosphorylation (Y1213) in stable PAE cells expressing wild-type VEGFR-1 when stimulated with 0.25nM PIGF.

Having established an expression system and kinase assay to study VEGFR-1 activation, we proceeded to study the activity of domain 5 double (E513A/K517A; T455E/K517A) and triple (T455W/E513A/K517A; T455E/E513A/K517A) VEGFR-1 mutants. The constructs were cloned into the mammalian expression vector pcDNA3.1 and used to generate stable PAE cell lines through chemical transfection (PEI; Aldrich 408727, 25 kDa branched). Most of the mutants showed weak expression levels compared to the wild-type (Figure 23a). Alternatively, we generated PAE cell lines stably expressing wild-type, domain 5_E513A/K517A and domain 5_T455W/E513A/K517A VEGFR-1 by lentivirus transduction. However, the expression levels of the various VEGFR-1 constructs in the PAE cell lines generated by lentiviral transduction were poor compared to the expression of wild-type VEGFR-1 in PAE cell lines generated by PEI transfection (Figure 23b). We suspect that the large size of the inserts (4 kb) reduced the viral packaging efficiency and hence led to weak expression of recombinant proteins. Therefore, we were unable to use these cell lines to study receptor phosphorylation of the domain 5 mutants upon ligand activation, and we sought an alternative system using chimeric VEGFR-1/2 constructs as described in the following section 7.3.2.

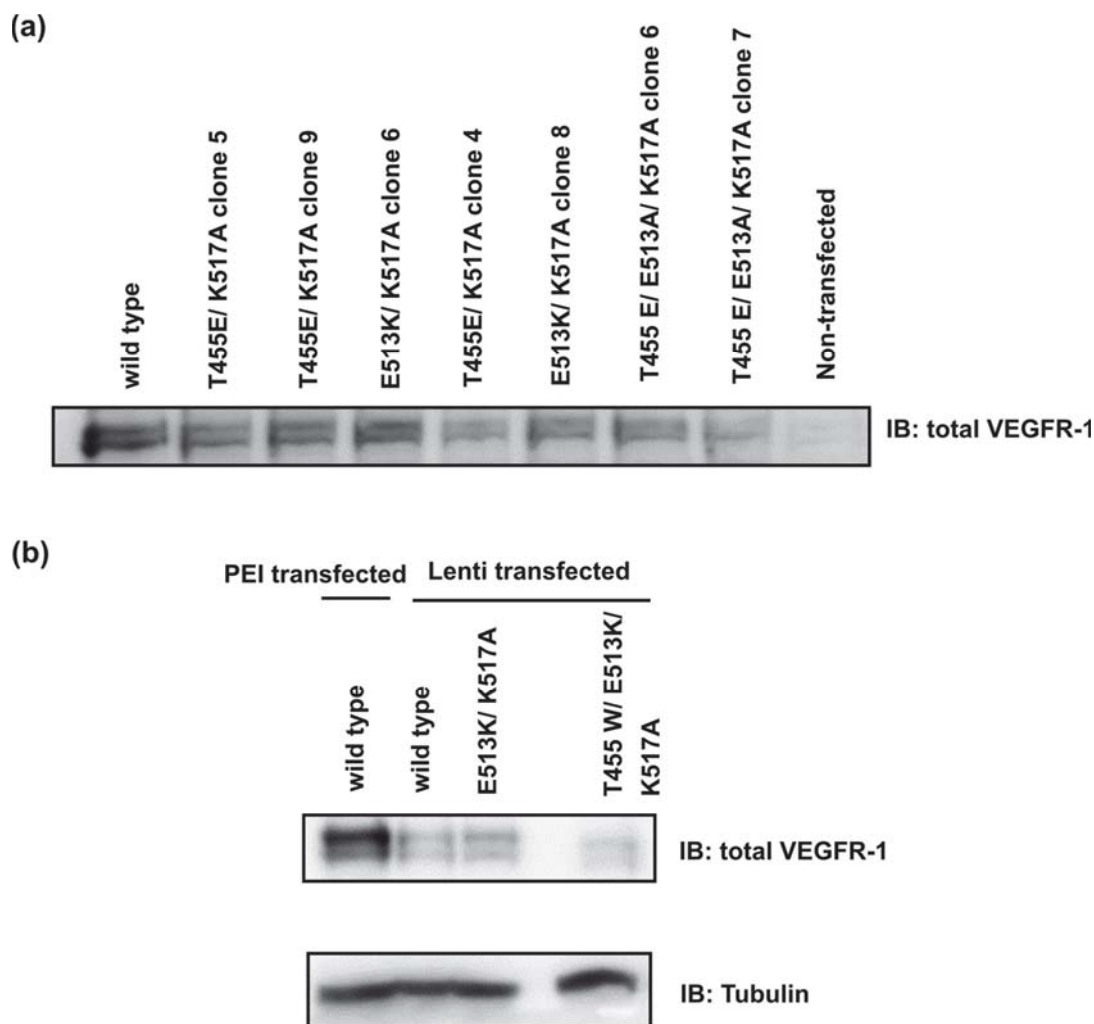


Figure 23: Stable PAE clones expressing wild-type and domain 5 mutants of VEGFR-1. (a) PAE cells lines expressing either wild-type, T455E/K517A, E513K/K517A or T455E/E513K/K517A VEGFR-1 were generated by chemical transfections with PEI. Whole cell lysates from different cell clones were analyzed by western blotting using an anti-VEGFR-1 antibody (2893S Cell Signaling). Samples from equal number of cells were loaded.. (b) PAE cells lines expressing either wild-type, E513K/K517A or T455E/E513K/K517A VEGFR-1 were generated by lentiviral transduction. Whole cell lysates were analyzed by western blotting using an anti-VEGFR-1 antibody (2893S Cell Signaling). The expression levels of VEGFR-1 were compared to those from PAE cells transfected with wild-type VEGFR-1 using PEI. Equal protein loading was confirmed with an anti- β -actin antibody.

7.3.2. Functional analysis of chimeric VEGFR-1/2 domain 5 mutants

As an alternative strategy to study VEGFR-1 activation and its dependency on the homotypic interactions involving domain 5, we generated chimeric VEGFR-1/2 constructs, consisting of the extracellular domain of VEGFR-1 (residues 1-752; wild-type, domain 5_E513K/K517A and domain 5_T455W/E513K/K517A), followed by the

intracellular domain of VEGFR-2 (residues 759-1356). Stable PAE cell lines were generated by chemical transfections (PEI; Aldrich 408727, 25 kDa branched). Upon clonal selection, the total expression levels of the chimeric receptor was assessed by Western blot using an anti-VEGFR-2 antibody, since the anti-VEGFR-1 antibody was specific for the intracellular domain of the receptor (Figure 24). We obtained a strong expressing clone for wild-type chimeric VEGFR-1/2 (clone 8; lane 3) but only weak expressing clones for the domain 5 mutants. Because of the unequal expression of wild-type and mutant PAE cell lines we were unable to carry out quantitative kinase activity studies in this system.

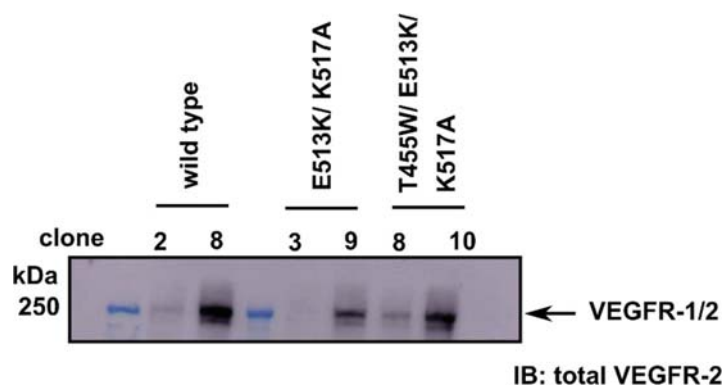


Figure 24: Stable PAE clones of VEGFR-1/2 wild-type and domain 5 mutants. PAE cells lines expressing either wild-type, E513K/K517A or T455E/E513K/K517A VEGFR-1/2 chimeras were generated by PEI transfections. Whole cell lysates from different cell clones were analyzed by western blotting using an anti-VEGFR-2 antibody. Samples from equal number of cells were loaded.

However, we could achieve similar expression levels between wild-type and domain 5_E513K/K517A VEGFR-1 constructs in transiently transfected NIH3T3 cells. Consequently, the cells were stimulated with 0.25 nM PIGF (Peprotech; 100-06) for 5 min according to our previous results (Figure 22) and receptor activation was assessed in whole cell lysates by immunoblotting with an antibody specific for pY1175, the major phosphorylation site of VEGFR-2. Wild-type VEGFR-1/2 showed considerably higher phosphorylation activity compared to chimeric mutant E513K/K517A (Figure 25). Similar kinase assays using the triple mutant T455W/E513K/K517A were inconclusive due to unequal expression of mutant and wild-type receptors. However, the results with the double mutant indicate that the homotypic contacts in domain 5 revealed by our

VEGFR-1 ECD/VEGF-A structure are functionally relevant and thus crucial for ligand induced dimerization and receptor activation.

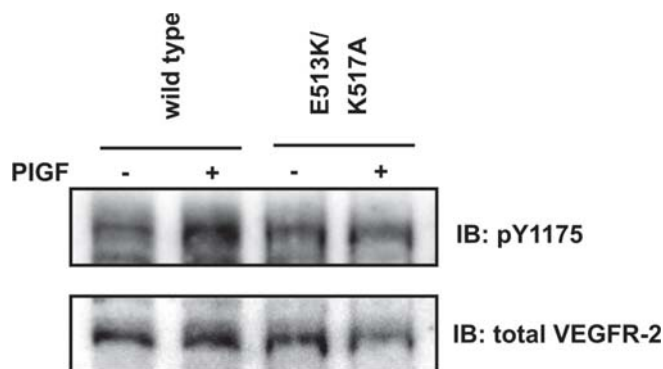


Figure 25: Effect of domain 5 mutations on activation of chimeric VEGFR1/2 constructs. NIH3T3 cells transiently expressing chimeric VEGFR-1/2 [VEGFR-1 ECD (residues 1-752) and intracellular domain of VEGFR-2 (residues 759-1356)] wild-type and domain 5 mutants were stimulated with 0.25 nM PIGF for 5 min. Phosphorylation activity was determined in whole cell lysates by immunoblotting with pY1175 and tVEGFR-2 (total) antibodies. Samples from equal number of cells were loaded.

7.3.3. Functional analysis of VEGFR-2 domain 5 mutants

To further verify the relevance and universality of the domain 5 homotypic contacts observed in our VEGFR-1 structure in receptor activation, we mutated the corresponding residues (T446, E508 and K512) in the domain 5 of VEGFR-2. We first tested whether HEK293 cells expressing wild-type VEGFR-2 were a suitable system to study ligand-induced receptor activation. Transient transfection were carried with several different transfection agents and the total levels of VEGFR-2 were assessed by immunoblotting. Lipofectamine 2000 and Lipofectamine 3000 showed superior transfection efficiency when compared to Fugene (Figure 26). Mock transfected cells were used as a negative control. However, the basal levels of receptor activation were too high. The spontaneous transactivation of the receptor kinase, possibly because of overexpression at the cell membrane, prevented us from using these cells to study the effect of domain 5 homotypic interactions on ligand-induced receptor activation (Figure 27).

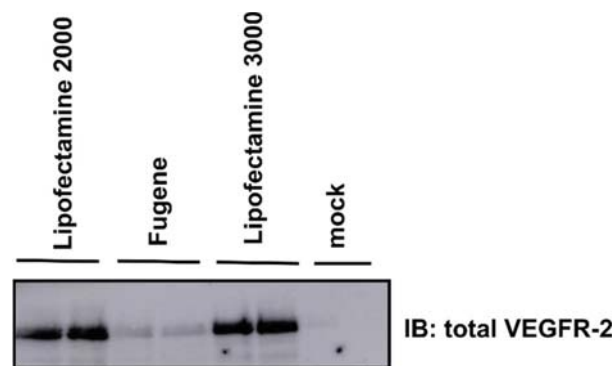


Figure 26: Effect of different transfection agents on the expression of VEGFR-2 in HEK293 cells. HEK293 cells were transfected with the pBE VEGFR-2 plasmid, using different transfection reagents: Lipofectamine 2000, Fugene and Lipofectamine 3000. Cells were harvested 25 h post-transfection and whole cell lysates were analyzed by western blotting using an anti-VEGFR-2 antibody. Samples from equal number of cells were loaded.

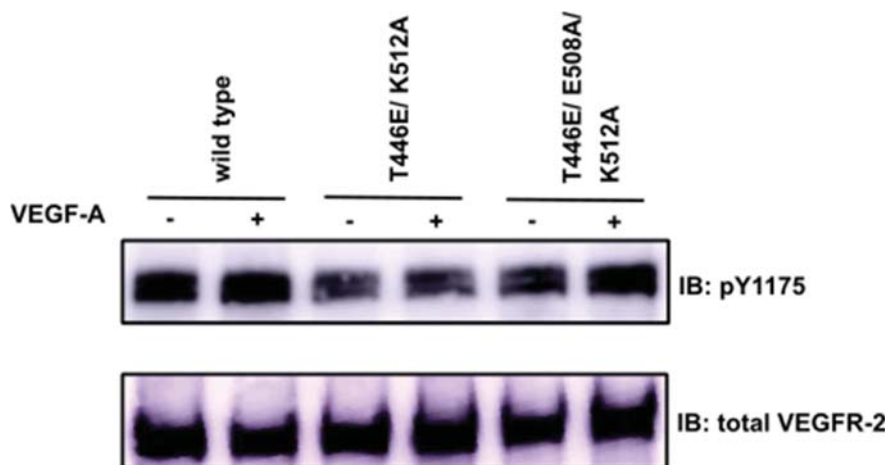


Figure 27: VEGFR-2 overexpression in HEK293 cells prevents ligand-induced activation. HEK293 cells transiently expressing VEGFR-2 wild-type and domain 5 mutants were stimulated with 1.5 nM VEGF-A₁₆₅. Phosphorylation activity was determined in whole-cell lysates by immunoblotting with pY1175 and total VEGFR-2 antibodies. Samples from equal number of cells were loaded.

On the contrary, we were successful in generating NIH3T3 cells expressing wild-type VEGFR-2 with low basal activity that was sensitive to ligand stimulation. The cells were transiently transfected using Lipofectamine 2000 and PEI, with PEI transfections being more efficient and giving clearer protein bands compared to Lipofectamine 2000 transfection. Therefore, we used transient transfections of NIH3T3 cells with PEI to express the domain 5 T446E/K512A and T446E/ E508A/K512A VEGFR-2 mutants. The cells were stimulated with 1.5 nM VEGF-A₁₆₅ for 10 min and receptor activation

was assessed in whole cell lysates by immunoblotting with an antibody specific for pY1175. Receptor phosphorylation was greatly reduced in domain 5 double (T446E/K512A) and triple (T446E/ E508A/K512A) mutants compared to the wild-type (Figure 28). This shows that the conserved key residues involved in domain 5 interactions are crucial for VEGF-A-induced VEGFR-2 tyrosine autophosphorylation.

In order to investigate the mutual importance of domain 5 and 7 homotypic interactions in VEGFR-2 activation, we made additional mutant constructs: domain 7_R726A, domain 7_R726A_domain 5_ T446E/K512A, domain 7_R726A_domain 5_T446E/E508K/K512A. The mutation R726A in domain 7 has been reported earlier to significantly reduce kinase activation due to the inability to form the inter-receptor salt bridge leading to destabilization of the receptor dimers (Hyde *et al.*, 2012; Yang *et al.*, 2010). Also, an analogous mutation R737A in domain 7 of VEGFR-3 together with domain 5 homotypic mutations showed an additional inhibitory effect in activation of VEGFR-3 (Leppänen *et al.*, 2013). However, these constructs could not be tested during this work due to lack of time.

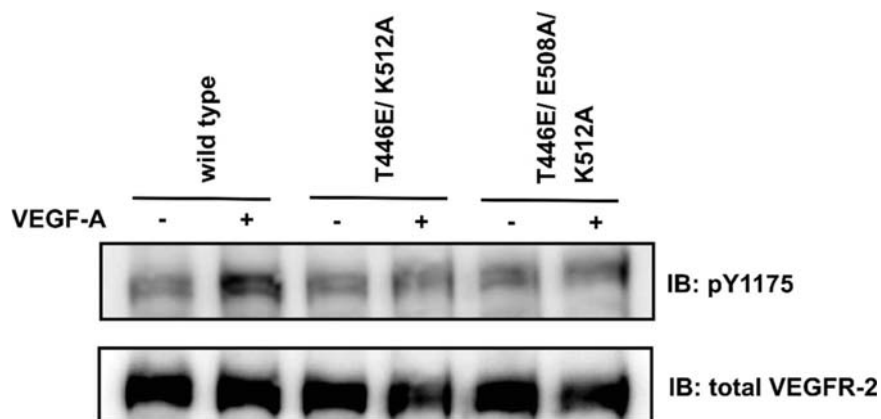


Figure 28: Effect of domain 5 mutations on VEGFR-2 activation. NIH3T3 cells transiently expressing VEGFR-2 wild-type and domain 5 mutants were stimulated with 1.5 nM VEGF-A₁₆₅. Phosphorylation activity was determined in whole-cell lysates by immunoblotting with pY1175 and total VEGFR-2 antibodies. Samples from equal number of cells were loaded.

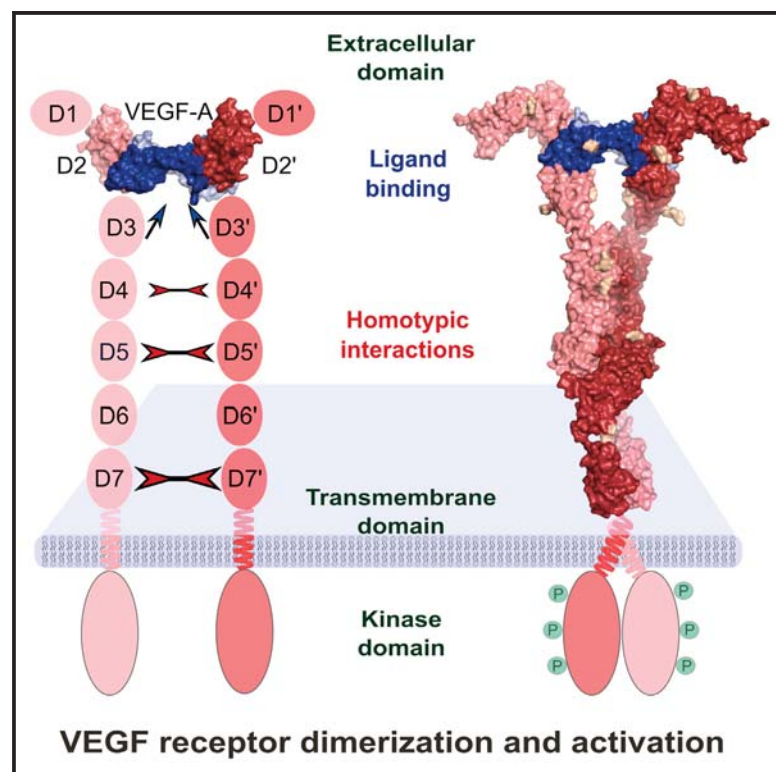
7.4 Structure of the full-length VEGFR-1 ECD in complex with VEGF-A

In this section, a re-print of the publication of results obtained during PhD is attached to give an overview. My contribution is the biochemical analysis of receptor mutants.

Structure

Structure of the Full-length VEGFR-1 Extracellular Domain in Complex with VEGF-A

Graphical Abstract



Authors

Sandra Markovic-Mueller,
Edward Stutfeld,
Mayanka Asthana, ..., Kaisa Kisko,
Guido Capitani, Kurt Ballmer-Hofer

Correspondence

kurt.ballmer-hofer@unibas.ch

In Brief

Markovic-Müller et al. describe the first full-length ectodomain structure of a type V receptor tyrosine kinase, VEGFR-1, in complex with its cognate ligand, VEGF-A. The structure reveals the details of regulatory homotypic receptor interactions representing putative targets for therapeutic receptor inhibition.

Highlights

- First full-length structure of the VEGFR-1 ectodomain bound to its cognate ligand
- Description of unique strategy to determine crystal structures at medium resolution
- Characterization of VEGFR ligand specificity and homotypic receptor interactions
- Paradigm for type V receptor tyrosine kinase activation and therapeutic inhibition

Accession Numbers

5T89



Structure of the Full-length VEGFR-1 Extracellular Domain in Complex with VEGF-A

Sandra Markovic-Mueller,^{1,5,6} Edward Stuttfeld,^{2,5} Mayanka Asthana,^{1,5} Tobias Weinert,¹ Spencer Bliven,^{1,4} Kenneth N. Goldie,³ Kaisa Kisko,¹ Guido Capitani,¹ and Kurt Ballmer-Hofer^{1,7,*}

¹Paul Scherrer Institute, Laboratory of Biomolecular Research, 5232 Villigen, Switzerland

²Biozentrum, University of Basel, 4056 Basel, Switzerland

³Center for Cellular Imaging and Nano Analytics (C-CINA), Biozentrum, University of Basel, 4056 Basel, Switzerland

⁴National Center for Biotechnology Information, National Library of Medicine, National Institutes of Health, Bethesda, MD 20894, USA

⁵Co-first author

⁶Present address: leadXpro AG, PARK INNOVAARE, 5234 Villigen, Switzerland

⁷Lead Contact

*Correspondence: kurt.ballmer-hofer@unibas.ch

<http://dx.doi.org/10.1016/j.str.2016.12.012>

SUMMARY

Vascular endothelial growth factors (VEGFs) regulate blood and lymph vessel development upon activation of three receptor tyrosine kinases: VEGFR-1, -2, and -3. Partial structures of VEGFR/VEGF complexes based on single-particle electron microscopy, small-angle X-ray scattering, and X-ray crystallography revealed the location of VEGF binding and domain arrangement of individual receptor subdomains. Here, we describe the structure of the full-length VEGFR-1 extracellular domain in complex with VEGF-A at 4 Å resolution. We combined X-ray crystallography, single-particle electron microscopy, and molecular modeling for structure determination and validation. The structure reveals the molecular details of ligand-induced receptor dimerization, in particular of homotypic receptor interactions in immunoglobulin homology domains 4, 5, and 7. Functional analyses of ligand binding and receptor activation confirm the relevance of these homotypic contacts and identify them as potential therapeutic sites to allosterically inhibit VEGFR-1 activity.

INTRODUCTION

The formation of functional blood and lymphatic vessels is a keystone during embryo development and is essential for supplying all organs with oxygen and nutrients and for disposal of catabolites. Vascular endothelial growth factors (VEGFs) are the main drivers of vasculogenesis, the *de novo* formation of vessels, and angiogenesis, the formation of new vessels from preexisting vasculature (reviewed in [Smith et al., 2015](#); [Shibuya, 2014](#); [Moens et al., 2014](#)). VEGFs activate VEGFR-1, -2, and -3, representing the type V subfamily of receptor tyrosine kinases (RTKs) in the human kinome ([Shibuya, 2013](#)).

Mutation or ablation of a specific VEGFR gave rise to distinct disease profiles ([Shibuya, 2014](#)), documenting signal diversity among these three receptors. Both ablation of VEGFR-1

and -2 were embryonic lethal; the former due to severe disorganization of blood vessels ([Fong et al., 1995](#)) and the latter because of the complete absence of endothelial cells ([Shalaby et al., 1995](#)). Interestingly, mice expressing kinase-deficient VEGFR-1 instead of wild-type showed only minor vascular defects ([Hiratsuka et al., 1998, 2001](#)). Deregulated expression of a soluble splice variant of VEGFR-1, encompassing only the extracellular domain (ECD) and acting as a ligand trap ([Kendall and Thomas, 1993](#)), is associated with vascular defects such as the placental deficiency preeclampsia ([Luttun and Carmeliet, 2003](#); [Maynard et al., 2003](#)) or corneal ([Ambati et al., 2006](#)) and retinal avascularity ([Luo et al., 2013](#)).

RTK activation requires ligand-mediated dimer or multimer formation, which instigates transmembrane signaling resulting in activation of the intracellular kinase domain ([Lemmon and Schlessinger, 2010](#)). The exact structural changes driving this process are unique for each RTK subfamily and are not known for VEGF receptors.

A low-resolution structure of a VEGFR-2 ECD/ligand complex showed that of the seven immunoglobulin homology domains (Ig domains) comprising the receptor ECD, Ig domains 1–3 form the ligand binding site while domains 4–7 are involved in homotypic receptor contacts, presumably regulating receptor dimerization and activation ([Ruch et al., 2007](#)). In addition, high-resolution information for Ig domains D2–3 and D1–2 of VEGFR-2 and -3, respectively, bound to VEGF ([Leppänen et al., 2010, 2013](#); [Brozzo et al., 2012](#)) is available. For VEGFR-1, there are X-ray structures for VEGF-A, -B, and placental growth factor (PIGF), respectively, in complex with D2 ([Christinger et al., 2004](#); [Wiesmann et al., 1997](#); [Iyer et al., 2010](#)). These structures show how the membrane distal Ig domains mediate ligand binding, in particular how three highly variable loops present in all VEGF family ligands interact with the receptor ECD. High-resolution information on the VEGFR membrane-proximal Ig domains has so far been obtained by crystallizing specific subdomains in isolation. The crystal structure of Ig domain 7, together with functional experiments using receptor mutants ([Yang et al., 2010](#)), revealed the importance of homotypic contacts between the conserved residues R726 and D731 present in the EF loop for ligand-induced activation of VEGFR-2. A recent crystal structure of Ig domains 4–5 of VEGFR-3 pointed to additional receptor-receptor interactions in D5 ([Leppänen et al., 2013](#)). These D5

interactions were a consequence of crystal packing. However, similar to the D7 contacts observed earlier for VEGFR-2 (Yang et al., 2010; Hyde et al., 2012; Ruch et al., 2007), functional analysis showed that these contacts are indispensable for receptor activation. We focused on the structural characterization of full-length VEGF receptor ECD complexes and succeeded in determining the structure of the VEGFR-1 ECD in complex with VEGF-A at 4 Å resolution. The structure allows for the first time detailed visualization of ligand binding and ligand-induced homotypic interactions in a complete VEGF receptor ECD/VEGF complex and opens new possibilities for future drug design.

RESULTS

Structure Determination of the VEGFR-1 Extracellular Domain/VEGF-A Complex

We determined the structural organization of the full-length ECD of VEGFR-1 in complex with VEGF-A using X-ray crystallography. Human VEGFR-1 baculovirus expression constructs encompassing Ig domains D1–7, D1–6, and D2–7 (Figure 1A) were expressed in insect cells, purified, and crystallized in complex with VEGF-A. Complex formation between ligand and receptor ECD proteins and monodispersity of the complexes was determined by size-exclusion chromatography coupled to multi-angle light scattering (SEC-MALS) and small-angle X-ray scattering (SAXS; Supplemental Experimental Procedures). VEGF-A co-eluted from an SEC column with the VEGFR-1 ECD (Figure S1A), and molecular weight determination by SEC-MALS indicated 1:1 dimer formation of the full-length VEGFR-1 ECD with VEGF-A (Figure S1B). In addition, an increase in the radius of gyration (R_g) and of the maximal length of the complex (D_{max}) in the presence of ligand was observed in the distance distribution function determined by SAXS, confirming the presence of a stable ligand/receptor complex (Figure S1C).

After various optimization rounds, we obtained crystals of the D1–6 complex diffracting to 4 Å that were suitable for structure determination (Table 1). Crystals belonged to space group C2 with one complex per asymmetric unit and a solvent content of 70%. Enabled by a novel data collection strategy (Weinert et al., 2015), the structure of the VEGFR-1 D1–6/VEGF-A complex was solved by a combination of molecular replacement (MR) and single-wavelength anomalous dispersion (SAD) using iodide-soaked crystals (Figure 1B). The resulting electron density map revealed the D2 region and the ligand, positioned by molecular replacement, and contained continuous electron density for the missing Ig domains (Figure S2). D3, D4, and D5 were placed by additional rounds of phased molecular replacement, and proper sequence assignment was performed by replacing the molecular replacement search models with the corresponding homology models generated by the SWISS-MODEL homology modeling server. Because of their less well-defined electron density and the lack of good homology modeling templates, D1 and D6 were modeled using the Foldit structure prediction game (Cooper et al., 2010). The best D1 and D6 models were selected for further manual refinement based on their performance as search models in molecular replacement (Figure S3).

Anomalous scattering of selenium-methionine (Se-Met) is a powerful structure and sequence validation tool. In the absence of diffracting Se-Met derivative crystals, we turned to sulfur SAD

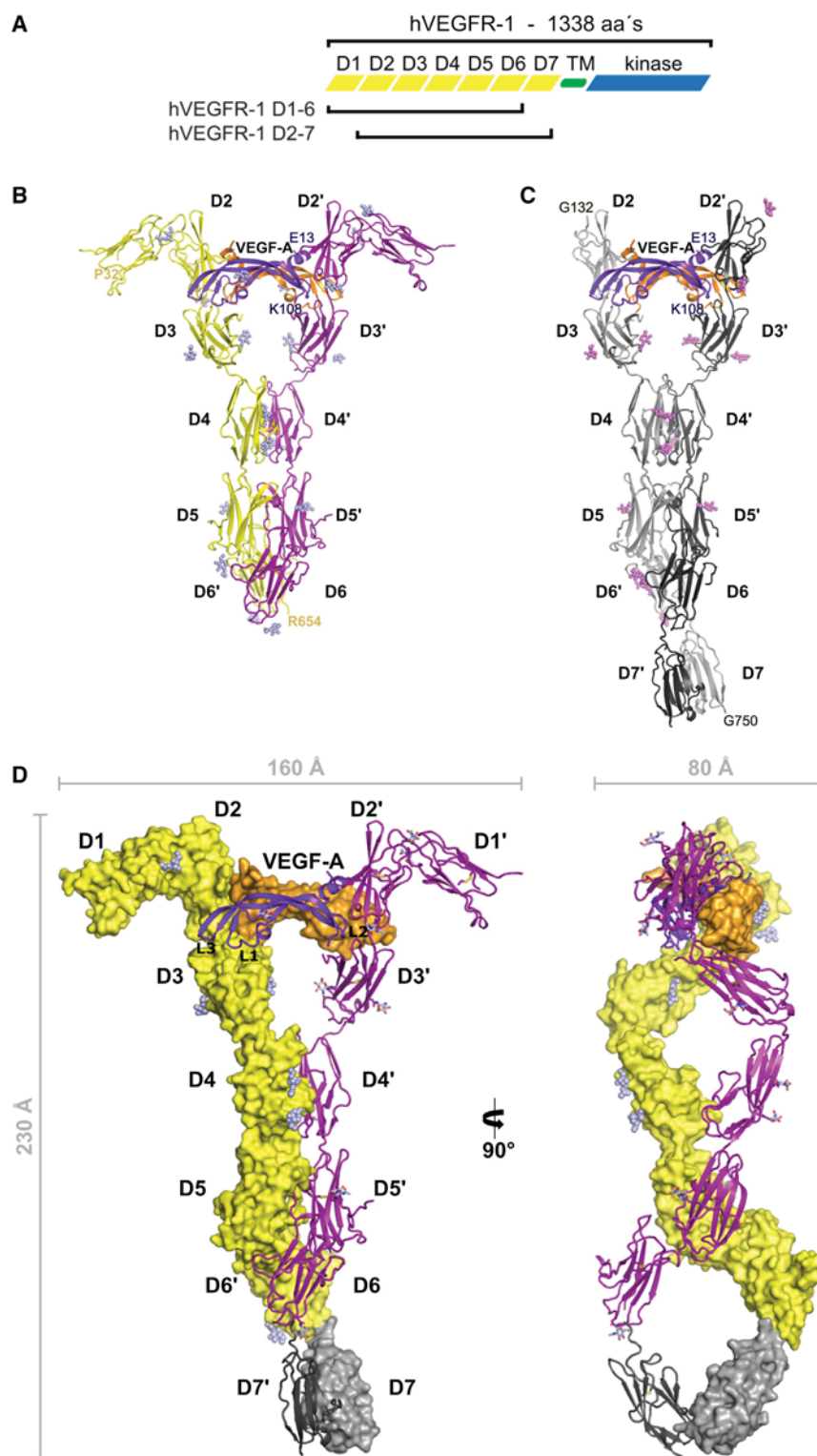
to validate our final model of the VEGFR-1 D1–6/VEGF-A complex (Figure 2). With weakly diffracting crystals, careful data collection was crucial to obtain the accuracy necessary for resolution of the small anomalous signals. Despite the crystals diffracting only to 4 Å resolution, more than half of all anomalous scatterers, including every disulfide bridge in the Ig domains and the VEGF-A ligand, as well as several methionines were assigned in the anomalous difference Fourier maps, verifying subunit placement as well as sequence assignment (Figure 2B). In addition, positive electron density present in the $F_o - F_c$ maps for N-linked glycans around the asparagine residues predicted to be glycosylated further aided in exact sequence assignment.

To complete the molecular structure of the VEGFR-1 ECD, we also used crystals of the VEGFR-1 D2–7/VEGF-A complex diffracting to 4.8 Å. The D1–6 complex structure was used as a search model for molecular replacement of the D2–7/VEGF-A complex (Figure 1C). To create a composite model of the D1–7/VEGF-A complex, we superimposed the two structures, D1–6/VEGF-A and D2–7/VEGF-A (root-mean-square deviation [RMSD] of 1.76 Å for 1,128 residues of the D2–6 region) and connected the D7 portion of the D2–7/VEGF-A model with the D1–6/VEGF-A-based model (Figure 1D).

Overall Architecture of the VEGFR-1 ECD/VEGF-A Complex

The structures of the D1–6 and the D2–7 VEGF-A complexes both show 2:2 stoichiometry and contain two sets of 1:1 complexes in the asymmetric unit related by 2-fold non-crystallographic symmetry (NCS). In the composite model of the VEGFR-1 ECD/VEGF-A complex (Figure 1D), two receptor chains are bridged with the dimeric VEGF-A ligand in the D2–3 region and related by 2-fold symmetry throughout the long axis of the complex. The complex has overall dimensions of ~ 160 Å \times ~ 230 Å \times ~ 80 Å and is characterized by the existence of three cavities: the upper one formed between the VEGF-A dimer D3 and D4 domains of two receptor chains (dimensions ~ 65 Å \times ~ 50 Å); the middle one between the D4 and D5 domains (~ 30 Å \times ~ 15 Å); and the lower one between the D5, D6, and D7 domains (~ 55 Å \times ~ 50 Å). VEGF-A binding to D2 and D3 induces a twisted arrangement between these two domains, with a bending angle of $\sim 135^\circ$. This is followed by intertwining of receptor chains in D4–5 bringing two protomers in close proximity to each other. The twist angle between D4 and D5 within the same chain is 60° . Additional homotypic contacts are observed between D7 domains. In our model the D7 dimer deviates from the D1–6/VEGF-A 2-fold axis, which is a consequence of crystal packing of the D2–7/VEGF-A complex. This finding suggests flexibility in the D6–7 region due to a longer linker between these two domains.

To confirm the overall structure of the VEGFR-1 ECD/VEGF-A complex, we additionally visualized the complex by negative stain electron microscopy (Figure 3A). The calculated class averages showed excellent agreement with projections of the crystal structure (Figure 3B). All class averages show dimeric VEGFR-1 ECD chains bridged by VEGF-A. Interestingly, a slight bend is observed in the membrane-proximal region, confirming the kinked D6–7 region seen in the D2–7/VEGF-A crystal structure. As there is a clear preference for the complex to adsorb to the grid showing the front view, only one class was generated of the side view.



Structure and Glycosylation of Individual Ig Domains

This is the largest structure determined so far in the VEGF receptor family and allows us to describe the structure and arrangement of the individual Ig domains of VEGFR-1. With the exception of D6, all Ig domains of VEGFR-1 belong to the I

Figure 1. Structure of the VEGFR-1 Extracellular Domain in Complex with VEGF-A

(A) Schematic overview of the domain organization of VEGFR-1. Crystallized constructs are indicated. Cartoon representation of the VEGFR-1 D1-6/VEGF-A complex (B) and of the VEGFR-1 D2-7/VEGF-A complex (C) structures. The chains of the VEGF-A homodimer are shown in purple and orange, the two chains of VEGFR-1 D1-6 in yellow and magenta, and the VEGFR-1 D2-7 chains in light and dark gray. N-linked glycans are depicted as spheres. The N- and C-terminal residues of VEGF-A, and VEGFR-1 D1-6 and D2-7, respectively, visualized in the two structures are indicated.

(D) Composite model of the VEGFR-1 ECD/VEGF-A complex. One half of the complex is represented as surface with N-linked glycans depicted as spheres and the other half as a cartoon with N-linked glycans depicted as sticks. The D7 homodimer shown in gray was positioned by superimposing VEGFR-1 D2-7/VEGF-A onto VEGFR-1 D1-6/VEGF-A. The dimensions of the complex and the axis of rotation relating the two views are also shown.

set of the Ig domain superfamily. D1 (residues 32–130) was modeled by Foldit players and subsequently rebuilt during refinement. Although the experimental electron density map suggested large disordered regions, the $2F_o - F_c$ maps allowed us to build all residues except the D-E loop (residues 78–84), which was disordered. Additional electron density around N100 confirmed the presence of an N-linked glycan, and the position of a disulfide bridge between C53 and C107 was validated by sulfur-SAD experiments. The structure of D2 (residues 132–225) was solved before (Wiesmann et al., 1997), and our structure additionally shows N-glycosylation of N164 and N196. D1 is bent away by $\sim 80^\circ$ from D2 and has no contact with the ligand. The bent conformations of the D1–2 modules of VEGFR-1 and VEGFR-3 (Leppänen et al., 2013) are very similar and can be aligned with an RMSD of 1.66 Å for 161 residues (Figure S4). D3 (residues 226–330) is an elongated Ig domain with N-glycosylation of N251 and N323. D4 (residues 333–426) is a smaller Ig domain not disulfide bridged between the β sheets and lacking β strand 4. D4 is glycosylated at N402 and N417. D5 (residues 428–554) is the largest Ig domain in VEGF receptors due to a long C-D loop that connects two β sheets. Residues 474–486 within this region were disordered and therefore omitted from the final model. In D5, we observed N-glycosylation of N547 and verified the positions of the disulfide bridge between

Table 1. Data Collection and Refinement Statistics

	VEGFR-1 D1-6/VEGF-A			VEGFR-1 D2-7/VEGF-A
Data Collection				
Crystal	Native	Iodide-SAD	Sulfur-SAD	Native
Wavelength (Å)	1	1.6	2.066	1
Space group	C2	C2	C2	C2
Unit cell				
a, b, c (Å)	166.7, 123.1, 167.4	166.7, 125.1, 167.9	166.6, 125.0, 168.3	163.5, 121.5, 141.6
α , β , γ (°)	90.0, 109.6, 90.0	90.0, 109.6, 90.0	90.0, 109.4, 90.0	90.0, 90.02, 90.0
Resolution (Å)	50–4.0 (4.14–4.0)	50–4.1 (4.21–4.1)	50–4.0 (4.11–4.0)	50–4.8 (4.972–4.8)
R _{meas} (%)	19.5 (194.7)	18.8 (221.6)	16.8 (277.4)	11.3 (190.4)
CC _{1/2}	0.998 (0.607)	1 (0.749)	1 (0.695)	0.999 (0.755)
I/ σ I	9.53 (1.28)	16.35 (1.76)	23.72 (1.50)	10.57 (1.15)
Completeness (%)	99.6 (99.4)	99.8 (99.9)	99.5 (95.9)	99.8 (99.85)
Redundancy	6.9 (7.1)	27.9/24.5	60.2 (26.7)	6.9 (6.8)
Refinement				
Resolution (Å)	20–4.0			20–4.8
No. of reflections	26,740			13,416
R _{work} /R _{free}	28.5/31.5			34.5/38.2
No. of atoms	11,400			11,106
Protein	11,078			10,882
Glycan	322			224
Water	–			–
B Factors				
Protein	182.5			301.8
Glycan	236.2			301.2
Water	–			–
RMSDs				
Bond lengths (Å)	0.004			0.004
Bond angles (°)	0.71			1.02

Only one crystal was used to obtain each of the above datasets. Values in parentheses are for the highest resolution shell.

C454 and C535 and of all methionines by S-SAD (Figure 2). With our data, we obtained for the first time structural information on D6 of VEGF receptors, which belongs to the C2 set of Ig domains. D6 (residues 555–654) contains strands of intermediate length in both β sheets, a disulfide bridge between C577 and C636, and an N-linked glycan at N625. D7 (residues 661–750) was modeled using D7 of VEGFR-2 (PDB: 3KVQ) as a template. Due to the low resolution of the VEGFR-1 D2–7 complex dataset, we do not further discuss its structural details. However, D7 of the two protomers form a dimeric arrangement as described in the crystal structure of isolated VEGFR-2 D7 (Yang et al., 2010).

VEGF-A Interacts with D2 and D3 of VEGFR-1

Ligand binding to VEGFR-1 takes place in Ig domains 2 and 3. With our structure, we can now describe the complete ligand binding site of VEGFR-1, while earlier published VEGFR-1 complex structures contained only D2 (Christinger et al., 2004; Iyer et al., 2010; Wiesmann et al., 1997). In the VEGFR-1 D1–6/VEGF-A model, residues 13–108 of VEGF-A₁₂₁ are visible in the electron density. Each receptor chain interacts with both

VEGF-A protomers (Figure 4A). The surface buried on one receptor chain by the bound VEGF-A dimer is $\sim 1,500 \text{ \AA}^2$, with D2 and D3 contributing similar interface areas ($\sim 800 \text{ \AA}^2$ for D2 versus $\sim 700 \text{ \AA}^2$ for D3). VEGF-A residues interacting with D2 are part of the N-terminal helix $\alpha 1$ of the ligand protomer A (M17, F18, Y21, Q22, and Y25) and of strands $\beta 2$ (I46, K48), $\beta 4$ (Q79, M81, I83), and $\beta 5$ (Q89, I91) of protomer B (Figure 4B). While the interface between ligand and D2 is largely hydrophobic, the contacts with D3 are hydrophilic, comprising a number of possible ionic interactions. There is an overall positive charge of the D3 region that comes in contact with the ligand. We identified several charged residues from all three loops (L1, L2, and L3) of VEGF-A interacting with D3. The most prominent conserved residue is E64 in L2 that engages five charged residues located in D3 of the receptor (N259, R261, R280, Q284, and N290) in hydrogen-bond- and salt-bridge-type interactions. Another residue from L2, D63, forms salt bridges with R224 located in the D2–3 linker (Figure 4C). In addition, E44 in L1 and K84 in L3 form hydrogen bonds with Q263 of D3. Loops 1 and 3 also carry hydrophobic residues such as P40, I43, and P85 that form a complementary surface with D3 of VEGFR-1. I43 protrudes

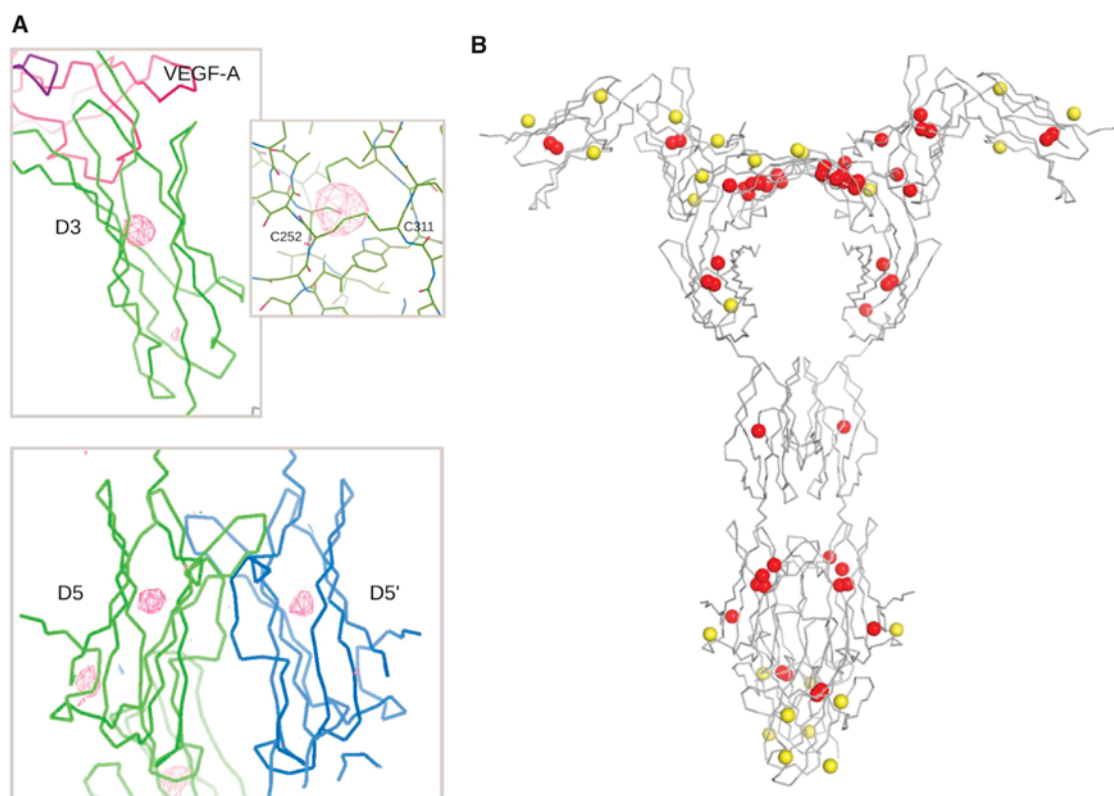


Figure 2. Native-SAD as Validation Tool

(A) Ribbon representation of VEGFR-1 D3 (upper panel) and VEGFR-1 D5 dimer (lower panel) with sulfur peaks detected in anomalous difference Fourier maps. The map is contoured to 4σ .

(B) Ribbon representation of the VEGFR-1 D1-6/VEGF-A complex structure with 86 sulfur atoms presented as spheres. Fifty-one sulfur atoms (60%) colored in red were detected at 3σ in anomalous difference Fourier maps. The sulfur atoms colored in yellow belong mostly to methionines and were not detected.

into the hydrophobic pocket on the D3 surface formed by V262, M264, V278, and F292. Due to the low resolution of our structure, some of the above described interactions remain tentative.

Structural comparison of receptor binding epitopes for the VEGFR-1 ligands VEGF-A, PIGF, and VEGF-B shows that all three ligands interact similarly with the D2 of VEGFR-1 (Figure S5). The interaction between the loop L2 of the three ligands with D3 is also very similar since D63 of VEGF-A is strictly conserved and E64 is conserved in PIGF and substituted by aspartate in VEGF-B. Differences are observed in the way the three ligands interact through the loops L1 and L3 with D3 of VEGFR-1. While the sequence and structure conservation in these regions is high between VEGF-A and PIGF, this is not the case for VEGF-B. Superposition of the VEGFR-1 D2/VEGF-B complex onto our structure tentatively reveals the structural arrangement of loops L1 and L3 of VEGF-B in relation to receptor domain D3. These loops are moved away from D3 and are not involved in any receptor/ligand interactions in agreement with a recent study (Anisimov et al., 2013) showing that VEGF-B does not require D3 for high-affinity binding. Anisimov et al. also showed that VEGF-B does not promote signaling downstream of VEGFR-1. PIGF and VEGF-A, on the other hand, are angiogenic ligands, and the interaction of L1 with D3 is important for receptor activation.

VEGFR-1 D4 and D5 Form Homotypic Interactions in the Presence of Ligand

The structure of the VEGFR-1 D1-6/VEGF-A complex reveals homotypic interactions in D4 and D5, covering altogether a solvent-accessible area of $\sim 1,073 \text{ \AA}^2$ per chain (Figures 5A and 5B). The interface between Ig domain 4 is small ($\sim 201 \text{ \AA}^2$ per chain) and includes several residues that may take part in hydrogen-bond interactions. R351 in the A-B loop interacts with K379 from the C-E loop, and K393 of the C-E loop could be positioned to interact with the backbone of either S380 or A381 of the adjacent C-E loop (Figure 5C). Determining which interaction is more likely is difficult at the resolution of our dataset. The interactions between the residues in the E-F loop proposed earlier based on a KIT ECD structure (Yuzawa et al., 2007) and the VEGFR-2 D7 structure (Yang et al., 2010) are not visible in our data.

The homotypic contacts in D5 are, like in VEGFR-3, centered on the fully conserved residues T455 (β strand B) and K517 (β strand E) that form hydrogen bonds with the backbone atoms of S436 and A434 of the other chain (Figure 5C). Furthermore, a glutamate residue in the D-E loop (E513) conserved in all VEGFRs interacts via hydrogen bond with Q429 and via a salt bridge with K433 of the other chain. While the fully conserved residues are part of the rigid β sheet, their interacting partners

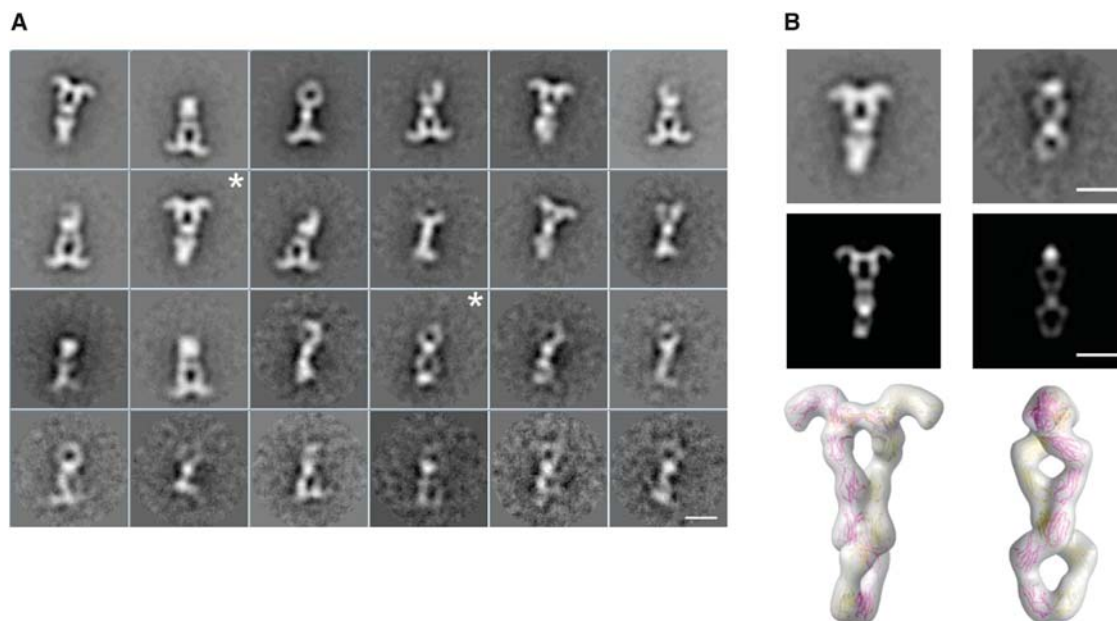


Figure 3. Negative -Staining EM Analysis of the VEGFR-1 D1-7/VEGF-A Complex

(A) A gallery of 24 2D class averages from image classification is shown.

(B) Comparison of the VEGFR-1 D1-7/VEGF-A EM class averages with the composite model shown in Figure 1. Representative class averages (labeled with a star in [A]) are compared with selected 2D projections and with the corresponding 3D volume models of the VEGFR-1 D1-7/VEGF-A complex. The volumes were filtered at 25 Å resolution. The class average in (B) was rotated by $\sim 180^\circ$ relative to its orientation in (A). Scale bars represent 10 nm.

are not conserved and belong to the flexible strands A and A' and the helical protrusion between them.

Homotypic Contacts in D4-7 Increase Ligand Binding and Are Essential for Receptor Activation

The purified receptor ECD was monomeric, indicating that the homotypic interactions in D4-7 are weak and apparently depend on ligand-mediated receptor dimerization (Figure S1). We used isothermal titration calorimetry to assess the contribution of the membrane-proximal Ig domains 4-7 to the binding affinity of the full-length ECD of VEGFR-1 for VEGF-A. Similar to VEGFR-3 (Leppänen et al., 2013), D1-7 of VEGFR-1 had significantly higher affinity for the ligand than D1-3 (Figure 6A). The binding affinity of VEGFR-1 D1-7 for VEGF-A was in the low nanomolar range (~ 2 nM) while the affinity of VEGF-A for VEGFR-1 D1-3 was 20 times lower (i.e., ~ 50 nM). Binding of VEGF-A to D1-3 was entropically favored while binding to D1-7 was enthalpically driven (Figure 6B). Thus, the presence of Ig domains 4-7 increased binding affinity for VEGF-A, presumably due to stabilization through homotypic receptor-receptor contacts in D4-7.

Based on the structural data described here and in our earlier work (Leppänen et al., 2010, 2013; Brozzo et al., 2012; Ruch et al., 2007; Kisko et al., 2011), we predicted that the contacts in D5 are essential for receptor function. We mutated the residues involved in the D5 interaction and determined receptor activity in transfected NIH3T3 cells. The activity of VEGFR-1 was too low to obtain high-quality biochemical data; therefore, we mutated the corresponding residues in D5 of VEGFR-2 based on a homology model of this domain (for details of the mutants used, see Figure 6D). In the mutant T446E/K512A, residue T446 was replaced by E and K512 by A, thus preventing

hydrogen-bond and salt-bridge formation in the dimeric receptor complex. This mutant showed drastically reduced ligand-induced receptor phosphorylation (Figure 6C). Taken together, these data show that the contacts in D5 revealed by our VEGFR-1 ECD/VEGF-A structure are essential for receptor activation.

DISCUSSION

We present here the first full-length VEGF receptor ECD structure in complex with one of its ligands, revealing all structural details of VEGF-A binding to VEGFR-1. Most importantly, our structure shows the structural details of the homotypic contacts in D4-7 in the context of the full-length receptor ECD. The functional analysis of these interactions proves their relevance for receptor activation. We propose that the exact positioning of ligand-bound receptor protomers in active dimers, which is essential for kinase activation, is mediated by the concerted interplay of receptor/ligand interactions in D2-3 and receptor-receptor interactions in D4, D5, and D7.

Receptor Binding Specificity of Distinct VEGF Ligands

Using chimeric receptor constructs, it was proposed earlier that D2 is responsible for the ligand specificity of VEGFRs (Davis-Smyth et al., 1996; Cursiefen et al., 2004; Holash et al., 2002). Structural and biochemical analysis also showed that D3 did not significantly increase affinity of VEGFR-1 ECD constructs toward VEGF-A (Wiesmann et al., 1997). Based on these earlier studies, interaction with D3 seems therefore not to increase the receptor binding affinity of VEGF. Our structure shows significant interaction of all three loops of VEGF with D3, suggesting

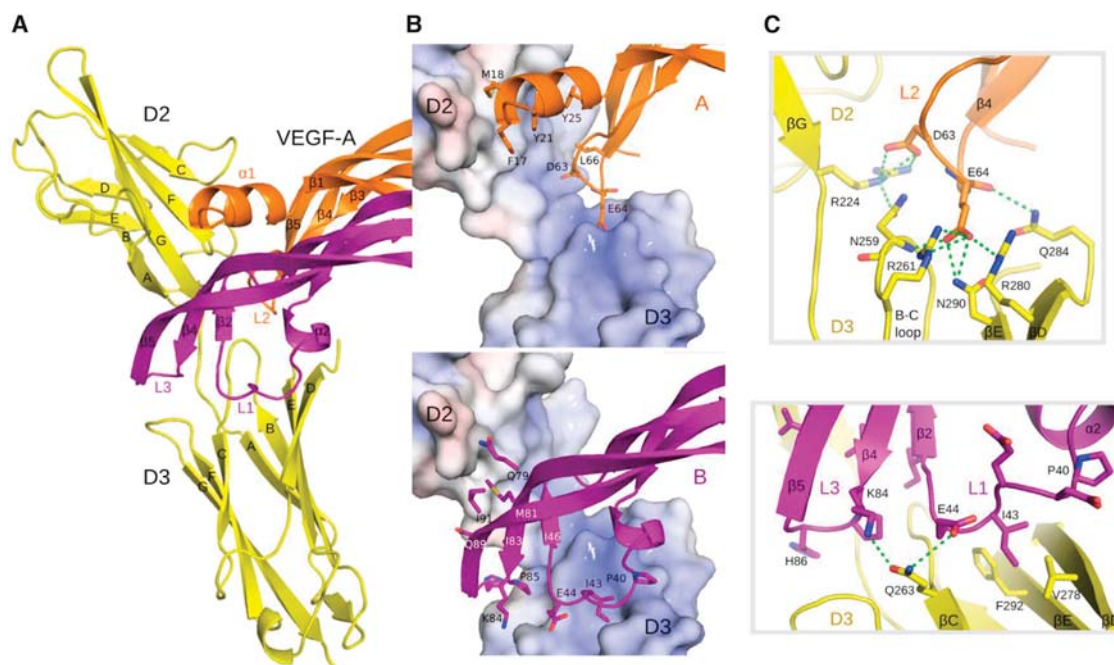


Figure 4. Binding Interface between VEGF-A and VEGFR-1 D2-3

(A) Cartoon representation of D2 and D3 of one receptor chain colored in yellow and VEGF-A chains in orange (chain A) and purple (chain B). Secondary structure elements are labeled. Three loops in VEGF-A are designated L1, L2, and L3.

(B) VEGFR-1 interaction with the VEGF-A monomer A including N-terminal helix $\alpha 1$ and loop 2 (upper panel) and with the VEGF-A monomer B including loops 1 and 3 (lower panel). The key residues of the ligand are highlighted as sticks and labeled. VEGFR-1 charge distribution at the interaction surface is presented as a surface potential model (calculated with the APBS module in PyMol).

(C) Interactions of charged residues in VEGF-A L2 (upper panel) and L1 and L3 (lower panel) with VEGFR-1 D3. Hydrogen bonds and salt bridges are shown as green dashed lines.

that, in the full-length receptor, both D2 and D3 are required for receptor signaling. D3/VEGF interaction apparently triggers receptor ECD intertwining, thus inducing homotypic interactions in D4-5 and D7, which are essential for receptor activation. We propose that the D3/VEGF interaction plays a role as a sensor for modification of homotypic interactions in D4-7 depending on the strength of the induced twist between D2 and D3. This might ultimately lead to different functional output by distinct VEGF ligands. With the structure of the VEGFR-1 ECD/VEGF-A complex and the comparison of receptor binding epitopes in VEGF-A, PlGF, and VEGF-B, we provide a structural basis for understanding the different signal outputs generated by these three VEGFR-1 ligands (Figure S5).

The next question that arises is why do VEGF-C, -D, and -E not bind to VEGFR-1? Sequence conservation between different VEGF family members varies in the three binding loops. While the residues in loop L2 are highly conserved within the VEGF family, there are significant sequence and structural differences in the N-terminal helix $\alpha 1$ and in loops L1 and L3, which presumably define receptor specificity of the ligands. The interactions between residues E44 in L1 and K84 in L3 of VEGF-A with D3 of VEGFR-1 are not conserved in VEGF-C, -D, and -E (Figure S6), and may thus determine receptor specificity.

Structural comparison of VEGF-A binding to VEGFR-1, as described here, with binding to VEGFR-2 (PDB: 3V2A) shows similar types of interactions. The ligands in the two structures have very similar structures and can be aligned with an RMSD

of 0.86 Å for 190 aligned residues. The difference exists in the orientation of D3 toward D2, where VEGF-A binding to VEGFR-1 induces a stronger twist by 11° between D2 and D3 (Figure S4). With the exception of E64 in VEGFR-1, which engages more residues in salt-bridge- and hydrogen-bond-type interactions, loop L2 interacts similarly with D3 of VEGFR-1 or VEGFR-2.

To fully understand the differences in the signaling output by VEGFRs upon binding to a particular VEGF ligand, one needs to consider also the role of co-receptors. Distinct ligands promote ternary complex formation, which has an impact on receptor trafficking and signaling (Ballmer-Hofer et al., 2011).

Role of Homotypic Receptor Contacts in VEGFR Activation

Our structural analysis describes for the first time the details of homotypic contacts in the membrane-proximal domain of type V RTKs in the context of a full-length ligand-bound receptor ECD. In addition, we show that mutation of the interacting interface attenuates receptor activity. This is in agreement with earlier findings showing that homotypic contacts in D4-7 are indispensable for activation of VEGFR-3 (Leppänen et al., 2013) and VEGFR-2 (Yang et al., 2010), and documents the strong similarity with type III RTKs such as PDGFR (Yang et al., 2008) and KIT (Yuzawa et al., 2007; Reshetnyak et al., 2015; Yang et al., 2010). Mutation of the interface of the homotypic contacts renders KIT oncogenic (Reshetnyak et al., 2015) and

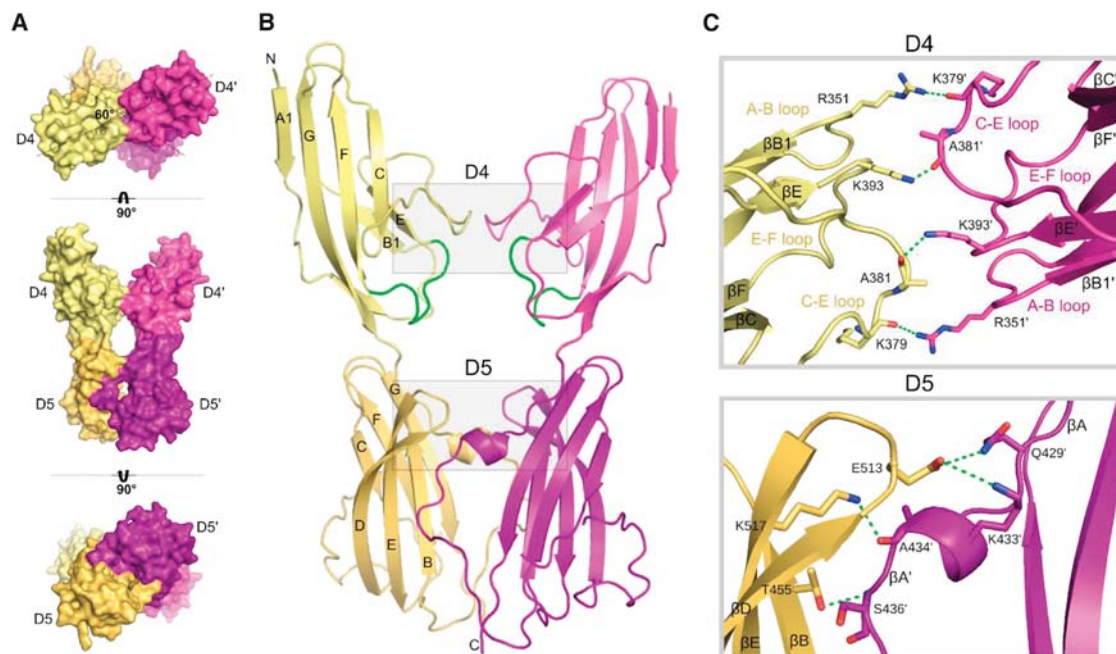


Figure 5. Homotypic Interactions between Ig domains 4 and 5 of VEGFR-1

(A) Surface representation of the D4–5 dimer. D4 on two chains are colored in pale yellow and light magenta and D5 is shown in yellow-orange and purple. The rotation axis relating the views is shown. The twist angle between D4 and D5 within the same chain is 60°.

(B) Cartoon representation of the D4–5 dimer with labeled β strands. The E-F loop in D4 is colored in green, illustrating that residues that are part of this loop in VEGFR-1 do not interact.

(C) Zoom-in view into the interface of D4 (top) and D5 (bottom). Interacting residues are shown as sticks and hydrogen bonds and salt bridges as green dashed lines.

promotes ligand-independent kinase activation. In agreement with this, we showed earlier that antibody-like molecules such as DARPin (Stumpp et al., 2008; Binz et al., 2004) binding D4 or D7 of VEGFR-2 block receptor signaling (Hyde et al., 2012). Ligand-induced homotypic ectodomain contacts in the membrane-proximal domain are thus required for tight control of type III and V receptors. A detailed comparison of type III and V receptor ECD structures and possible implications for the mechanism of receptor activation was published recently by Verstraete et al. (2011).

Receptor-receptor interactions in D4 revealed in this work are in agreement with earlier studies on VEGFR-1 (Barleon et al., 1997) and VEGFR-2 (Shinkai et al., 1998) that pointed at the importance of this domain in ligand-induced receptor dimerization. Similar interactions were, on the other hand, not observed in the VEGFR-3 D4–5 structure (Leppänen et al., 2013). Since the D4 interactions in VEGFR-1 occur through the C-E loop, which is longer in this receptor compared with the other homologs, they might only be relevant for VEGFR-1 functionality. In our structure, we did not observe the previously proposed D4 interactions between residues in the E-F loop of KIT (Yuzawa et al., 2007).

Homotypic interactions in D5 have interesting structural characteristics, with one interacting side composed of a rigid β sheet (β strands B, D, and E) and the other side being more flexible (strands A and A'; Figure 5C). The flexible strands A and A' are directly linked to D4, suggesting an order of homotypic contact formation following ligand binding (i.e., formation of interactions in D4 will be transmitted downstream to D5). This may also

explain heterodimer formation giving rise to VEGFR-1/VEGFR-2 (Cudmore et al., 2012) and VEGFR-2/VEGFR-3 (Harris et al., 2013) ligand complexes, where one interacting face is rigid and fully conserved and the other more flexible, allowing for differential bond formation.

Here, we show detailed structural information for the isolated ECD of VEGFR-1 in complex with ligand. In cells, however, the receptor ECD is membrane bound and separated from the transmembrane domain (TMD) via a short linker. We showed earlier that a distinct conformation of the TMD is required for VEGFR activation (Manni et al., 2014; Dell'Era Dosch and Ballmer-Hofer, 2010). It is therefore likely that the conformation of the most membrane-proximal D7 domain and the linker separating it from the TMD is affected by the presence of the TMD. In other words, the exact structure of D7 in a ligand-bound, membrane-associated receptor might differ from the structure determined for the soluble ECD described here. So far, only low-resolution single-particle electron microscopy structures are available for such membrane-proximal domains in the epidermal growth factor receptor (Mi et al., 2008) and KIT (Opatowsky et al., 2014), respectively. We propose that the D7 interactions initially observed in VEGFR-2 (Yang et al., 2010; Ruch et al., 2007), and now confirmed for VEGFR-1, represent a checkpoint during formation of active receptor dimers. The restriction of mobility toward the TMD imposed by homotypic contacts in D5 and D7 may be responsible for stringent control of VEGFR activation.

Taken together, the availability of the structural details of the full-length VEGFR-1 ECD in complex with VEGF-A presented

determined by MR-SAD, as implemented in the program suite PHASER (McCoy et al., 2007). The partial molecular replacement solution obtained using the structure of the VEGFR-1 D2/VEGF-A complex (PDB: 1QTY) as a search model allowed for the identification of heavy atom sites and substructure completion. Initial phases were improved by solvent flattening and extended to 4 Å by 2-fold non-crystallographic symmetry averaging with the program DM (Cowtan et al., 2012). The missing Ig-homology domains were positioned by phased molecular replacement in MOLREP (Vagin and Teplyaev, 2010) using the following structures as search models in the following order: for D4 VEGFR-3 D4 (PDB: 4BSJ), for D5 VEGFR-3 D5 (PDB: 4BSJ), and for D3 VEGFR-2 D3 (PDB: 2X1X). To construct a model with the full VEGFR-1 sequence, we created homology models for the Ig domains D3-D5 using the corresponding MR search models as templates in SWISS-MODEL (Biasini et al., 2014). The homology models were superimposed onto the domains positioned by molecular replacement and single Ig domains were connected generating the VEGFR-1 D2-D5/VEGF-A model.

We first attempted to fit D1 and D6 using homology models as well, but the resulting models had a poor fit without clear difference density to guide model building. To overcome this, D1 and D6 were submitted to the Foldit structure prediction game (Cooper et al., 2010). Players were provided a set of five starting models from I-TASSER (Zhang, 2008). Players then modified the structure to minimize the Rosetta energy function; 339 and 443 players participated in the D1 and D6 puzzles, respectively, over a 2-week period. A very diverse set of models was generated, which were clustered to within 2 Å RMSD. The 1,000 top-scoring models were then used for molecular replacement with PHASER. A candidate model was chosen with high log likelihood gain and translational function Z score for further manual refinement (Figure S2). The D6 and D1 models were added sequentially to the VEGFR-1 D2-D5/VEGF-A model, followed by manual rebuilding in COOT (Emsley and Cowtan, 2004) and refinement in PHENIX (Adams et al., 2002) as for the homology models. NCS, secondary structure, and reference structure restraints were applied throughout the refinement process. For the final refined structure, Ramachandran values were 83.6% favored, 13.8% allowed, and 2.6% outlier.

The structure of the VEGFR-1 D2-7/VEGF-A complex was determined to 4.8-Å resolution by molecular replacement in PHASER using the D2-6 part of the VEGFR-1 D1-6/VEGF-A structure and the structure of the VEGFR-2 D7 dimer (PDB: 3KVQ) as search models. The structure was improved by rigid-body refinement in PHENIX. A composite model of the full-length VEGFR-1 ECD/VEGF-A complex was constructed in COOT by secondary structure match superposition of the D1-6 and D2-7 structures (RMSD of 1.76 Å for 1,128 residues of the D2-6 region).

Native SAD Experiments

Highly redundant diffraction data were collected from a very large native crystal (700 μm) of the VEGFR-1 D1-6/VEGF-A complex at an X-ray energy of 6 keV (2.0663 Å wavelength) applying a recently described method (Weinert et al., 2015). Individual datasets of 360° were measured from multiple positions and orientations of the crystal giving 4,320° in total with the anomalous signal extending to 4.5 Å. The final VEGFR-1 D1-6/VEGF-A model was refined against these long-wavelength data in PHENIX, which allowed for calculation of anomalous difference Fourier maps for sulfur. The anomalous peaks around all disulfide bridges in Ig domains and in the VEGF ligand and additionally around several methionine sulfurs confirmed the accuracy of the model.

ACCESSION NUMBERS

The VEGFR-1 D1-6/VEGF-A structure has been deposited in the PDB: 5T89.

SUPPLEMENTAL INFORMATION

Supplemental Information includes Supplemental Experimental Procedures, six figures, and one PDB file and can be found with this article online at <http://dx.doi.org/10.1016/j.str.2016.12.012>.

AUTHOR CONTRIBUTIONS

E.S. and S.M.M. produced, purified and crystallized proteins, performed electron microscopic and crystallographic experiments, and wrote the manuscript.

M.A. performed the biochemical analysis of receptor mutants. E.S. and K.K. performed SAXS experiments. T.W. assisted in diffraction data acquisition, structure phasing, and validation. S.B. initiated and analyzed the Foldit molecular modeling and contributed to structure refinement. K.N.G. assisted in electron microscopy data acquisition and analysis. G.C. was involved in structure refinement and manuscript preparation. K.B.-H. conceived and planned the experiments and wrote the manuscript.

ACKNOWLEDGMENTS

K.B.-H. thanks the Swiss National Science Foundation (grant 31003A-130463) and Oncosuisse (grant OC2 01200-08-2007) for continuous support of his research. S.B. was supported by the Intramural Research Program of the NCBI, National Library of Medicine, and NIH (United States). We are also grateful to Thomas Schleier, Kate Thielges, and Julia Kostin for technical assistance and the staff of the X06SA and X06DA beamlines of the Swiss Light Source for their support during data collection. We thank the Foldit players and Firas Khatib for modeling D1 and D6 (<https://fold.it/portal/info/credits>).

Received: September 11, 2016

Revised: November 14, 2016

Accepted: December 21, 2016

Published: January 19, 2017

REFERENCES

- Adams, P.D., Grosse-Kunstleve, R.W., Hung, L.W., Ioerger, T.R., McCoy, A.J., Moriarty, N.W., Read, R.J., Sacchettini, J.C., Sauter, N.K., and Terwilliger, T.C. (2002). PHENIX: building new software for automated crystallographic structure determination. *Acta Crystallogr. D. Biol. Crystallogr.* **58**, 1948–1954.
- Ambati, B.K., Nozaki, M., Singh, N., Takeda, A., Jani, P.D., Suthar, T., Albuquerque, R.J., Richter, E., Sakurai, E., Newcomb, M.T., et al. (2006). Corneal avascularity is due to soluble VEGF receptor-1. *Nature* **443**, 993–997.
- Anisimov, A., Leppänen, V.M., Tvorogov, D., Zarkada, G., Jeltsch, M., Holopainen, T., Kajjalainen, S., and Alitalo, K. (2013). The basis for the distinct biological activities of vascular endothelial growth factor receptor-1 ligands. *Sci. Signal.* **6**, ra52.
- Ballmer-Hofer, K., Andersson, A.E., Ratcliffe, L.E., and Berger, P. (2011). Neuropilin-1 promotes VEGFR-2 trafficking through Rab11 vesicles thereby specifying signal output. *Blood* **118**, 816–826.
- Barleon, B., Totzke, F., Herzog, C., Blanke, S., Kremmer, E., Siemeister, G., Marmé, D., and Martiny-Baron, G. (1997). Mapping of the sites for ligand binding and receptor dimerization at the extracellular domain of the vascular endothelial growth factor receptor FLT-1. *J. Biol. Chem.* **272**, 10382–10388.
- Biasini, M., Bienert, S., Waterhouse, A., Arnold, K., Studer, G., Schmidt, T., Kiefer, F., Cassarino, T.G., Bertoni, M., Bordoli, L., et al. (2014). SWISS-MODEL: modelling protein tertiary and quaternary structure using evolutionary information. *Nucleic Acids Res.* **42**, W252–W258.
- Binz, H.K., Amstutz, P., Kohl, A., Stumpp, M.T., Briand, C., Forrer, P., Grutter, M.G., and Pluckthun, A. (2004). High-affinity binders selected from designed ankyrin repeat protein libraries. *Nat. Biotechnol.* **22**, 575–582.
- Brozzo, M.S., Bjelic, S., Kisko, K., Schleier, T., Leppänen, V.M., Alitalo, K., Winkler, F.K., and Ballmer-Hofer, K. (2012). Thermodynamic and structural description of allosterically regulated VEGF receptor 2 dimerization. *Blood* **119**, 1781–1788.
- Christinger, H.W., Fuh, G., de Vos, A.M., and Wiesmann, C. (2004). The crystal structure of PIGF in complex with domain 2 of VEGFR1. *J. Biol. Chem.* **279**, 10382–10388.
- Collaborative Computational Project, Number 4 (1994). The CCP4 suite: programs for protein crystallography. *Acta Crystallogr. D. Biol. Crystallogr.* **50**, 760–763.
- Cooper, S., Khatib, F., Treuille, A., Barbero, J., Lee, J., Beenen, M., Leaver-Fay, A., Baker, D., Popovic, Z., and Players, F. (2010). Predicting protein structures with a multiplayer online game. *Nature* **466**, 756–760.
- Cowtan, K., Zhang, K., and Main, P. (2012). Crystallography of biological macromolecules. In *International Tables for Crystallography Volume F*, E. Arnold,

- D.M. Himmel, and M.G. Rossmann, eds. (International Union of Crystallography), pp. 385–400.
- Cudmore, M.J., Hewett, P.W., Ahmad, S., Wang, K.Q., Cai, M., Al-Ani, B., Fujisawa, T., Ma, B., Sissaoui, S., Ramma, W., et al. (2012). The role of heterodimerization between VEGFR-1 and VEGFR-2 in the regulation of endothelial cell homeostasis. *Nat. Commun.* **3**, 972.
- Cursiefen, C., Chen, L., Borges, L.P., Jackson, D., Cao, J., Radziejewski, C., D'Amore, P.A., Dana, M.R., Wiegand, S.J., and Streilein, J.W. (2004). VEGF-A stimulates lymphangiogenesis and hemangiogenesis in inflammatory neovascularization via macrophage recruitment. *J. Clin. Invest.* **113**, 1040–1050.
- Davis-Smyth, T., Chen, H., Park, J., Presta, L.G., and Ferrara, N. (1996). The second immunoglobulin-like domain of the VEGF tyrosine kinase receptor Flt-1 determines ligand binding and may initiate a signal transduction cascade. *EMBO J.* **15**, 4919–4927.
- Dell'Era Dosch, D., and Ballmer-Hofer, K. (2010). Transmembrane domain-mediated orientation of receptor monomers in active VEGFR-2 dimers. *FASEB J.* **24**, 32–38.
- Emsley, P., and Cowtan, K. (2004). Coot: model-building tools for molecular graphics. *Acta Crystallogr. D. Biol. Crystallogr.* **60**, 2126–2132.
- Fong, G.H., Rossant, J., Gertsenstein, M., and Breitman, M.L. (1995). Role of the Flt-1 receptor tyrosine kinase in regulating the assembly of vascular endothelium. *Nature* **376**, 66–70.
- Harris, N.C., Davydova, N., Roufail, S., Paquet-Fifield, S., Paavonen, K., Karnezis, T., Zhang, Y.F., Sato, T., Rothacker, J., Nice, E.C., et al. (2013). The propeptides of VEGF-D determine heparin binding, receptor heterodimerization and effects on tumor biology. *J. Biol. Chem.* **288**, 8176–8186.
- Hiratsuka, S., Minowa, O., Kuno, J., Noda, T., and Shibuya, M. (1998). Flt-1 lacking the tyrosine kinase domain is sufficient for normal development and angiogenesis in mice. *Proc. Natl. Acad. Sci. USA* **95**, 9349–9354.
- Hiratsuka, S., Maru, Y., Okada, A., Seiki, M., Noda, T., and Shibuya, M. (2001). Involvement of Flt-1 tyrosine kinase (vascular endothelial growth factor receptor-1) in pathological angiogenesis. *Cancer Res.* **61**, 1207–1213.
- Holash, J., Davis, S., Papadopoulos, N., Croll, S.D., Ho, L., Russell, M., Boland, P., Leidich, R., Hylton, D., Burova, E., et al. (2002). VEGF-Trap: a VEGF blocker with potent antitumor effects. *Proc. Natl. Acad. Sci. USA* **99**, 11393–11398.
- Hyde, C.A., Giese, A., Stutfeld, E., Abram, S.J., Villemagne, D., Schleier, T., Binz, H.K., and Ballmer-Hofer, K. (2012). Targeting the extracellular domains D4 and D7 of VEGFR-2 reveals allosteric receptor regulatory sites. *Mol. Cell Biol.* **32**, 3802–3813.
- Iyer, S., Darley, P.I., and Acharya, K.R. (2010). Structural insights into the binding of VEGF-B by VEGFR-1D2: recognition and specificity. *J. Biol. Chem.* **285**, 23779–23789.
- Kabsch, W. (1993). Automatic processing of rotation diffraction data from crystals of initially unknown symmetry and cell constants. *J. Appl. Crystallogr.* **26**, 795–800.
- Kendall, R.L., and Thomas, K.A. (1993). Inhibition of vascular endothelial cell growth factor activity by an endogenously encoded soluble receptor. *Proc. Natl. Acad. Sci. USA* **90**, 10705–10709.
- Kisko, K., Brozzo, M.S., Missimer, J., Schleier, T., Menzel, A., Leppänen, V.M., Alitalo, K., Walzthoeni, T., Aebersold, R., and Ballmer-Hofer, K. (2011). Structural analysis of vascular endothelial growth factor receptor-2/ligand complexes by small-angle X-ray solution scattering. *FASEB J.* **25**, 2980–2986.
- Lemmon, M.A., and Schlessinger, J. (2010). Cell signaling by receptor tyrosine kinases. *Cell* **141**, 1117–1134.
- Leppänen, V.M., Prota, A.E., Jeltsch, M., Anisimov, A., Kalkkinen, N., Strandin, T., Lankinen, H., Goldman, A., Ballmer-Hofer, K., and Alitalo, K. (2010). Structural determinants of growth factor binding and specificity by VEGF receptor 2. *Proc. Natl. Acad. Sci. USA* **107**, 2425–2430.
- Leppänen, V.M., Tvorogov, D., Kisko, K., Prota, A.E., Jeltsch, M., Anisimov, A., Markovic-Mueller, S., Stutfeld, E., Goldie, K.N., Ballmer-Hofer, K., et al. (2013). Structural and mechanistic insights into VEGF receptor 3 ligand binding and activation. *Proc. Natl. Acad. Sci. USA* **110**, 12960–12965.
- Luo, L., Uehara, H., Zhang, X., Das, S.K., Olsen, T., Holt, D., Simonis, J.M., Jackman, K., Singh, N., Miya, T.R., et al. (2013). Photoreceptor avascular privilege is shielded by soluble VEGF receptor-1. *Elife* **2**, e00324.
- Luttun, A., and Carmeliet, P. (2003). Soluble VEGF receptor Flt1: the elusive preeclampsia factor discovered? *J. Clin. Invest.* **111**, 600–602.
- Manni, S., Mineev, K.S., Usmanova, D., Lyukmanova, E.N., Shulepko, M.A., Kirpichnikov, M.P., Winter, J., Matkovic, M., Deupi, X., Arseniev, A.S., et al. (2014). Structural and functional characterization of alternative transmembrane domain conformations in VEGF receptor 2 activation. *Structure* **22**, 1077–1089.
- Massena, S., Christoffersson, G., Vagesjo, E., Seigneux, C., Gustafsson, K., Binet, F., Herrera, H.C., Giraud, A., Lomei, J., Westrom, S., et al. (2015). Identification and characterization of VEGF-A-responsive neutrophils expressing VEGFR1, CD49d and CXCR4 in mice and humans. *Blood* **126**, 2016–2026.
- Maynard, S.E., Min, J.Y., Merchan, J., Lim, K.H., Li, J., Mondal, S., Libermann, T.A., Morgan, J.P., Sellke, F.W., Stillman, I.E., et al. (2003). Excess placental soluble fms-like tyrosine kinase 1 (sFlt1) may contribute to endothelial dysfunction, hypertension, and proteinuria in preeclampsia. *J. Clin. Invest.* **111**, 649–658.
- McCoy, A.J., Grosse-Kunstleve, R.W., Adams, P.D., Winn, M.D., Storoni, L.C., and Read, R.J. (2007). Phaser crystallographic software. *J. Appl. Crystallogr.* **40**, 658–674.
- Mi, L.Z., Grey, M.J., Nishida, N., Walz, T., Lu, C., and Springer, T.A. (2008). Functional and structural stability of the epidermal growth factor receptor in detergent micelles and phospholipid nanodiscs. *Biochemistry* **47**, 10314–10323.
- Moens, S., Goveia, J., Stapor, P.C., Cantelmo, A.R., and Carmeliet, P. (2014). The multifaceted activity of VEGF in angiogenesis - implications for therapy responses. *Cytokine Growth Factor Rev.* **25**, 473–482.
- Opatowsky, Y., Lax, I., Tome, F., Bleichert, F., Unger, V.M., and Schlessinger, J. (2014). Structure, domain organization, and different conformational states of stem cell factor-induced intact KIT dimers. *Proc. Natl. Acad. Sci. USA* **111**, 1772–1777.
- Reshetnyak, A.V., Opatowsky, Y., Boggan, T.J., Folta-Stogniew, E., Tome, F., Lax, I., and Schlessinger, J. (2015). The strength and cooperativity of KIT ectodomain contacts determine normal ligand-dependent stimulation or oncogenic activation in cancer. *Mol. Cell* **57**, 191–201.
- Ruch, C., Skiniotis, G., Steinmetz, M.O., Walz, T., and Ballmer-Hofer, K. (2007). Structure of a VEGF-VEGF receptor complex determined by electron microscopy. *Nat. Struct. Mol. Biol.* **14**, 249–250.
- Schomber, T., Kopfstein, L., Djonov, V., Albrecht, I., Baeriswyl, V., Strittmatter, K., and Christofori, G. (2007). Placental growth factor-1 attenuates vascular endothelial growth factor-A-dependent tumor angiogenesis during beta cell carcinogenesis. *Cancer Res.* **67**, 10840–10848.
- Shalaby, F., Rossant, J., Yamaguchi, T.P., Gertsenstein, M., Wu, X.F., Breitman, M.L., and Schuh, A.C. (1995). Failure of blood-island formation and vasculogenesis in Flk-1-deficient mice. *Nature* **376**, 62–66.
- Shibuya, M. (2013). VEGFR and type-V RTK activation and signaling. *Cold Spring Harb. Perspect. Biol.* **5**, a009092.
- Shibuya, M. (2014). VEGF-VEGFR signals in health and disease. *Biomol. Ther.* **22**, 1–9.
- Shinkai, A., Ito, M., Anazawa, H., Yamaguchi, S., Shitara, K., and Shibuya, M. (1998). Mapping of the sites involved in ligand association and dissociation at the extracellular domain of the kinase insert domain-containing receptor for vascular endothelial growth factor. *J. Biol. Chem.* **273**, 31283–31288.
- Smith, G.A., Fearnley, G.W., Harrison, M.A., Tomlinson, D.C., Wheatcroft, S.B., and Ponnambalam, S. (2015). Vascular endothelial growth factors: multi-tasking functionality in metabolism, health and disease. *J. Inherit. Metab. Dis.* **38**, 753–763.
- Stumpp, M.T., Binz, H.K., and Amstutz, P. (2008). DARPin: a new generation of protein therapeutics. *Drug Discov. Today* **13**, 695–701.
- Vagin, A., and Teplyakov, A. (2010). Molecular replacement with MOLREP. *Acta Crystallogr. D. Biol. Crystallogr.* **66**, 22–25.

- Van de Veire, S., Stalmans, I., Heindryckx, F., Oura, H., Tijeras-Raballand, A., Schmidt, T., Loges, S., Albrecht, I., Jonckx, B., Vinckier, S., et al. (2010). Further pharmacological and genetic evidence for the efficacy of PIGF inhibition in cancer and eye disease. *Cell* *141*, 178–190.
- Verstraete, K., Vandriessche, G., Januar, M., Elegheert, J., Shkumatov, A.V., Desfosses, A., Svergun, D.I., Gutsche, I., Vergauwen, B., and Savvides, S.N. (2011). Structural insights into the extracellular assembly of the hematopoietic Flt3 signaling complex. *Blood* *118*, 60–68.
- Waltersperger, S., Olieric, V., Pradervand, C., Gletting, W., Salathe, M., Fuchs, M.R., Curtin, A., Wang, X., Ebner, S., Panepucci, E., et al. (2015). PRIGo: a new multi-axis goniometer for macromolecular crystallography. *J. Synchrotron. Radiat.* *22*, 895–900.
- Weinert, T., Olieric, V., Waltersperger, S., Panepucci, E., Chen, L., Zhang, H., Zhou, D., Rose, J., Ebihara, A., Kuramitsu, S., et al. (2015). Fast native-SAD phasing for routine macromolecular structure determination. *Nat. Methods* *12*, 131–133.
- Wiesmann, C., Fuh, G., Christinger, H.W., Eigenbrot, C., Wells, J.A., and de Vos, A.M. (1997). Crystal structure at 1.7 Å resolution of VEGF in complex with domain 2 of the Flt-1 receptor. *Cell* *91*, 695–704.
- Yang, Y., Yuzawa, S., and Schlessinger, J. (2008). Contacts between membrane proximal regions of the PDGF receptor ectodomain are required for receptor activation but not for receptor dimerization. *Proc. Natl. Acad. Sci. USA* *105*, 7681–7686.
- Yang, Y., Xie, P., Opatowsky, Y., and Schlessinger, J. (2010). Direct contacts between extracellular membrane-proximal domains are required for VEGF receptor activation and cell signaling. *Proc. Natl. Acad. Sci. USA* *107*, 1906–1911.
- Yuzawa, S., Opatowsky, Y., Zhang, Z., Mandiyan, V., Lax, I., and Schlessinger, J. (2007). Structural basis for activation of the receptor tyrosine kinase KIT by stem cell factor. *Cell* *130*, 323–334.
- Zhang, Y. (2008). I-TASSER server for protein 3D structure prediction. *BMC Bioinformatics* *9*, 40.

Structure, Volume 25

Supplemental Information

Structure of the Full-length VEGFR-1

Extracellular Domain in Complex with VEGF-A

Sandra Markovic-Mueller, Edward Stutfeld, Mayanka Asthana, Tobias Weinert, Spencer Bliven, Kenneth N. Goldie, Kaisa Kisko, Guido Capitani, and Kurt Ballmer-Hofer

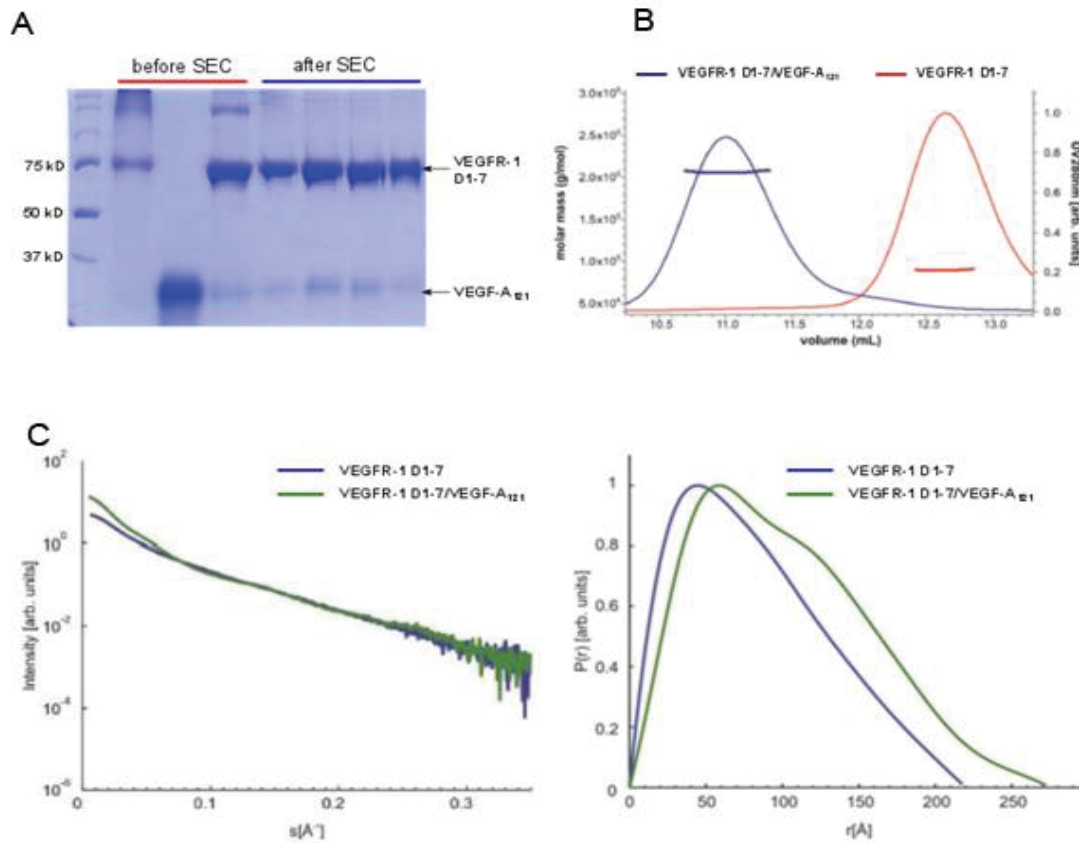


Figure S1 related to Figure 1 and 6. Purification and biophysical characterization of the VEGFR-1 ECD monomer and the VEGFR-1 ECD/VEGF-A complex in solution.

A, SDS-PAGE analysis of purified VEGFR-1 ECD, VEGF-A₁₂₁ and the VEGFR-1 ECD/VEGF-A₁₂₁ complex. The preformed complex was purified by size exclusion chromatography (SEC) on Superdex 200 and used for further biophysical and structural analyses. **B**, Size exclusion coupled to multi-angle light scattering (SEC-MALS) of VEGFR-1 ECD alone and in complex with VEGF-A₁₂₁. The UV-profiles are shown along with the mass distribution of each peak calculated from the MALS data. Experimentally determined M_r values were, for the VEGFR-1 ECD 89.7 kDa and for the VEGFR-1 ECD/VEGF-A₁₂₁ complex 206.3 kDa (theoretical values 83.3 and 196.8 kDa, respectively). **C**, SAXS analysis of VEGFR-1 ECD and of the complex with VEGF-A₁₂₁. Left panel: Scattering intensity as a function of scattering vectors. Right panel: GNOM distance distribution functions.

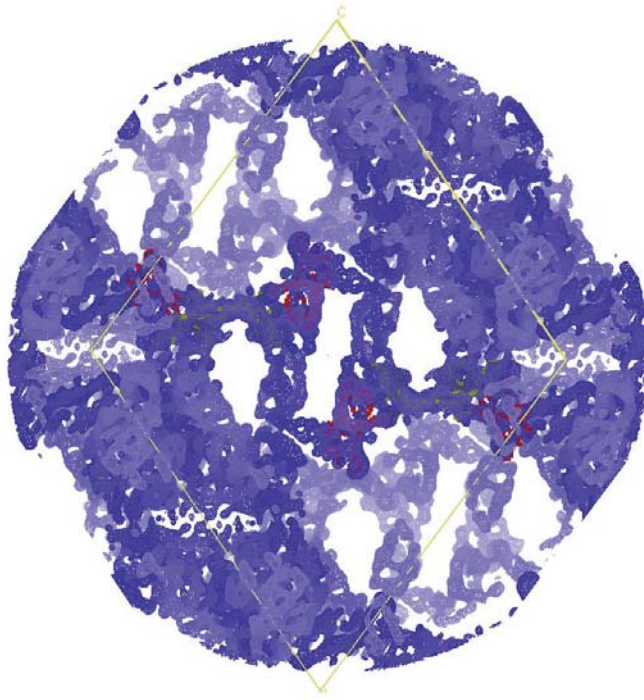
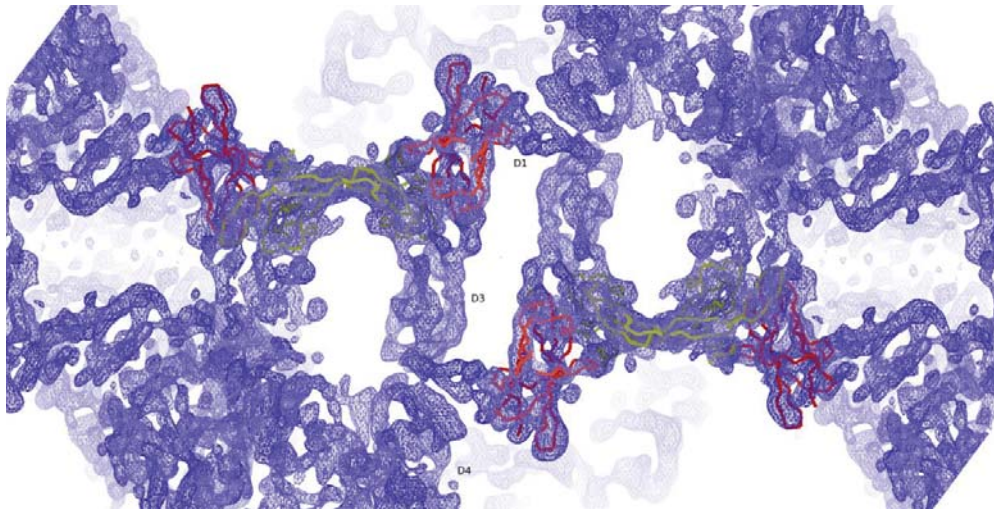
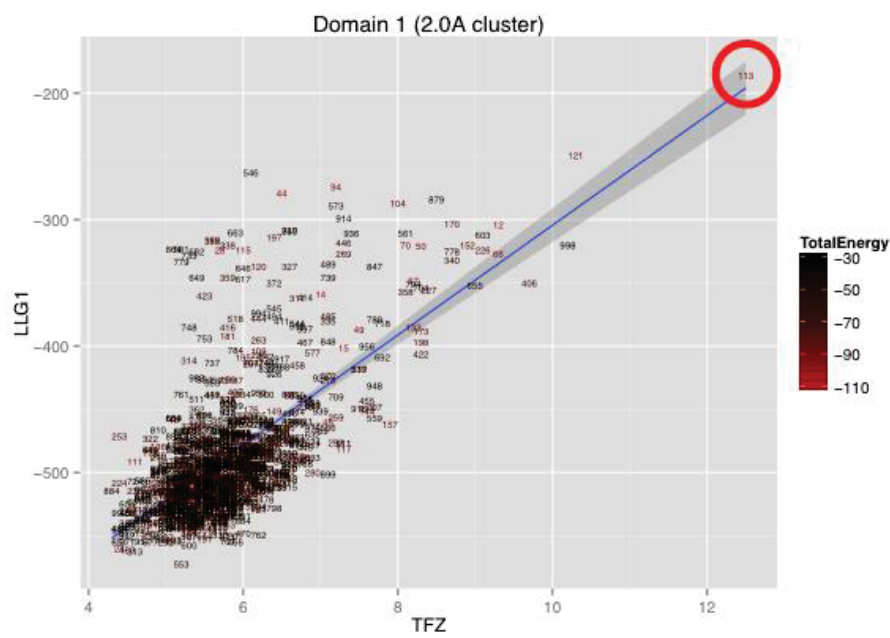
A**B**

Figure S2, related to Figure 1. Quality of the experimental electron density map.

Electron density map as obtained from MR-SAD phasing in PHASER and subsequent density modification in DM. The map is contoured at 1.5σ and exhibits clear solvent-protein boundaries. The figure is centered on two VEGFR-1 D2/VEGF-A complexes positioned by molecular replacement and related by 2-fold crystallographic symmetry around y axis (VEGFR-1 D2 is colored red, VEGF-A is colored yellow). **A**, view on the whole unit cell along the y axis. **B**, Zoom-in of panel a. The density corresponding to Ig-domains D1, D3 and D4 is indicated by labels.

A



B

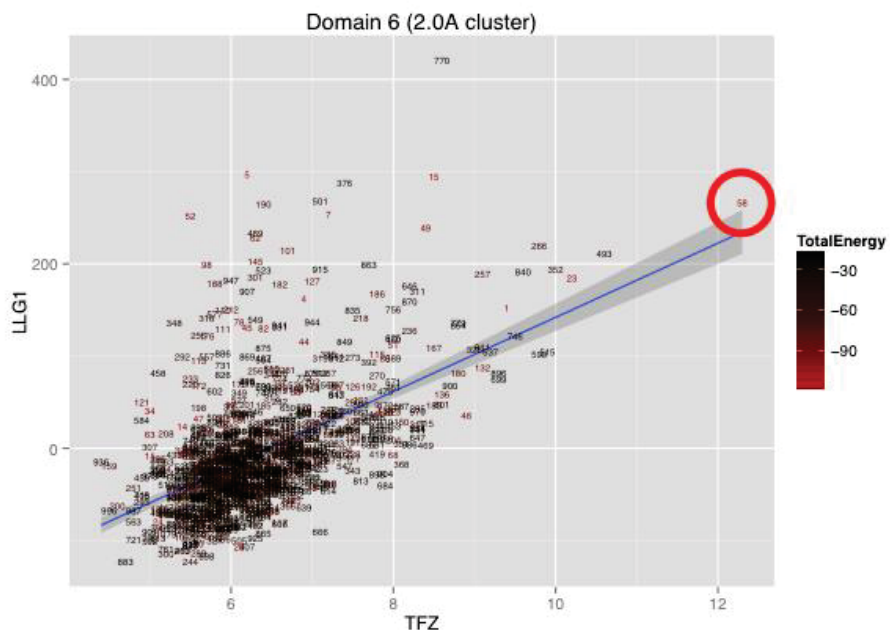


Figure S3 related to Figure 1. PHASER scores for molecular replacement of Foldit models for Ig-domain 1 (A) and Ig-domain 6 (B). Translation function z-scores (TFZ) and log-likelihood gains for the fitted domain (LLG1) were used to select a model for further use (red circle). Electron density fit only weakly correlated with Rosetta energy (Total Energy, color with labels giving ranked energy).

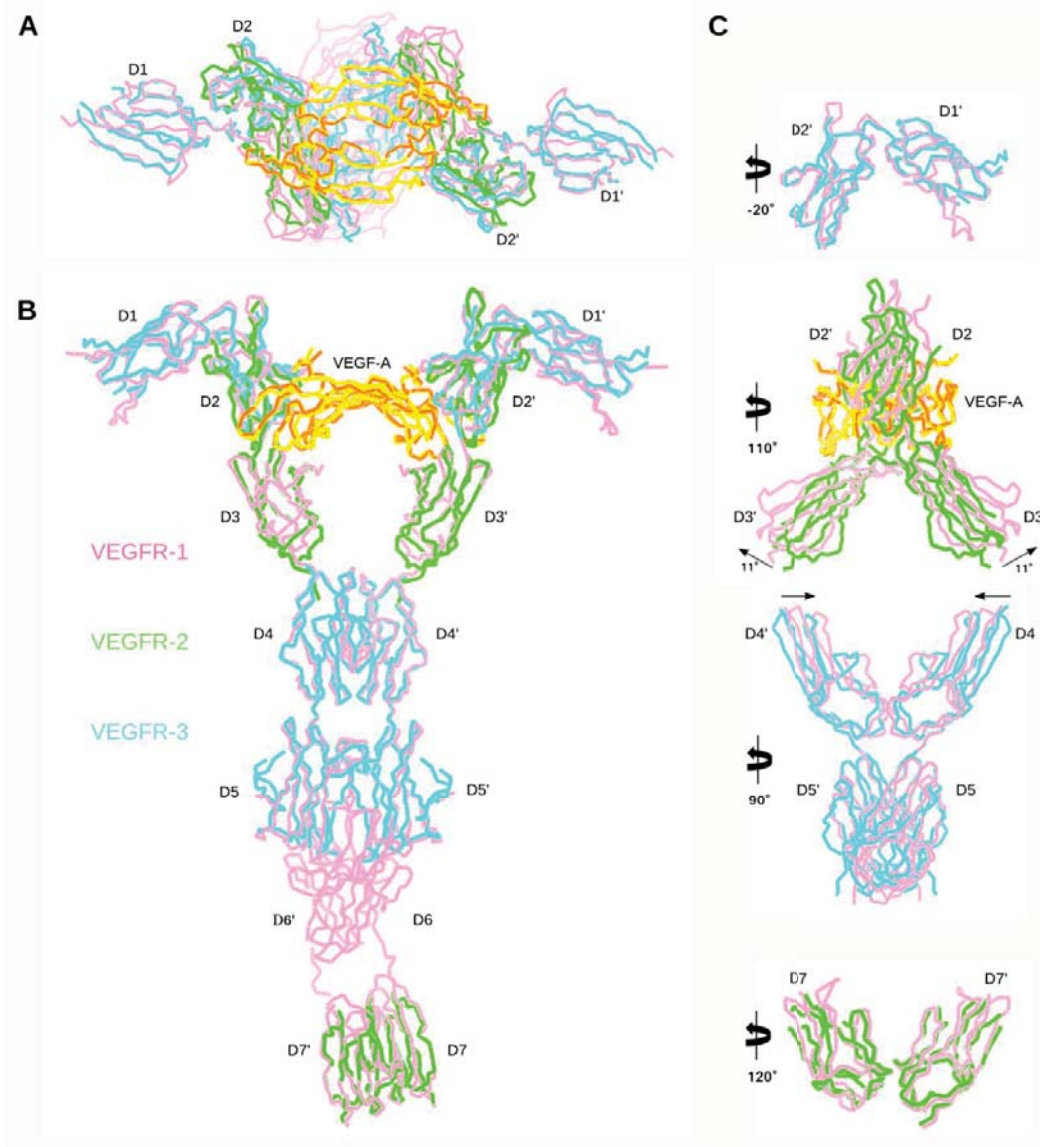


Figure S4 related to Figure 1. Comparison of the VEGFR-1 ECD/VEGF-A complex with known partial structures of VEGFR-2 and VEGFR-3.

A, Top, and **B**, side views of the VEGFR-1 ECD / VEGF-A model (pink/yellow) with four known partial structures of VEGFR-2 (green) or VEGFR-3 (cyan) superimposed. From N- to C-terminus: VEGFR-3 D1-2 (PDB: 4BSK); VEGFR-2 D2-3/VEGF-A complex (PDB: 3V2A) (green/orange); VEGFR-3 D4-5 dimer (PDB: 4BSJ); and VEGFR-2 D7 dimer (PDB: 3KVQ). Structural alignments were obtained by SSM superposition in Coot. **C**, The same four superpositions presented separately. Rotations relative to the orientation in **B** are designated.

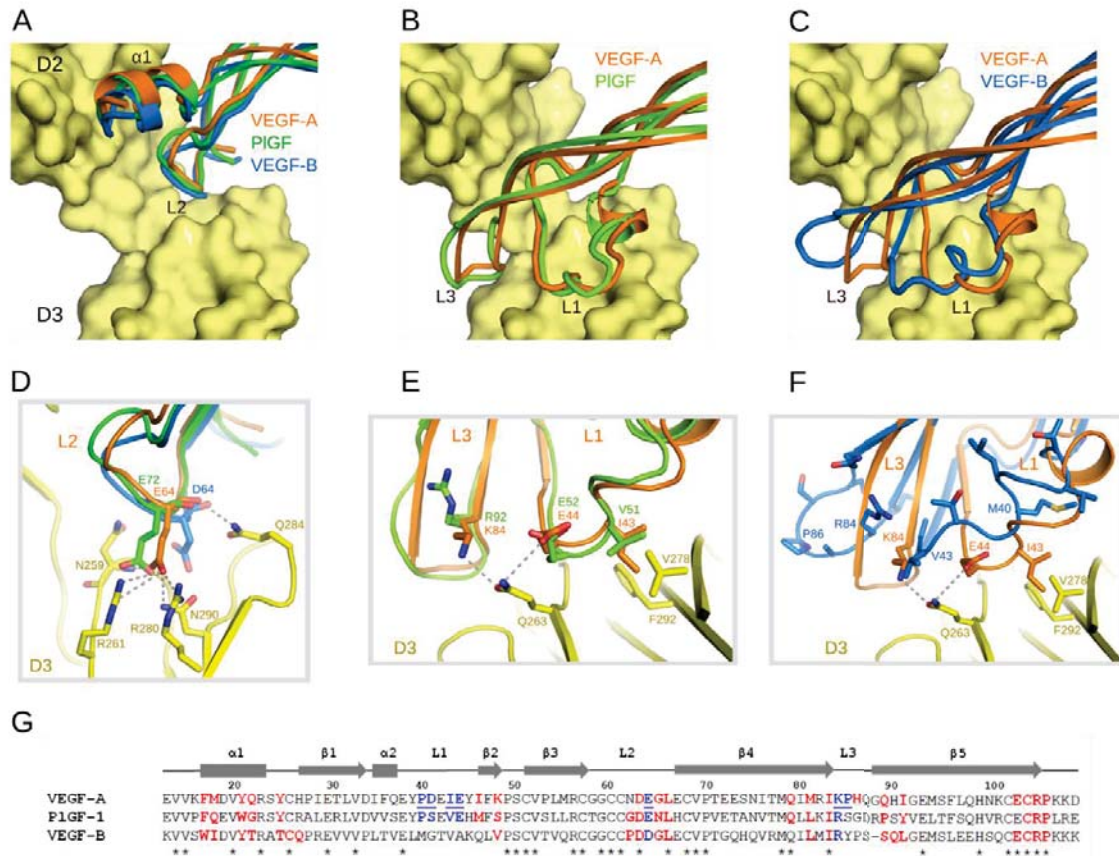


Figure S5. Related to Figure 4. Structural comparison of receptor binding epitopes in VEGF-A, PIGF and VEGF-B.

A-C, Interaction of VEGF-A (orange) with VEGFR-1 D2-3 (yellow) as in Figure 4b. VEGFR-1 D2 complexes with PIGF (PDB: 1RV6) and VEGF-B (PDB: 2XAC) were superimposed onto D2 of the VEGFR-1 D1-6/VEGF-A complex structure. Parts of the ligands are shown: **A**, monomer A, helix $\alpha 1$ and loop 2; **B** and **C**, monomer B, loops 1 and 3. **D**, Interaction of E64 of VEGF-A with VEGFR-1 D3 and comparison with the corresponding residues in PIGF (E72) and VEGF-B (D64). Hydrogen bonds and salt bridges are shown as gray dashed lines. **E**, **F**, Interaction of VEGF-A L1 and L3 with VEGFR-1 D3 with the same loops of PIGF (**E**) and VEGF-B (**F**) superimposed. There is a high sequence and structure homology between L1 and L3 of VEGF-A and PIGF. L1 and L3 of VEGF-B have clearly different structural features. **G**, Structure-based sequence alignment of VEGF-A (13-109), PIGF (21-115) and VEGF-B (13-109). Residues that interact with VEGFR-1 D2 are colored in red. VEGF-A residues that interact with VEGFR-1 D3 are colored in blue and underlined and the homologues residues in PIGF and VEGF-B that could play similar roles are colored in blue.

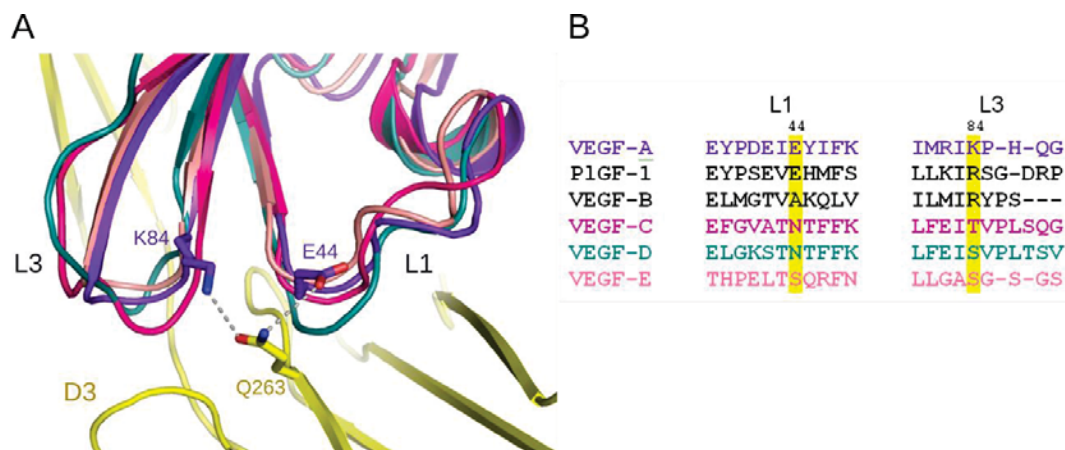


Figure S6 related to Figure 4. Structural comparison of the loops L1 and L3 of different VEGF family members.

A, Interactions between the loops L1 and L3 of VEGF-A (purple) and VEGFR-1 D3 (yellow). The key interacting residues are shown as sticks and hydrogen bonds as gray dashed lines. VEGF-C (magenta, PDB: 2X1W), VEGF-D (deep teal, PDB: 2XV7) and VEGF-E (salmon, PDB: 3V6B) were superimposed onto our VEGFR-1 structure to compare L1 and L3 loops. **B**, Sequence alignment of the L1 and L3 regions of different VEGFs. VEGF-A residues E44 and K84 that interact with Q263 of VEGFR-1 and their counterparts in other VEGFs are highlighted in yellow.

Supplemental Experimental Procedures

Production and purification of recombinant proteins

Human VEGF-A₁₂₁ (here denoted as VEGF-A) was produced in *Pichia pastoris* as described before (Scheidegger et al., 1999). Human VEGFR-1 D1-3 (residues 1-339), D1-6 (residues 1-660), D2-7 (residues 132-750) and D1-7 (residues 1-750) were expressed as secreted proteins in Sf21 insect cells, as described previously (Brozzo et al., 2012). The proteins were purified from culture supernatant by immobilized metal affinity chromatography (IMAC) followed by size exclusion chromatography (SEC) on Superdex 200 HR 16/600 (GE Healthcare) equilibrated in 25 mM HEPES pH 7.5 and 500 mM NaCl. For the formation of VEGFR-1 ECD/VEGF-A complexes, an equimolar amount of receptor and ligand were mixed and the complexes were purified by SEC.

Size exclusion chromatography coupled to multi-angle light scattering (SEC-MALS)

100 μ l protein samples at a concentration of 1 mg/ml were injected onto a Superdex 200 HR 10/300 column for SEC-MALS determination (GE Healthcare). The column was equilibrated in 25 mM HEPES pH 7.5, 500 mM NaCl at 20°C, using an Agilent 1100 HPLC system. Light scattering and differential refractive index were recorded using a Wyatt miniDAWN Tristar detector and a Wyatt Optilab rRex detector, respectively. Wyatt Astra software was used to collect and process the data and to calculate the molar mass from a global fit of the light scattering signals from three detectors at different angles and the differential refractive index signal.

Small angle X-ray solution scattering (SAXS)

SAXS data acquisition was performed at the X12SA-beamline (cSAXS) at the Swiss Light Source at the Paul Scherrer Institute in Villigen, Switzerland. The intensities of the scattered X-rays were recorded on a Pilatus 2M detector using a wavelength of $\lambda = 1 \text{ \AA}$. Data was collected in the scattering vector range of $0.008 \text{ \AA}^{-1} - 0.4 \text{ \AA}^{-1}$, where the length of the scattering vector is given as $s = 4\pi\sin\theta/\lambda$ (2θ is the scattering angle). Silver behenate was used as a standard for calibration of the s-range (Huang et al., 1993). Three concentrations were measured per protein sample using quartz capillaries with a diameter of 1 mm (Hilgenberg GmbH). To record background scattering, the protein buffer was measured in the same capillaries prior to protein data acquisition. Exposures of 0.5 s were taken at ten different spots along the capillary. The data was monitored for radiation damage and all frames showing no radiation damage were merged and averaged for further data processing. The collected SAXS data were integrated and radially averaged utilizing our own MATLAB-scripts (J. Missimer & K. Kisko, unpublished). Using PRIMUS from the ATSAS (Petoukhov et al., 2012) program package¹⁴, the background scattering was subtracted and data of different concentrations were merged. In order to check for proper protein folding of all measured samples Kratky-plots were calculated. The distance distribution function $P(r)$ was calculated using GNOM and the program AUTOGNOM.

Negative stain single particle electron microscopy (EM)

In order to stabilize the VEGFR-1 D1-7/VEGF-A complex for negative stain EM, samples were prepared using GraFix (Kastner et al., 2008). Briefly, 150 pmol of the complex were applied onto a 5-20 % glycerol gradient containing 20 mM HEPES pH 7.5, 150 mM NaCl in the presence or absence of 0.2% glutaraldehyde. The samples were centrifuged for 18 hrs at 40'000 rpm in a SW60Ti rotor (Beckman-Coulter), which correlates to an average RCF value of $164'326 \times g$. The gradients were harvested from bottom to top with a peristaltic pump collecting 120

μ l fractions. Protein containing fractions were detected using Roti[®]-Quant reagent (Carl Roth GmbH + Co. KG) for protein quantitation according to Bradford. In addition, protein containing fractions were analyzed by SDS-PAGE to verify the presence of the complex. Cross-linking reactions were quenched with the addition of 5x quenching buffer (20 mM HEPES pH 7.5, 150 mM NaCl, 0.4 M glycine). For negative stain EM, 5 μ l of undiluted sample was adsorbed to a freshly glow discharged thin carbon film supported on a 200 mesh copper grid and incubated for 1 min. at room temperature. The excess sample was blotted away using filter paper. Three consecutive washes using 20 mM HEPES pH 7.5, 150 mM NaCl and one wash with 2% uranyl acetate was performed followed by 20 s staining with fresh 2% uranyl acetate. Negative stain EM data were collected on a CM-100 microscope (Philips) equipped with a Veleta 2k x 2k CCD camera (Olympus). The voltage used was 80 kV and the magnification was set to a nominal value of 130'000 x. From 126 micrographs 4883 particles were picked manually using XMIPP (Scheres et al., 2008). Inferior particles and particles with a z-score >3 were discarded. 4536 particles were boxed in 100 x 100 pixel boxes and subjected to alignment and classification into 24 2D class averages using maximum-likelihood target function (ML2D) implemented in XMIPP using 100 iterations (Scheres et al., 2005). After 49 iterations ML2D reached convergence.

Comparison of the crystal and EM structure of the VEGFR-1 D1-7/VEGF-A complex

The composite model of the VEGFR-1 D1-7/VEGF-A complex was converted into density volume filtered to 25 Å resolution using the Bsoft software package (Heymann and Belnap, 2007). The volume was then used to calculate projections at an angular interval of 15° with the SPIDER image processing suite (Frank et al., 1996). The projections with the most similar features to the experimental 2D averages were selected. Density volumes and ribbon diagrams were displayed and oriented with the UCSF Chimera package (Pettersen et al., 2004).

Isothermal titration calorimetry (ITC)

The measurements on VEGFR-1 were performed at 20°C in 25 mM HEPES pH 7.5, and 150 mM NaCl (ITC-buffer) using an iTC200 calorimeter (MicroCal[®], GE Healthcare). The proteins were purified on a Superdex 200 10/300 column (GE Healthcare) equilibrated in ITC-buffer and dialyzed against ITC-buffer overnight at 4°C prior to analysis. The calorimeter cell contained VEGFR-1 D1-7 or VEGFR-1 D1-3 at concentrations ranging from 4.4 to 30 μ M and the ligand VEGF-A₁₂₁ was used in the syringe at concentrations ranging from 22.5 to 100 μ M. All samples were equilibrated to the measurement temperature and degassed prior to ITC analysis. The following settings were applied: one initial injection of 1 μ l followed by 15 injections of 2.6 μ l at an injection speed of 1 μ l/s with a data filter of 1 s and 300 s recovery time between each peak. The software Origin 7.0 (OriginLab[®]) was used for data analysis.

Cell transfection and determination of receptor activity

NIH 3T3 cells were grown in 10% calf serum in Dulbecco's Modified Eagle's Medium (DMEM) and transfected using a modified peGFP-N1 vectors (Takara Bio Europe/Clontech) carrying either wt VEGFR-2, or a mutant T446E/K512A where residue K512 was replaced by A and T446 by E. All expression vectors were generated by Gibson assembly (Gibson et al., 2009). 8 μ g DNA in 0.8 ml serum-free medium were mixed with 16 μ l PEI (Polyethyleneimine, stock 1 mg/ml, Aldrich 408727, 25 kDa branched), incubated for 10 minutes at RT for the complex to form. The medium in the culture dishes was replaced with 1.6 ml DMEM containing 0.5% serum and the DNA/PEI complex was added for 5 hrs. Cells were incubated for 20 hrs after addition of 1 ml DME with 10%

serum. The cells were serum-starved in DMEM supplemented with 1% bovine serum albumin (BSA) and stimulated with 1.5 nM VEGF-A for 10 min at 37°C. Cell lysates were prepared in lysis buffer (50 mM Tris pH 7.5, 100 mM NaCl, and 0.5% w/v Triton X-100) supplemented with protease inhibitor cocktail (Roche diagnostics, Risch-Rotkreuz Switzerland), phosphatase inhibitors (200 μ M Na_3VO_4 , 10 mM NaF, 10 mM sodium pyrophosphate, 30 mM p-nitrophenyl-phosphate, 80 mM glycerophosphate, and 20 μ M phenylarsine oxide), and 10% glycerol. Cell lysates were diluted with Lämmli buffer (20 mM Tris pH 6.8, 5% SDS, 10% mercaptoethanol, 0.02% bromphenol blue) and the proteins separated on 8% SDS polyacrylamide gels and blotted to Polyvinylidene (PVDF, Thermofisher Scientific, Zug Switzerland) membranes. We used 55B11 (2479, Cell Signaling Technology Europe) and phospho-Y1175 (2478, Cell Signaling Technology Europe) for determining VEGFR-2 activity. All primary antibodies were used at dilutions of 1:1'000, followed by secondary alkaline phosphatase-coupled antibodies (6440-04, Southern Biotech, Birmingham USA) at a dilution of 1:10'000. The blots were developed with AP chemiluminescent detection substrate (Life Technologies, Carlsbad USA) and the immunoblots were analyzed on a GE Healthcare ImageQuant RT ECL scanner and densitometrically quantified using the ImageJ gel analysis plugin. Relative activity is given as the ratio of the intensities of the bands corresponding to VEGF treated versus non-treated receptor detected by phospho-Y1175 antibody.

Supplemental References

Brozzo, M.S., Bjelic, S., Kisko, K., Schleier, T., Leppänen, V.M., Alitalo, K., Winkler, F.K., and Ballmer-Hofer, K. (2012). Thermodynamic and structural description of allosterically regulated VEGF receptor 2 dimerization. *Blood* *119*, 1781-1788.

Frank, J., Radermacher, M., Penczek, P., Zhu, J., Li, Y., Ladjadj, M., and Leith, A. (1996). SPIDER and WEB: processing and visualization of images in 3D electron microscopy and related fields. *J Struct Biol* *116*, 190-199.

Gibson, D.G., Young, L., Chuang, R.Y., Venter, J.C., Hutchison, C.A., III, and Smith, H.O. (2009). Enzymatic assembly of DNA molecules up to several hundred kilobases. *Nat. Methods* *6*, 343-345.

Heymann, J.B. and Belnap, D.M. (2007). Bsoft: image processing and molecular modeling for electron microscopy. *J. Struct. Biol* *157*, 3-18.

Huang, T.C., Blanton, T.N., and Wu, Y. (1993). X-ray-powder diffraction analysis of silver behenate, a possible low-angle diffraction standard. *J. Appl. Crystallogr.* *26*, 180-184.

Kastner, B., Fischer, N., Golas, M.M., Sander, B., Dube, P., Boehringer, D., Hartmuth, K., Deckert, J., Hauer, F., Wolf, E. et al. (2008). GraFix: sample preparation for single-particle electron cryomicroscopy. *Nat. Methods* *5*, 53-55.

Petoukhov, M.V., Franke, D., Shkumatov, A.V., Tria, G., Kikhney, A.G., Gajda, M., Gorba, C., Mertens, H.D., Konarev, P.V., and Svergun, D.I. (2012). New developments in the program package for small-angle scattering data analysis. *J. Appl. Crystallogr.* *45*, 342-350.

Pettersen, E.F., Goddard, T.D., Huang, C.C., Couch, G.S., Greenblatt, D.M., Meng, E.C., and Ferrin, T.E. (2004). UCSF Chimera--a visualization system for exploratory research and analysis. *J. Comput. Chem.* *25*, 1605-1612.

Scheidegger, P., Weiglhofer, W., Suarez, S., Kaser-Hotz, B., Steiner, R., Ballmer-Hofer, K., and Jaussi, R. (1999). Vascular endothelial growth factor (VEGF) and its receptors in tumor-bearing dogs. *Biol. Chem.* *380*, 1449-1454.

Scheres, S.H., Nunez-Ramirez, R., Sorzano, C.O., Carazo, J.M., and Marabini, R. (2008). Image processing for electron microscopy single-particle analysis using XMIPP. *Nat. Protoc.* *3*, 977-990.

Scheres, S.H., Valle, M., Nunez, R., Sorzano, C.O., Marabini, R., Herman, G.T., and Carazo, J.M. (2005).
Maximum-likelihood multi-reference refinement for electron microscopy images. *J. Mol. Biol.* 348, 139-149.

8. Discussion and Outlook

VEGFRs, upon binding to their cognate ligands, initiate signaling cascades across the plasma membrane for carrying out processes such as angiogenesis and lymphangiogenesis. The ligand binds to the receptor ECD and induces distinct conformational changes promoting dimerization and instigating TM signaling resulting in intracellular kinase activation. Low-resolution structural information on the VEGFR-2 ECD/ligand complex, derived from single particle EM and SAXS, revealed that Ig-homology domains 1-3 are involved in ligand binding while membrane proximal domains 4-7 form homotypic contacts presumably required for receptor activation (Kisko *et al.*, 2011; Ruch *et al.*, 2007). High-resolution structural data on ligand binding to subdomains 1-3 show the details of the interactions between the variable loops present in VEGF ligands and the receptor domains. A high-resolution crystal structure and functional studies of the membrane proximal Ig-homology domain 7 document the relevance of the homotypic contacts mediated by conserved charged residues, namely R726 and D731 present in the β E-F loop, in activation of the VEGFR-2 complexed with ligand (Hyde *et al.*, 2012; Yang *et al.*, 2010). Structural information of Ig-homology domains 4-5 of VEGFR-3 show weak lateral interactions in domain 4 and close homotypic contacts in domain 5 between receptor monomers (Leppänen *et al.*, 2013). Thus, although information on small isolated subdomains for VEGFR-2 exists, the exact mechanism of how the ligand induces interactions in the membrane proximal domain leading to receptor activation remains unclear.

8.1. Crystallization of VEGFR-2 ECD ligand complexes

A great motivation for this thesis was to identify conformational changes present in the membrane proximal Ig-homology domains of VEGFR-2 which are triggered by ligand binding. To carry out such a structural study, appropriate systems for the expression, purification and characterization of various VEGFR-2 constructs were required. In this thesis, we describe the successful establishment of such systems, as well as initial approaches employed for their crystallization.

Protein expression in *Pichia pastoris* was not pursued because earlier expression trials in the laboratory resulted in the generation of degraded protein. *E.coli* expression also

lead to misfolded protein in inclusion bodies (Stuttfeld, 2011). In earlier studies carried out for determining the crystal structures of single VEGFR Ig-homology domains, *E.coli* expression could be used only after refolding (Christinger *et al.*, 2004; Iyer *et al.*, 2010; Wiesmann *et al.*, 1997; Yang *et al.*, 2010). In order to produce larger VEGFR ECD fragments, eukaryotic expression systems are more suitable to achieve properly folded recombinant proteins (Aricescu *et al.*, 2006). Therefore, we chose to express the recombinant receptor proteins in mammalian or insect cells, and we achieved protein yields up to several milligrams (0.5-13 mg/l). It is known that there are several potential N-glycosylation sites within the ECD of the VEGFRs (Terman *et al.*, 1991), which might hamper protein crystallization. Moreover, recombinant proteins produced in insect cells are heterogeneously glycosylated, which makes deglycosylation by EndoF or PNGase only partially successful (Hollister *et al.*, 2002). Thus, expression in HEK293S GnTi-cells is a promising option in order to obtain homogeneously glycosylated proteins. As a matter of fact, there are some reported structures of RTK ECDs where the recombinant proteins were expressed in HEK293S GnTi- cells (Shim *et al.*, 2010; Verstraete *et al.*, 2011). In order to overcome the low expression yields in glycosylation-deficient HEK293S GnTi- cells, a baculovirus-mediated gene transduction system for mammalian cells (BacMam) has been developed (Dukkipati *et al.*, 2008), and successfully applied to solve the structure of the platelet-derived growth factor receptor (PDGFR) Ig-homology domains 1-3 in complex with PDGF (Shim *et al.*, 2010). In this thesis, I adapted this system for establishing recombinant protein production of VEGFR-2 ECD subdomain constructs. However, even using high-titer virus in high volumes did not yield high protein expression in mammalian cells when compared to chemically transfected HEK293T or HEK293S GnTi- cells, possibly due to poor efficiency of our recombinant baculoviruses for transducing mammalian cells (Figure 8). There are only a few recently published studies exploring factors for improving the entry of baculoviruses in mammalian cells, for which the mechanism has been less well known (Mansouri *et al.*, 2016; O'Flynn *et al.*, 2012).

Since we were unable to generate enough protein for crystallization studies from HEK293S GnTi- cells using the BacMam system, we explored alternative stable mammalian expression systems, such as the HEK293 EBNA system. HEK293 EBNA cells express the EBNA-1 protein, which drives the episomal amplification of expression plasmids carrying the origin of replication derived from the EBV. Thus,

these cells under selection pressure (Puromycin) are expected to increase recombinant protein expression levels by permitting more plasmid copies to persist in the transfected cells throughout the production phase. We established high expression suspension cultures and obtained homogeneous protein of high purity from mammalian HEK293 EBNA cells for the mouse VEGFR-2 ECD constructs, which share a sequence identity of 80% with the human VEGFR-2 ECD. Unfortunately, excessive crystallization trials of both glycosylated and deglycosylated mouse VEGFR-2 ECD proteins did not give rise to any crystals. On the other hand, using the above established HEK293 EBNA expression system in a followup study from our lab gave for the first time highly diffracting crystals of domains 4-5 (allosteric site) of human VEGFR-2 (Thieltges *et al.*, 2018).

Since our extensive crystallization trials with differently glycosylated constructs were unsuccessful, we sought an alternative method to facilitate crystallization. We successfully generated VEGFR-2 ECD/VEGF-A/antibody fragment complexes for co-crystallization trials (Griffin *et al.*, 2011). The antibody fragments aid in stabilizing flexible protein domains to a distinct conformation leading to improved structural homogeneity of the sample. ScFvs have been commonly used for crystallization studies. A comparative evaluation of scFv and Fab fragments showed that the presence of both constant domains can further stabilize the variable domains in the Fab fragment (Rothlisberger *et al.*, 2005). Crystallization of the extracellular region of another RTK, HER2 (also known as Neu receptor), was aided by a Fab called herceptin (Cho *et al.*, 2003). The need for such crystallization chaperones for VEGFR-2 becomes evident when one considers that the Ig-homology domains present in the ECD are connected with flexible linkers, particularly domains 1-2, which exist in a bent conformation, as suggested by the structural data on VEGFR-3 and VEGFR-1 (Leppänen *et al.*, 2013) (Section 7.4). This structural conservation indicates that the flexibility in domain 1 may be physiologically essential, for receptor function, and might be required for interacting with co-receptors such as neuropilins. Also, binding studies on VEGFR-2 ECD/VEGF complexes suggest a regulatory role of Ig-homology domain 1 (Shinkai *et al.*, 1998). Therefore, we chose scFv and Fab fragments of antibodies targeting either domain 1 or domains 2-3 of VEGFR-2 ECD to stabilize the highly flexible ligand-binding region of the receptor (Figures 12 and 14). In addition to the flexibility due to the linker regions, VEGFR-2 ECD complexes also lack the stability in

the membrane proximal regions, which in the physiologically relevant form of the receptor is provided by the TMD embedded in the cell membrane. It has been shown earlier by our lab that distinct conformation of the TMD is crucial for stabilizing ligand-receptor complex formation and activation (Dell'Era Dosch *et al.*, 2010; Manni *et al.*, 2014b). We therefore sought to mimic this stabilization by generating complexes with receptor constructs containing a GCN-4 leucine zipper domain at the C-terminal of the membrane proximal domain 7.

Extensive crystallization trials of VEGFR-2 ECD/VEGF-A complexes with or without stabilizing antibody fragments did not yield crystals. It is possible that flexible loops other than those in the ligand-binding domain and other unstructured regions in the protein impair crystallization. Indeed, bioinformatics analysis predicted the presence of extensive disordered regions in VEGFR-2 ECD domains 3 and 5 (Figure 15). New constructs with redefined domain boundaries based on a preliminary limited proteolysis study presented in this thesis on hVEGFR-2 ECD/VEGF-A complex might be helpful. Treatment with subtilisin, α -chymotrypsin and trypsin gave a stable, lower molecular weight fragment after longer incubation times, which contains presumably fewer disordered regions than the intact protein (Figure 16). The fragments and interfaces obtained by limited proteolysis can be identified by a mass spectrometry analysis. Other strategies to design new constructs include replacing flexible tails and interdomain regions and rational mutagenesis of surface residues, which could make proteins amenable for crystallization, were also not pursued for time reasons during this thesis. Finally, crystallization trials of isolated Ig-homology domains could be beneficial, although this strategy would fail to unravel the interplay between the ligand binding domains and membrane proximal domains.

8.2. Role of VEGFR-2 ECD in receptor dimerization and activation

It has been shown that VEGFR-2 forms dimers even in the absence of ligand when expressed at physiological levels, but complete phosphorylation in the kinase domain is only achieved upon ligand binding to the ECD (Sarabipour *et al.*, 2016). ITC and MST studies presented here gave us insight into the distinct roles of individual extracellular subdomains in ligand-mediated dimerization of VEGFR-2 (Figures 18 and 19). The biophysical studies confirmed the ability of complex formation between

VEGFR-2 ECD and VEGF-A in a 2:1 stoichiometry, considering the disulfide-linked ligand dimer as a single molecule. Thermodynamic analysis of receptor binding to VEGF, carried out by ITC, revealed the counterintuitive finding that the Gibbs free energy of ligand binding to full length ECD is less negative by 1.12 kcal/mol compared to that of ligand binding with domains 1-3. The comparative data from the two biophysical studies also show that the presence of membrane proximal domains (4-7) attenuate the receptor affinity for the ligand by approximately 10 fold, although the precise value for ligand binding to VEGFR-2 domains 1-3 could not be determined by MST, due to reaching the detection limit of the technique,. The study shows that ligand interactions with domains 2-3 are thermodynamically highly favourable, whereas homotypic interactions in domains 4-7 occur with an enthalpic penalty. This result is in agreement with a previous study, which demonstrated that binding of VEGF to recombinantly produced ECD protein, encompassing Ig-homology domains 1-7 of VEGFR-2 is 1.0-1.7 kcal/mol less favourable than binding to Ig-homology domains 2-3 (Brozzo *et al.*, 2012). It is also in agreement with another system, fibroblast growth factor receptor 3, where the ECD prevents dimerization in the absence of ligand with a ΔG of 1 kcal/mol (Chen *et al.*, 2010). A previous study also shows that deletion of domains 4-7 of VEGFR-2 leads to constitutive ligand independent receptor activation (Tao *et al.*, 2001). It can be postulated that the energetically unfavorable interactions in domains 4-7 are required for proofreading, to prevent ligand-independent self-association of VEGFR-2 monomers, while properly positioning inactive dimers upon ligand activation. It is essential to prevent any erroneous signaling by VEGF that might disrupt homeostasis of blood and lymph vessels.

On the other hand, ITC shows that the homologous VEGFR-1 ECD binds VEGF-A with 10 fold higher affinity compared to VEGFR-2 ECD (Section 7.4). Moreover, the presence of the membrane proximal domains 4-7 in VEGFR-1 increases ligand binding affinity by 20 fold when compared with ligand binding affinity to domains 1-3. This is in contrast to VEGFR-2, where domains 4-7 significantly reduce ligand binding affinity. These studies show that membrane proximal Ig-homology domains enhance ligand binding to VEGFR-1 in line with the fact that VEGFR-1 acts as a strong decoy for VEGF-A. In addition, the soluble splice variant of VEGFR-1 (sVEGFR-1) comprising domains 1-6, has been shown to act as a strong VEGF binding antagonist (Kendall *et al.*, 1993). ITC analysis showed that the presence of the membrane proximal domains

4-7 in VEGFR-3 also enhance affinity for VEGF-C and the thermodynamic data suggest that ligand binding is both enthalpically and entropically favourable (Leppänen *et al.*, 2013). Several knock out studies in mice showed that precisely regulated VEGF-A concentrations are required for spatially and temporally tightly controlled vessel homeostasis (Fong *et al.*, 1995; Fong *et al.*, 1999; Hiratsuka *et al.*, 2005). Thus, RTKs follow a strictly ordered sequence of receptor activation where ligand binding allows the exact positioning of the subdomains present in the ECD and consequently promote a stable thermodynamic state distinct from preformed inactive ligand-free dimers.

8.3. Functional role of homotypic interactions in the VEGFR-1 ECD

Structural characterization of the full-length VEGFR-1 ECD complexed with VEGF-A revealed for the first time the details of ligand binding and ligand-induced interactions between the receptor monomers at the molecular level (Section 7.4). The structure shows homotypic interactions taking place in domains 4 and 5 in the ligand bound receptor, which seem to be essential for maintaining the conformation of receptor dimers that are essential for activation. Our latest VEGFR-1 structure and the already existing structural data on other VEGFR homologues show that the interface of domain 5 is large and the interactions involve fully conserved residues forming hydrogen bonds with residues in the adjacent receptor monomer (Brozzo *et al.*, 2012; Leppänen *et al.*, 2013; Ruch *et al.*, 2007). Therefore, we hypothesized that domain 5 interactions are indispensable for receptor function. In order to understand their role in receptor activation, we designed cell-based assays comparing the activity of mutant constructs that interfere with the homotypic contacts in VEGFR-1 domain 5. In order to perform these studies, we needed to optimize the cell expression system for VEGFR-1 to be able to detect ligand-induced receptor activation. Initially, we created stably expressing PAE cells using chemical transfections as well as lentiviral transductions (Figure 23). The advantage of stable transgene expression is that it permanently integrates the plasmid DNA into the genome of the host cells, leading to constitutive expression of the protein of interest. The PAE cell line was chosen as it is suitable for *in vitro* studies of EC function. Stable PAE cells expressing wild-type VEGFR-1 were used for identifying and optimizing the antibodies required for functional assays (Figure 21). Furthermore, these cells were used for carrying out time course studies of VEGFR-1

activation induced by various ligands (PIGF and VEGF-A₁₆₅), which revealed very quick maximal activation of VEGFR-1 upon binding to PIGF (Figure 22). It appears that the cells maintain a narrow window of receptor activation, which is crucial to prevent overstimulation and deregulation. Our findings are in agreement with those of another study, where VEGFR-1 expressed in human umbilical vein ECs, achieved maximal activation 5 min after PIGF-1 stimulation (the PIGF-1 used in this study was expressed in-house in HEK293 cells) (Hoffmann *et al.*, 2013). The weak kinase activity of VEGFR-1 in PAE cells led us to explore alternative ways to assess ligand-induced VEGFR-1 activation. One such approach was to co-immunoprecipitate (Co-IP) VEGFR-1 (using antibodies against VEGFR-1 or pan phosphoantibodies) and p85. p85 is the regulatory subunit of PI-3 KINASE, whose activity is required for the cytoskeletal changes occurring during migration of fibroblasts and epithelial cells, and is activated downstream of VEGFR-1 (Toker *et al.*, 1997). However, PAE cell lysates co-immunoprecipitated with anti-VEGFR-1 did not show any PI-3 KINASE activity (data not shown). It is possible that the antibodies used for Co-IP might have interfered with the interaction site, preventing p85 binding. Successful pull-down experiments of VEGFR-1 have been performed on lysates of primary dermal microvascular ECs, which however, have usually high expression levels of VEGFR-1 and hence make detection easier (Anisimov *et al.*, 2013). Since the results with PI-3 KINASE were inconclusive, we sought an alternative target for probing VEGFR-1 activity. The serine/threonine kinase Akt is known to be activated downstream of PI-3 KINASE by VEGFR-2 to mediate EC survival signals (Dayanir *et al.*, 2001). It has been postulated that it may be one of the targets of VEGFR-1 activation as well (Hudson *et al.*, 2014; Tchaikovski *et al.*, 2008). However, we did not observe any Akt phosphorylation upon PIGF stimulation of PAE cells expressing wild-type VEGFR-1 (data not shown). Natalie Hudson and colleagues could only observe significant Akt phosphorylation in whole-cell lysates of retinal tissues after a prolonged stimulation of 25 min (Hudson *et al.*, 2014). As these were primary cells with sufficiently high levels of endogenously expressed VEGFR-1, detection of Akt activation might have been easier in this study. As an alternative approach to study the role of domain 5 interactions in VEGFR-1 activation, we also introduced these mutations in the juxtamembrane activated VEGFR-1 constructs. These either lacked the three serines or had a replacement with ANGG sequence from VEGFR-2, in the JMD for enhancing the receptor activity. These

constructs were made in accordance with an earlier study by Gille *et al.*, which attributes the divergence in the juxtamembrane region for the strikingly different kinase activity of the two homologous receptors (Gille *et al.*, 2000). We also made PAE stable cell lines expressing chimeric VEGFR-1/2 constructs comprising the ECD of VEGFR-1 and the intracellular domain of VEGFR-2, harbouring the K517A/E513K mutations in domain 5, which were expected to show disruption in the homotypic contacts identified in the high-resolution VEGFR-1 ECD structure. However, we could not use stable PAE cells for studying receptor kinase activity of the domain 5 mutants due to unequal expression levels of wild-type and mutant constructs of either VEGFR-1 or chimeric VEGFR-1/2 because of inconsistent genomic integration (Figure 23a and 24). Hence we shifted our system of study to transiently expressing HEK293 and NIH3T3 cells. Although transient transfections have their own limitations, including the requirement for new cell transfections for each experiment, the need for large amounts of recombinant DNA and the heterogeneity of expression between different DNA batches, they have the ability for rapid protein expression within days compared to several months, required for stable gene expression. Addressing the lower efficiency associated with transient transfection, we optimized two parameters: cell-seeding density and transfection reagents: Lipofectamine 2000 and Lipofectamine 3000 showed improved transfection efficiency in HEK293 cells. However, VEGFR-1 overexpression in transiently transfected HEK293 cells led to constitutive receptor activation and was therefore, unsuitable for ligand-induced functional assays. On the other hand, NIH3T3 cells transiently transfected using branched PEI (25kDa) gave sharper protein bands and expression levels that allowed the detection of ligand-induced phosphorylation activity.

Based on these results, we generated NIH3T3 cells expressing the chimeric VEGFR-1/2 constructs. When stimulated by PIGF, these cells showed drastically reduced phosphorylation activity at Y1175 when compared to the wild-type receptor (Figure 25). The kinase activity of these chimeric constructs depends on domain 5 interactions in the VEGFR-1 ECD, as the kinase domains of VEGFR-1 and VEGFR-2 are highly conserved with 70.1% homology (Rahimi, 2006). Indeed, substitution of the C-terminal kinase domain present in VEGFR-1 with that of VEGFR-2 promotes VEGFR-1 activation and EC proliferation (Meyer *et al.*, 2006). We could further show that homologous mutations in domain 5 of VEGFR-2 severely reduced Y1175

autophosphorylation activity upon ligand stimulation (Figure 28). Interestingly, the triple mutants (T446E/E508A/K512A) did not show further reduction in phosphorylation activity when compared to the double VEGFR-2 mutants (T446E/K512A). This suggests that disrupting the hydrogen bonds formed by residues T455 and K517 of VEGFR-1 and the corresponding residues T446 and K512 in VEGFR-2 are sufficient to destabilize the conformation of the ECD and prevent kinase activation. These *in vitro* kinase assays validate the molecular interactions suggested by the VEGFR-1 ECD/VEGF-A structure and emphasize that domain 5 mediated homotypic interactions are crucial for the activation of VEGFRs. Our study is also in agreement with the work of Veli-Matti Leppanen and colleagues who showed the partial structure of another receptor homologue, VEGFR-3, as a homodimer of domains 4-5 (Leppänen *et al.*, 2013). Based on their data, residues T446 and K516 on domain 5 are essential for receptor activity. Taken together these data show that these homotypic interactions are very well conserved amongst all three VEGFRs. Similar homotypic interactions were also shown to be present in the membrane proximal Ig-homology domain 7 of VEGFR-2 ECD, and they were also shown to fulfill a regulatory function for receptor activation (Yang *et al.*, 2010). Our group has also shown previously that mutating domain 4 in VEGFR-2 leads to complete receptor inhibition (Hyde *et al.*, 2012). Similar activation mechanisms requiring formation of homotypic interactions are also observed in other type III RTKs, such as stem cell growth factor receptor (c-Kit) and PDGFR, where the ECD is comprised of five Ig-homology domains (Yang *et al.*, 2008; Yuzawa *et al.*, 2007). Crystallographic data for c-Kit showed that ligand binding to Ig-homology domains 1-3 does not lead to any significant conformational changes in this region. However, ligand binding induces conformational rearrangements in Ig-homology domains 4-5, leading to salt bridge formation by residues E386 and R381 located in Ig-homology domain 4. The functional relevance of these residues was proven by mutational analyses (Yuzawa *et al.*, 2007). The only exception is the Fms-like tyrosine kinase 3, where the crystal structure of the receptor ECD in complex with its ligand suggests a novel ligand binding mechanism where the receptor monomers are not involved in homotypic interactions (Verstraete *et al.*, 2011).

Several studies showed that receptor dimerization is essential but not sufficient for kinase activation (Bell *et al.*, 2000; Dell'Era Dosch *et al.*, 2010). The described homotypic interactions may represent a proofreading mechanism requiring distinct

orientation of receptor monomers in active, ligand-bound dimeric receptors. On the other hand, inhibition of receptor activity in the absence of ligand may also depend on domains 4-7. Correct dimerization of the ECD is further transmitted to the TMD to achieve the precise orientation of the two receptors required for full kinase activation (Manni *et al.*, 2014b). A recent NMR and molecular dynamics simulation study showed that a specific TMD helix conformation is associated with receptor activity. The data revealed that TMDs in active constructs were rotated by 180° relative to the inactive state (Manni *et al.*, 2014b).

In conclusion, the structural and thermodynamic studies of VEGFR-2 and the biochemical studies on VEGFR-1 presented in this study show that ligand binding to Ig-homology domains 2-3 of two receptor protomers promotes further conformational changes in the membrane proximal Ig-homology domains 4, 5 and 7 (Figure 29). This leads to precise positioning of monomers in the active receptor kinase dimer. These findings open new possibilities for developing novel anti-angiogenic compounds specifically targeting the homotypic interactions described here.

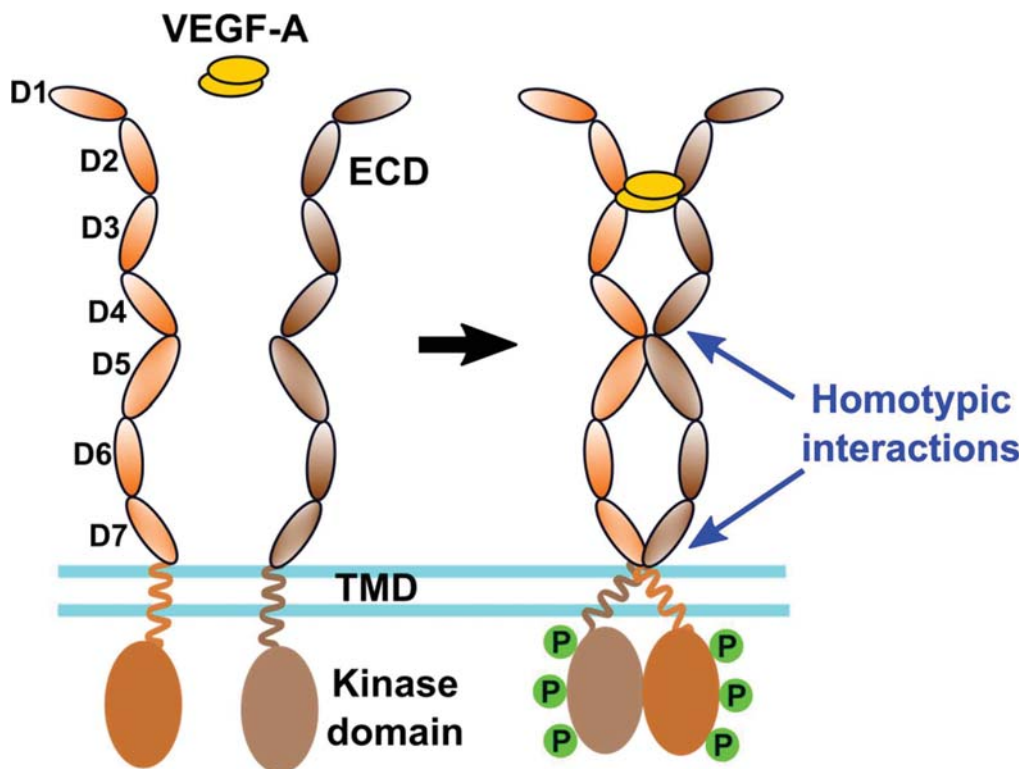


Figure 29: Schematic representation of VEGFR-1 and -2 dimerization and activation induced by ligand VEGF-A.

9. Conclusion

VEGFRs and their ligands are among the most prominent regulators of angiogenic and lymphatic development. Disturbance of their tight and multi-level regulation of downstream signaling results in numerous pathological conditions and are relevant in cancer progression and in various ischemic and inflammatory diseases (Carmeliet *et al.*, 2000). Biophysical and structure-function studies of this receptor system will contribute highly relevant information for elucidating the exact molecular mechanisms involved in receptor activation. Distinct Ig-homology domains are promising target sites for the development of highly specific compounds for future medical applications such as for instance therapies restricting aberrant angiogenesis.

We could verify by two in solution native-like environment based biophysical methods that dimerization of the VEGFR-2 ECD upon ligand binding depends on two types of modules interacting with each other: ligand binding to Ig-homology domains 2-3 are highly favourable thermodynamic interactions while homotypic interactions arising in Ig-homology domains 4-7 comes with an unfavourable endothermic enthalpy. Hence we propose that the membrane proximal domains in the ECD play an important role in maintaining the receptor in an inactive state in the absence of ligand while being essential for receptor activation by VEGF. These findings document that dimerization per se is not sufficient for receptor activation. We assume that specific orientation of distinct subdomains is required to accomplish receptor interactions acting as checkpoints for kinase activation.

The molecular details revealed by X-ray crystallography on VEGFR-1 were analyzed by carrying out functional experiments involving ligand binding and receptor activation. *In vitro* EC assays showed that VEGFR-1, upon binding to PlGF, leads to autophosphorylation of tyrosine residue 1213 present in the C-terminal domain. The introduction of mutations in the residues involved in the observed domain 5 interactions following ligand binding to VEGFR-1, resulted in reduced phosphorylation activity of VEGFR-1/2 chimeric constructs. In addition, similar mutations in the homologous residues in domain 5 of VEGFR-2 significantly decreased autophosphorylation activity. The above results suggest that Ig-homology domain 5 interactions are well conserved among the VEGFR family members. We propose that the hydrogen bonds and salt

bridges involved in homotypic interactions in domains 5 and 7 lead to local structural rigidity and alignment of the ECD thereby promoting TMD reorientation which then leads to VEGFR kinase activation.

Based on the conformational and functional insights acquired in this thesis on VEGFR-1 and 2, novel drugs either suppressing or activating vessel growth can be developed in the future.

10. Acknowledgement

First and foremost I would like to express my sincere gratitude to my advisor, Prof. Dr. Kurt Ballmer-Hofer for the opportunity he has given to me to pursue my Ph.D. under his able guidance, in his research group. His immense knowledge in the field motivated me to address new scientific questions and the challenges involved.

I would like to thank my thesis committee members Dr. Philipp Berger and Prof. Dr. Timm Maier profusely for their insightful comments and words of encouragement. Their feedback helped me to widen my research from different perspectives.

I am also grateful to Dr. Timothy Sharpe for permitting me to use the biophysics facility at Biozentrum and for his help in collection and assimilation of data. His in-depth know-how in the field and perpetual guidance helped me to work on difficult proteins. I convey my thanks to Dr. Richard Kammerer and Dr. Roger Benoit whose insight into molecular biology has resulted in designing and expressing many constructs used in the study. I would like to thank Dr. May Marsh Sharpe and Laura Vera for their assistance at SLS facility and also their direct involvement in crystallization trials of my proteins.

My special thanks goes to my fellow lab mates - Dragana Avramovic, Nagjie Alijaj, Milicia Bugarski, Dr. Caroline Hyde, Antonietta Gasperina, Dr. Petra Hillmann-Wuellner, Dr. Kaisa Kisko, Julia Kostin, Sandro Leuscher, Dr. Sandro Manni, Dr. Sandra Markovic-Mueller, Dr. Maysam Mansouri, Dr. Maria Mitsi, Dr. Aurelien Rizk, Ulla Suter, Thomas Schleier, Lydia Schmitz, Katherine Thieltges, Cornelia Walther, Richard West and Ye Xie - for their enormous support extended to me in carrying out experiments and holding discussions at length during my trying times.

I would like to extend my sincerest thanks to my parents and in-laws for boosting my morale throughout my writing of this thesis. My heartfelt thanks to my husband, Ashish, whose unconditional love, patience and continued support in my academic endeavours over the past several years has enabled me to complete this thesis. And finally the happiness and affection which I receive from my daughter has helped me in finishing, which at one point of time in my life seemed to be far-fetched.

11. References

Abedi,H., and Zachary,I. (1997). Vascular endothelial growth factor stimulates tyrosine phosphorylation and recruitment to new focal adhesions of focal adhesion kinase and paxillin in endothelial cells. *J. Biol. Chem.* 272, 15442-15451.

Albuquerque,R.J., Hayashi,T., Cho,W.G., Kleinman,M.E., Dridi,S., Takeda,A., Baffi,J.Z., Yamada,K., Kaneko,H., Green,M.G., Chappell,J., Wilting,J., Weich,H.A., Yamagami,S., Amano,S., Mizuki,N., Alexander,J.S., Peterson,M.L., Brekken,R.A., Hirashima,M., Capoor,S., Usui,T., Ambati,B.K., and Ambati,J. (2009). Alternatively spliced vascular endothelial growth factor receptor-2 is an essential endogenous inhibitor of lymphatic vessel growth. *Nat Med* 15, 1023-1030.

Anisimov,A., Leppänen,V.M., Tvorogov,D., Zarkada,G., Jeltsch,M., Holopainen,T., Kajjalainen,S., and Alitalo,K. (2013). The basis for the distinct biological activities of vascular endothelial growth factor receptor-1 ligands. *Sci. Signal.* 6, ra52.

Aricescu,A.R., Lu,W., and Jones,E.Y. (2006). A time- and cost-efficient system for high-level protein production in mammalian cells. *Acta Crystallogr. D. Biol. Crystallogr.* 62, 1243-1250.

Autiero,M., Waltenberger,J., Communi,D., Kranz,A., Moons,L., Lambrechts,D., Kroll,J., Plaisance,S., De Mol,M., Bono,F., Kliche,S., Fellbrich,G., Ballmer-Hofer,K., Maglione,D., Mayr-Beyrle,U., Dewerschin,M., Dombrowski,S., Stanimirovic,D., Van Hummelen,P., Dehio,C., Hicklin,D.J., Persico,G., Herbert,J.M., Communi,D., Shibuya,M., Collen,D., Conway,E.M., and Carmeliet,P. (2003). Role of PlGF in the intra- and intermolecular cross talk between the VEGF receptors Flt1 and Flk1. *Nat Med* 9, 936-943.

Baish,J.W., and Jain,R.K. (2000). Fractals and cancer. *Cancer Res.* 60, 3683-3688.

Baldwin,M.E., Halford,M.M., Roufail,S., Williams,R.A., Hibbs,M.L., Grail,D., Kubo,H., Stacker,S.A., and Achen,M.G. (2005). Vascular endothelial growth factor D is dispensable for development of the lymphatic system. *Mol. Cell Biol.* 25, 2441-2449.

Ballmer-Hofer,K., Hyde,A.C., Schleier,T., and Avramovic,D. (2018). ScFvs as Allosteric Inhibitors of VEGFR-2: Novel Tools to Harness VEGF Signaling. *Int. J. Mol. Sci.* 19, 1334.

Bates,D.O., and Harper,S.J. (2002). Regulation of vascular permeability by vascular endothelial growth factors. *Vascul. Pharmacol.* 39, 225-237.

Bell,C.A., Tynan,J.A., Hart,K.C., Meyer,A.N., Robertson,S.C., and Donoghue,D.J. (2000). Rotational coupling of the transmembrane and kinase domains of the neu receptor tyrosine kinase. *Mol. Biol. Cell* 11, 3589-3599.

Bellomo,D., Headrick,J.P., Silins,G.U., Paterson,C.A., Thomas,P.S., Gartside,M., Mould,A., Cahill,M.M., Tonks,I.D., Grimmond,S.M., Townson,S., Wells,C., Little,M., Cummings,M.C., Hayward,N.K., and Kay,G.F. (2000). Mice lacking the vascular endothelial growth factor-B gene (Vegfb) have smaller hearts, dysfunctional coronary vasculature, and impaired recovery from cardiac ischemia. *Circ. Res.* 86, E29-E35.

Bergers,G., and Hanahan,D. (2008). Modes of resistance to anti-angiogenic therapy. *Nat Rev Cancer* 8, 592-603.

Berger, I., Fitzgerald, D.J., and Richmond, T.J. (2004). Baculovirus expression system for heterologous multiprotein complexes. *Nat. Biotechnol.* 22, 1583-1587.

Biswas, P., Sengupta, S., Choudhary, R., Home, S., Paul, A., and Sinha, S. (2011). Comparing ranibizumab with bevacizumab. *Ophthalmology* 118, 600.

Brozzo, M.S., Bjelic, S., Kisko, K., Schleier, T., Leppänen, V.M., Alitalo, K., Winkler, F.K., and Ballmer-Hofer, K. (2012). Thermodynamic and structural description of allosterically regulated VEGF receptor 2 dimerization. *Blood* 119, 1781-1788.

Bry, M., Kivela, R., Leppanen, V.M., and Alitalo, K. (2014). Vascular endothelial growth factor-B in physiology and disease. *Physiol. Rev.* 94, 779-794.

Caldwell, R.B., Bartoli, M., Behzadian, M.A., El Remessy, A.E., Al Shabrawey, M., Platt, D.H., and Caldwell, R.W. (2003). Vascular endothelial growth factor and diabetic retinopathy: pathophysiological mechanisms and treatment perspectives. *Diabetes Metab Res. Rev.* 19, 442-455.

Carmeliet, P. (2003). Angiogenesis in health and disease. *Nat. Med.* 9, 653-660.

Carmeliet, P., Ferreira, V., Breier, G., Pollefeyt, S., Kieckens, L., Gertsenstein, M., Fahrig, M., Vandenhoek, A., Harpal, K., Eberhardt, C., Declercq, C., Pawling, J., Moons, L., Collen, D., Risau, W., and Nagy, A. (1996). Abnormal blood vessel development and lethality in embryos lacking a single VEGF allele. *Nature* 380, 435-439.

Carmeliet, P., and Jain, R.K. (2000). Angiogenesis in cancer and other diseases. *Nature* 407, 249-257.

Carmeliet, P., and Jain, R.K. (2011). Molecular mechanisms and clinical applications of angiogenesis. *Nature* 473, 298-307.

Carmeliet, P., Moons, L., Luttun, A., Vincenti, V., Compernelle, V., De Mol, M., Wu, Y., Bono, F., Devy, L., Beck, H., Scholz, D., Acker, T., DiPalma, T., Dewerchin, M., Noel, A., Stalmans, I., Barra, A., Blacher, S., Vandendriessche, T., Ponten, A., Eriksson, U., Plate, K.H., Foidart, J.M., Schaper, W., Charnock-Jones, D.S., Hicklin, D.J., Herbert, J.M., Collen, D., and Persico, M.G. (2001). Synergism between vascular endothelial growth factor and placental growth factor contributes to angiogenesis and plasma extravasation in pathological conditions. *Nat Med* 7, 575-583.

Carmeliet, P., Ng, Y.S., Nuyens, D., Theilmeier, G., Brusselmans, K., Cornelissen, I., Ehler, E., Kakkar, V., V, Stalmans, I., Mattot, V., Perriard, J., Dewerchin, M., Flameng, W., Nagy, A., Lupu, F., Moons, L., Collen, D., Amore, P.A., and Shima, D.T. (1999). Impaired myocardial angiogenesis and ischemic cardiomyopathy in mice lacking the vascular endothelial growth factor isoforms VEGF164 and VEGF188. *Nat Med* 5, 495-502.

Carneiro, A.M., Silva, R.M., Veludo, M.J., Barbosa, A., Ruiz-Moreno, J.M., Falcao, M.S., Brandao, E.M., and Falcao-Reis, F.M. (2011). Ranibizumab treatment for choroidal neovascularization from causes other than age-related macular degeneration and pathological myopia. *Ophthalmologica* 225, 81-88.

Chen, L., Placone, J., Novicky, L., and Hristova, K. (2010). The extracellular domain of fibroblast growth factor receptor 3 inhibits ligand-independent dimerization. *Sci. Signal.* 3, ra86.

Cho,H.S., Mason,K., Ramyar,K.X., Stanley,A.M., Gabelli,S.B., Denney,D.W., Jr., and Leahy,D.J. (2003). Structure of the extracellular region of HER2 alone and in complex with the Herceptin Fab. *Nature* **421**, 756-760.

Christinger,H.W., Fuh,G., de Vos,A.M., and Wiesmann,C. (2004). The crystal structure of PIGF in complex with domain 2 of VEGFR1. *J. Biol. Chem.* **279**, 10382-10388.

Claesson-Welsh,L. (2016). VEGF receptor signal transduction - A brief update. *Vascul. Pharmacol.* **86**, 14-17.

Claffey,K.P., Senger,D.R., and Spiegelman,B.M. (1995). Structural requirements for dimerization, glycosylation, secretion, and biological function of VPF/VEGF. *Biochim. Biophys. Acta* **1246**, 1-9.

Cudmore,M.J., Hewett,P.W., Ahmad,S., Wang,K.Q., Cai,M., Al-Ani,B., Fujisawa,T., Ma,B., Sissaoui,S., Ramma,W., Miller,M.R., Newby,D.E., Gu,Y., Barleon,B., Weich,H., and Ahmed,A. (2012). The role of heterodimerization between VEGFR-1 and VEGFR-2 in the regulation of endothelial cell homeostasis. *Nat. Commun.* **3**, 972.

Cunningham,S.A., Arrate,M.P., Brock,T.A., and Waxham,M.N. (1997). Interactions of FLT-1 and KDR with phospholipase C α : identification of the phosphotyrosine binding sites. *Biochem. Biophys. Res. Commun.* **240**, 635-639.

Davydova,N., Harris,N.C., Roufail,S., Paquet-Fifield,S., Ishaq,M., Streltsov,V.A., Williams,S.P., Karnezis,T., Stacker,S.A., and Achen,M.G. (2016). Differential Receptor Binding and Regulatory Mechanisms for the Lymphangiogenic Growth Factors Vascular Endothelial Growth Factor (VEGF)-C and -D. *J. Biol. Chem.* **291**, 27265-27278.

Dayanir,V., Meyer,R.D., Lashkari,K., and Rahimi,N. (2001). Identification of tyrosine residues in vascular endothelial growth factor receptor-2/FLK-1 involved in activation of phosphatidylinositol-3 kinase and cell proliferation. *J. Biol. Chem.* **276**, 17686-17692.

Dell'Era Dosch,D., and Ballmer-Hofer,K. (2010). Transmembrane domain-mediated orientation of receptor monomers in active VEGFR-2 dimers. *FASEB J.* **24**, 32-38.

Dewerchin,M., and Carmeliet,P. (2012). PIGF: a multitasking cytokine with disease-restricted activity. *Cold Spring Harb. Perspect. Med.* **2**, a011056.

Dhondt,J., Peeraer,E., Verheyen,A., Nuydens,R., Buyschaert,I., Poesen,K., VanGeyte,K., Beerens,M., Shibuya,M., Haigh,J.J., Meert,T., Carmeliet,P., and Lambrechts,D. (2011). Neuronal FLT1 receptor and its selective ligand VEGF-B protect against retrograde degeneration of sensory neurons. *FASEB J.* **25**, 1461-1473.

Dixelius,J., Makinen,T., Wirzenius,M., Karkkainen,M., Wernstedt,C., Alitalo,K., and Claesson-Welsh,L. (2003). Ligand-induced vascular endothelial growth factor receptor-3 (VEGFR-3) heterodimerization with VEGFR-2 in primary lymphatic endothelial cells regulates tyrosine phosphorylation sites. *J. Biol. Chem.* **278**, 40973-40979.

Djonov,V.G., Kurz,H., and Burri,P.H. (2002). Optimality in the developing vascular system: branching remodeling by means of intussusception as an efficient adaptation mechanism. *Dev. Dyn.* **224**, 391-402.

Dougher,M., and Terman,B.I. (1999). Autophosphorylation of KDR in the kinase domain is required for maximal VEGF-stimulated kinase activity and receptor internalization. *Oncogene* 18, 1619-1627.

Dukkipati,A., Park,H.H., Waghay,D., Fischer,S., and Garcia,K.C. (2008). BacMam system for high-level expression of recombinant soluble and membrane glycoproteins for structural studies. *Protein Expr. Purif.* 62, 160-170.

Dumont,D.J., Jussila,L., Taipale,J., Lymboussaki,A., Mustonen,T., Pajusola,K., Breitman,M., and Alitalo,K. (1998). Cardiovascular failure in mouse embryos deficient in VEGF receptor-3. *Science* 282, 946-949.

Ebos,J.M., Bocci,G., Man,S., Thorpe,P.E., Hicklin,D.J., Zhou,D., Jia,X., and Kerbel,R.S. (2004). A naturally occurring soluble form of vascular endothelial growth factor receptor 2 detected in mouse and human plasma. *Mol. Cancer Res.* 2, 315-326.

Eichmann,A., and Simons,M. (2012). VEGF signaling inside vascular endothelial cells and beyond. *Curr. Opin. Cell Biol.* 24, 188-193.

Enholm,B., Paavonen,K., Ristimaki,A., Kumar,V., Gunji,Y., Klefstrom,J., Kivinen,L., Laiho,M., Olofsson,B., Joukov,V., Eriksson,U., and Alitalo,K. (1997). Comparison of VEGF, VEGF-B, VEGF-C and Ang-1 mRNA regulation by serum, growth factors, oncoproteins and hypoxia. *Oncogene* 14, 2475-2483.

Fan,X., Rai,A., Kambham,N., Sung,J.F., Singh,N., Pettitt,M., Dhal,S., Agrawal,R., Sutton,R.E., Druzin,M.L., Gambhir,S.S., Ambati,B.K., Cross,J.C., and Nayak,N.R. (2014). Endometrial VEGF induces placental sFLT1 and leads to pregnancy complications. *J Clin Invest* 124, 4941-4952.

Ferrara,N., Carver Moore,K., Chen,H., Dowd,M., Lu,L., O Shea,K.S., Powell,B.L., Hillan,K.J., and Moore,M.W. (1996). Heterozygous embryonic lethality induced by targeted inactivation of the VEGF gene. *Nature* 380, 439-442.

Fitzgerald,D.J., Berger,P., Schaffitzel,C., Yamada,K., Richmond,T.J., and Berger,I. (2006). Protein complex expression by using multigene baculoviral vectors. *Nat. Methods* 3, 1021-1032.

Folkman,J. (1971). Tumor angiogenesis: therapeutic implications. *N. Engl. J. Med.* 285, 1182-1186.

Fong,G.H., Rossant,J., Gertsenstein,M., and Breitman,M.L. (1995). Role of the Flt-1 receptor tyrosine kinase in regulating the assembly of vascular endothelium. *Nature* 376, 66-70.

Fong,G.H., Zhang,L., Bryce,D.M., and Peng,J. (1999). Increased hemangioblast commitment, not vascular disorganization, is the primary defect in flt-1 knock-out mice. *Development* 126, 3015-3025.

Fournier,E., Dubreuil,P., Birnbaum,D., and Borg,J.P. (1995). Mutation at tyrosine residue 1337 abrogates ligand-dependent transforming capacity of the FLT4 receptor. *Oncogene* 11, 921-931.

Galvagni,F., Pennacchini,S., Salameh,A., Rocchigiani,M., Neri,F., Orlandini,M., Petraglia,F., Gotta,S., Sardone,G.L., Matteucci,G., Terstappen,G.C., and Oliviero,S. (2010). Endothelial

cell adhesion to the extracellular matrix induces c-Src-dependent VEGFR-3 phosphorylation without the activation of the receptor intrinsic kinase activity. *Circ. Res.* **106**, 1839-1848.

Gariano,R.F., and Gardner,T.W. (2005). Retinal angiogenesis in development and disease. *Nature* **438**, 960-966.

Geiser,M., Cébe,R., Drewello,D., and Schmitz,R. (2001). Integration of PCR fragments at any specific site within cloning vectors without the use of restriction enzymes and DNA ligase. *Biotechniques* **31**, 88-90, 92.

Gibson,D.G., Young,L., Chuang,R.Y., Venter,J.C., Hutchison,C.A., III, and Smith,H.O. (2009). Enzymatic assembly of DNA molecules up to several hundred kilobases. *Nat. Methods* **6**, 343-345.

Gille,H., Kowalski,J., Yu,L., Chen,H., Pisabarro,M.T., Davis,S.T., and Ferrara,N. (2000). A repressor sequence in the juxtamembrane domain of Flt-1 (VEGFR-1) constitutively inhibits vascular endothelial growth factor-dependent phosphatidylinositol 3'-kinase activation and endothelial cell migration. *EMBO J.* **19**, 4064-4073.

Gluzman-Poltorak,Z., Cohen,T., Herzog,Y., and Neufeld,G. (2000). Neuropilin-2 and neuropilin-1 are receptors for the 165-amino acid form of vascular endothelial growth factor (VEGF) and of placenta growth factor-2, but only neuropilin-2 functions as a receptor for the 145-amino acid form of VEGF. *The Journal of biological chemistry* **275**, 18040-18045.

Griffin,L., and Lawson,A. (2011). Antibody fragments as tools in crystallography. *Clin. Exp. Immunol.* **165**, 285-291.

Gu,F., Li,X., Kong,J., Pan,B., Sun,M., Zheng,L., and Yao,Y. (2013). VEGF111b, a new member of VEGFxxx isoforms and induced by mitomycin C, inhibits angiogenesis. *Biochem. Biophys. Res. Commun.* **441**, 18-24.

Hagberg,C.E., Falkevall,A., Wang,X., Larsson,E., Huusko,J., Nilsson,I., van Meeteren,L.A., Samén,E., Lu,L., Vanwildemeersch,M., Klar,J., Genove,G., Pietras,K., Stone-Elander,S., Claesson-Welsh,L., Yla-Herttuala,S., Lindahl,P., and Eriksson,U. (2010). Vascular endothelial growth factor B controls endothelial fatty acid uptake. *Nature* **464**, 917-921.

Hattori,K., Heissig,B., Wu,Y., Dias,S., Tejada,R., Ferris,B., Hicklin,D.J., Zhu,Z., Bohlen,P., Witte,L., Hendrikx,J., Hackett,N.R., Crystal,R.G., Moore,M.A., Werb,Z., Lyden,D., and Rafii,S. (2002). Placental growth factor reconstitutes hematopoiesis by recruiting VEGFR1(+) stem cells from bone-marrow microenvironment. *Nat Med* **8**, 841-849.

Hiratsuka,S., Minowa,O., Kuno,J., Noda,T., and Shibuya,M. (1998). Flt-1 lacking the tyrosine kinase domain is sufficient for normal development and angiogenesis in mice. *Proc. Natl. Acad. Sci. USA* **95**, 9349-9354.

Hiratsuka,S., Nakao,K., Nakamura,K., Katsuki,M., Maru,Y., and Shibuya,M. (2005). Membrane fixation of vascular endothelial growth factor receptor 1 ligand-binding domain is important for vasculogenesis and angiogenesis in mice. *Mol. Cell Biol.* **25**, 346-354.

Hoffmann,D.C., Willenborg,S., Koch,M., Zwolanek,D., Mueller,S., Becker,A.K., Metzger,S., Ehrbar,M., Kurschat,P., Hellmich,M., Hubbell,J.A., and Eming,S.A. (2013). Proteolytic processing regulates Placental growth factor activities. *J. Biol. Chem.* **288**, 17976-17989.

Holash,J., Davis,S., Papadopoulos,N., Croll,S.D., Ho,L., Russell,M., Boland,P., Leidich,R., Hylton,D., Burova,E., Ioffe,E., Huang,T., Radziejewski,C., Bailey,K., Fandl,J.P., Daly,T., Wiegand,S.J., Yancopoulos,G.D., and Rudge,J.S. (2002). VEGF-Trap: A VEGF blocker with potent antitumor effects. *Proc. Natl. Acad. Sci. USA* **99**, 11393-11398.

Holash,J., Wiegand,S.J., and Yancopoulos,G.D. (1999). New model of tumor angiogenesis: dynamic balance between vessel regression and growth mediated by angiopoietins and VEGF. *Oncogene* **18**, 5356-5362.

Hollister,J., Grabenhorst,E., Nimitz,M., Conradt,H., and Jarvis,D.L. (2002). Engineering the protein N-glycosylation pathway in insect cells for production of biantennary, complex N-glycans. *Biochemistry* **41**, 15093-15104.

Houck,K.A., Ferrara,N., Winer,J., Cachianes,G., Li,B., and Leung,D.W. (1991). The vascular endothelial growth factor family: identification of a fourth molecular species and characterization of alternative splicing of RNA. *Mol. Endocrinol.* **5**, 1806-1814.

Hudson,N., Powner,M.B., Sarker,M.H., Burgoyne,T., Campbell,M., Ockrim,Z.K., Martinelli,R., Futter,C.E., Grant,M.B., Fraser,P.A., Shima,D.T., Greenwood,J., and Turowski,P. (2014). Differential apicobasal VEGF signaling at vascular blood-neural barriers. *Dev. Cell* **30**, 541-552.

Hyde,C.A., Giese,A., Stuttfeld,E., Abram,S.J., Villemagne,D., Schleier,T., Binz,H.K., and Ballmer-Hofer,K. (2012). Targeting the extracellular domains D4 and D7 of VEGFR-2 reveals allosteric receptor regulatory sites. *Mol. Cell Biol.* **32**, 3802-3813.

Igarashi,K., Isohara,T., Kato,T., Shigeta,K., Yamano,T., and Uno,I. (1998). Tyrosine 1213 of Flt-1 is a major binding site of Nck and SHP-2. *Biochem. Biophys. Res. Commun.* **246**, 95-99.

Iyer,S., Darley,P.I., and Acharya,K.R. (2010). Structural insights into the binding of VEGF-B by VEGFR-1D2: Recognition and specificity. *J. Biol. Chem.* **285**, 23779-23789.

Jakobsson,L., Bentley,K., and Gerhardt,H. (2009). VEGFRs and Notch: a dynamic collaboration in vascular patterning. *Biochem Soc. Trans.* **37**, 1233-1236.

Jeltsch,M., Karpanen,T., Strandin,T., Aho,K., Lankinen,H., and Alitalo,K. (2006). Vascular endothelial growth factor (VEGF)/VEGF-C mosaic molecules reveal specificity determinants and feature novel receptor binding patterns. *J. Biol. Chem.* **281**, 12187-12195.

Jerabek-Willemsen,M., Wienken,C.J., Braun,D., Baaske,P., and Duhr,S. (2011). Molecular interaction studies using microscale thermophoresis. *Assay. Drug Dev. Technol.* **9**, 342-353.

Joory,K.D., Levick,J.R., Mortimer,P.S., and Bates,D.O. (2006). Vascular endothelial growth factor-C (VEGF-C) expression in normal human tissues. *Lymphat. Res. Biol.* **4**, 73-82.

Joukov,V., Pajusola,K., Kaipainen,A., Chilov,D., Lahtinen,I., Kukk,E., Saksela,O., Kalkkinen,N., and Alitalo,K. (1996). A novel vascular endothelial growth factor, VEGF-C, is a ligand for the Flt4 (VEGFR-3) and KDR (VEGFR-2) receptor tyrosine kinases. *EMBO J.* **15**, 290-298.

Joukov,V., Sorsa,T., Kumar,V., Jeltsch,M., Claesson-Welsh,L., Cao,Y., Saksela,O., Kalkkinen,N., and Alitalo,K. (1997). Proteolytic processing regulates receptor specificity and activity of VEGF-C. *EMBO J.* **16**, 3898-3911.

Kabrun,N., Buhring,H.J., Choi,K., Ullrich,A., Risau,W., and Keller,G. (1997). Flk-1 expression defines a population of early embryonic hematopoietic precursors. *Development* 124, 2039-2048.

Karkkainen,M.J., Haiko,P., Sainio,K., Partanen,J., Taipale,J., Petrova,T.V., Jeltsch,M., Jackson,D.G., Talikka,M., Rauvala,H., Betsholtz,C., and Alitalo,K. (2003). Vascular endothelial growth factor C is required for sprouting of the first lymphatic vessels from embryonic veins. *Nat Immunol* 5, 74-80.

Kendall,R.L., Rutledge,R.Z., Mao,X., Tebben,A.J., Hungate,R.W., and Thomas,K. (1999). Vascular endothelial growth factor receptor KDR tyrosine kinase activity is increased by autophosphorylation of two activation loop tyrosine residues. *J. Biol. Chem.* 274, 6453-6460.

Kendall,R.L., and Thomas,K.A. (1993). Inhibition of vascular endothelial cell growth factor activity by an endogenously encoded soluble receptor. *Proc. Natl. Acad. Sci. USA* 90, 10705-10709.

Keyt,B.A., Berleau,L.T., Nguyen,H.V., Chen,H., Heinsohn,H., Vandlen,R., and Ferrara,N. (1996). The carboxyl-terminal domain (111-165) of vascular endothelial growth factor is critical for its mitogenic potency. *J. Biol. Chem.* 271, 7788-7795.

Kiba,A., Sagara,H., Hara,T., and Shibuya,M. (2003). VEGFR-2-specific ligand VEGF-E induces non-edematous hyper-vascularization in mice. *Biochem. Biophys. Res. Commun.* 301, 371-377.

Kim,L.A., and D'Amore,P.A. (2012). A Brief History of Anti-VEGF for the Treatment of Ocular Angiogenesis. *Am. J. Pathol.* 181, 376-379.

Kisko,K., Brozzo,M.S., Missimer,J., Schleier,T., Menzel,A., Leppänen,V.M., Alitalo,K., Walzthoeni,T., Aebersold,R., and Ballmer-Hofer,K. (2011). Structural analysis of vascular endothelial growth factor receptor-2/ligand complexes by small-angle X-ray solution scattering. *FASEB J.* 25, 2980-2986.

Kivela,R., Bry,M., Robciuc,M.R., Rasanen,M., Taavitsainen,M., Silvola,J.M., Saraste,A., Hulmi,J.J., Anisimov,A., Mayranpaa,M.I., Lindeman,J.H., Eklund,L., Hellberg,S., Hlushchuk,R., Zhuang,Z.W., Simons,M., Djonov,V., Knuuti,J., Mervaala,E., and Alitalo,K. (2014). VEGF-B-induced vascular growth leads to metabolic reprogramming and ischemia resistance in the heart. *EMBO Mol. Med.* 6, 307-321.

Koch,S., and Claesson-Welsh,L. (2012). Signal transduction by vascular endothelial growth factor receptors. *Cold Spring Harb. Perspect. Med.* 2, a006502.

Koch,S., Tugues,S., Li,X., Gualandi,L., and Claesson-Welsh,L. (2011). Signal transduction by vascular endothelial growth factor receptors. *Biochem. J.* 437, 169-183.

Krupitskaya,Y., and Wakelee,H.A. (2009). Ramucirumab, a fully human mAb to the transmembrane signaling tyrosine kinase VEGFR-2 for the potential treatment of cancer. *Curr. Opin. Investig. Drugs* 10, 597-605.

Lamallice,L., Houle,F., Jourdan,G., and Huot,J. (2004). Phosphorylation of tyrosine 1214 on VEGFR2 is required for VEGF-induced activation of Cdc42 upstream of SAPK2/p38. *Oncogene* 23, 434-445.

Lanahan,A.A., Hermans,K., Claes,F., Kerley-Hamilton,J.S., Zhuang,Z.W., Giordano,F.J., Carmeliet,P., and Simons,M. (2010). VEGF Receptor 2 Endocytic Trafficking Regulates Arterial Morphogenesis. *Dev Cell* *18*, 713-724.

Lange,T., Gutman-Raviv,N., Baruch,L., Machluf,M., and Neufeld,G. (2003). VEGF162 : A new heparin binding VEGF splice form that is expressed in transformed human cells. *J. Biol. Chem.* *278*, 17164-17169.

Lee,S., Chen,T.T., Barber,C.L., Jordan,M.C., Murdock,J., Desai,S., Ferrara,N., Nagy,A., Roos,K.P., and Iruela-Arispe,M.L. (2007). Autocrine VEGF signaling is required for vascular homeostasis. *Cell* *130*, 691-703.

Lee,S., Jilani,S.M., Nikolova,G.V., Carpizo,D., and Iruela-Arispe,M.L. (2005). Processing of VEGF-A by matrix metalloproteinases regulates bioavailability and vascular patterning in tumors. *J. Cell Biol.* *169*, 681-691.

Leppänen,V.M., Jeltsch,M., Anisimov,A., Tvorogov,D., Aho,K., Kalkkinen,N., Toivanen,P., Yla-Herttuala,S., Ballmer-Hofer,K., and Alitalo,K. (2011). Structural determinants of vascular endothelial growth factor-D - receptor binding and specificity. *Blood* *117*, 1507-1515.

Leppänen,V.M., Tvorogov,D., Kisko,K., Prota,A.E., Jeltsch,M., Anisimov,A., Markovic-Mueller,S., Stutfeld,E., Goldie,K.N., Ballmer-Hofer,K., and Alitalo,K. (2013). Structural and mechanistic insights into VEGF receptor 3 ligand binding and activation. *Proc. Natl. Acad. Sci. USA* *110*, 12960-12965.

Lundkvist,A., Lee,S., Iruela-Arispe,L., Betsholtz,C., and Gerhardt,H. (2007). Growth factor gradients in vascular patterning. *Novartis Found. Symp.* *283*, 194-201.

Luttun,A., Tjwa,M., Moons,L., Wu,Y., Angelillo-Scherrer,A., Liao,F., Nagy,J.A., Hooper,A., Priller,J., De Klerck,B., Compennolle,V., Daci,E., Bohlen,P., Dewerchin,M., Herbert,J.M., Fava,R., Matthys,P., Carmeliet,G., Collen,D., Dvorak,H.F., Hicklin,D.J., and Carmeliet,P. (2002). Revascularization of ischemic tissues by PlGF treatment, and inhibition of tumor angiogenesis, arthritis and atherosclerosis by anti-Flt1. *Nat Med* *8*, 831-840.

Lyttle,D.J., Fraser,K.M., Fleming,S.B., Mercer,A.A., and Robinson,A.J. (1994). Homologs of vascular endothelial growth factor are encoded by the poxvirus orf virus. *J. Virol.* *68*, 84-92.

Maes,C., Stockmans,I., Moermans,K., Van Loveren,R., Smets,N., Carmeliet,P., Bouillon,R., and Carmeliet,G. (2004). Soluble VEGF isoforms are essential for establishing epiphyseal vascularization and regulating chondrocyte development and survival. *J. Clin. Invest.* *113*, 188-199.

Maglione,D., Guerriero,V., Viglietto,G., Ferraro,M.G., Aprelikova,O., Alitalo,K., Del Vecchio,S., Lei,K.J., Chou,J.Y., and Persico,M.G. (1993). Two alternative mRNAs coding for the angiogenic factor, placenta growth factor (PlGF), are transcribed from a single gene of chromosome 14. *Oncogene* *8*, 925-931.

Makinen,T., Olofsson,B., Karpanen,T., Hellman,U., Soker,S., Klagsbrun,M., Eriksson,U., and Alitalo,K. (1999). Differential binding of vascular endothelial growth factor B splice and proteolytic isoforms to neuropilin-1. *J. Biol. Chem.* *274*, 21217-21222.

Makinen,T., Veikkola,T., Mustjoki,S., Karpanen,T., Catimel,B., Nice,E.C., Wise,L., Mercer,A., Kowalski,H., Kerjaschki,D., Stacker,S.A., Achen,M.G., and Alitalo,K. (2001). Isolated

lymphatic endothelial cells transduce growth, survival and migratory signals via the VEGF-C/D receptor VEGFR-3. *EMBO J.* 20, 4762-4773.

Manni,S., Kisko,K., Schleier,T., Missimer,J., and Ballmer-Hofer,K. (2014a). Functional and structural characterization of the kinase insert and the carboxy terminal domain in VEGF receptor 2 activation. *FASEB J* 28, 4914-4923.

Manni,S., Mineev,K.S., Usmanova,D., Lyukmanova,E.N., Shulepko,M.A., Kirpichnikov,M.P., Winter,J., Matkovic,M., Deupi,X., Arseniev,A.S., and Ballmer-Hofer,K. (2014b). Structural and functional characterization of alternative transmembrane domain conformations in VEGF receptor 2 activation. *Structure* 22, 1077-1089.

Mansouri,M., Bellon-Echeverria,I., Rizk,A., Ehsaei,Z., Cianciolo,C.C., Silva,C.S., Xie,Y., Boyce,F.M., Davis,M.W., Neuhauss,S.C., Taylor,V., Ballmer-Hofer,K., Berger,I., and Berger,P. (2016). Highly efficient baculovirus-mediated multigene delivery in primary cells. *Nat. Commun.* 7, 11529.

Matsumoto,T., Bohman,S., Dixelius,J., Berge,T., Dimberg,A., Magnusson,P., Wang,L., Wikner,C., Qi,J.H., Wernstedt,C., Wu,J., Bruheim,S., Mugishima,H., Mukhopadhyay,D., Spurkland,A., and Claesson-Welsh,L. (2005). VEGF receptor-2 Y951 signaling and a role for the adapter molecule TSAd in tumor angiogenesis. *EMBO J.* 24, 2342-2353.

Matsumoto,T., and Claesson-Welsh,L. (2001). VEGF Receptor Signal Transduction. *Sci. STKE* 2001, RE21.

Maynard,S.E., Min,J.Y., Merchan,J., Lim,K.H., Li,J., Mondal,S., Libermann,T.A., Morgan,J.P., Sellke,F.W., Stillman,I.E., Epstein,F.H., Sukhatme,V.P., and Karumanchi,S.A. (2003). Excess placental soluble fms-like tyrosine kinase 1 (sFlt1) may contribute to endothelial dysfunction, hypertension, and proteinuria in preeclampsia. *J. Clin. Invest.* 111, 649-658.

Meyer,M., Clauss,M., Lepple,W.A., Waltenberger,J., Augustin,H.G., Ziche,M., Lanz,C., Buttner,M., Rziha,H.J., and Dehio,C. (1999). A novel vascular endothelial growth factor encoded by Orf virus, VEGF-E, mediates angiogenesis via signalling through VEGFR-2 (KDR) but not VEGFR-1 (Flt-1) receptor tyrosine kinases. *EMBO J.* 18, 363-374.

Meyer,R.D., Mohammadi,M., and Rahimi,N. (2006). A single amino acid substitution in the activation loop defines the decoy characteristic of VEGFR-1/FLT-1. *J. Biol. Chem.* 281, 867-875.

Motzer,R.J., Hutson,T.E., Glen,H., Michaelson,M.D., Molina,A., Eisen,T., Jassem,J., Zolnierak,J., Maroto,J.P., Mellado,B., Melichar,B., Tomasek,J., Kremer,A., Kim,H.J., Wood,K., Dutcus,C., and Larkin,J. (2015). Lenvatinib, everolimus, and the combination in patients with metastatic renal cell carcinoma: a randomised, phase 2, open-label, multicentre trial. *Lancet Oncol.* 16, 1473-1482.

Nagy,J.A., Chang,S.H., Shih,S.C., Dvorak,A.M., and Dvorak,H.F. (2010). Heterogeneity of the tumor vasculature. *Semin. Thromb. Hemost.* 36, 321-331.

Nilsson,I., Bahram,F., Li,X., Gualandi,L., Koch,S., Jarvius,M., Soderberg,O., Anisimov,A., Kholova,I., Pytowski,B., Baldwin,M., Yla-Herttuala,S., Alitalo,K., Kreuger,J., and Claesson-Welsh,L. (2010). VEGF receptor 2/-3 heterodimers detected in situ by proximity ligation on angiogenic sprouts. *EMBO J.* 29, 1377-1388.

O'Flynn,N.M., Patel,A., Kadlec,J., and Jones,I.M. (2012). Improving promiscuous mammalian cell entry by the baculovirus *Autographa californica* multiple nuclear polyhedrosis virus. *Biosci. Rep.* **33**, 23-36.

Ogawa,S., Oku,A., Sawano,A., Yamaguchi,S., Yazaki,Y., and Shibuya,M. (1998). A novel type of vascular endothelial growth factor, VEGF-E (NZ-7 VEGF), preferentially utilizes KDR/Fik-1 receptor and carries a potent mitotic activity without heparin-binding domain. *J. Biol. Chem.* **273**, 31273-31282.

Olofsson,B., Pajusola,K., Kaipainen,A., von Euler,G., Joukov,V., Saksela,O., Orpana,A., Pettersson,R.F., Alitalo,K., and Eriksson,U. (1996a). Vascular endothelial growth factor B, a novel growth factor for endothelial cells. *Proc. Natl. Acad. Sci. USA* **93**, 2576-2581.

Olofsson,B., Pajusola,K., von Euler,G., Chilov,D., Alitalo,K., and Eriksson,U. (1996b). Genomic organization of the mouse and human genes for vascular endothelial growth factor B (VEGF-B) and characterization of a second splice isoform. *J. Biol. Chem.* **271**, 19310-19317.

Pajusola,K., Aprelikova,O., Pelicci,G., Weich,H., Claesson-Welsh,L., and Alitalo,K. (1994). Signalling properties of FLT4, a proteolytically processed receptor tyrosine kinase related to two VEGF receptors. *Oncogene* **9**, 3545-3555.

Persico,M.G., Vincenti,V., and DiPalma,T. (1999). Structure, expression and receptor-binding properties of placenta growth factor (PlGF). *Curr. Top. Microbiol. Immunol.* **237**, 31-40.

Prilusky,J., Felder,C.E., Zeev-Ben-Mordehai,T., Rydberg,E.H., Man,O., Beckmann,J.S., Silman,I., and Sussman,J.L. (2005). FoldIndex: a simple tool to predict whether a given protein sequence is intrinsically unfolded. *Bioinformatics.* **21**, 3435-3438.

Rahimi,N. (2006). VEGFR-1 and VEGFR-2: two non-identical twins with a unique physiognomy. *Front Biosci.* **11**, 818-829.

Reeves,P.J., Callewaert,N., Contreras,R., and Khorana,H.G. (2002). Structure and function in rhodopsin: high-level expression of rhodopsin with restricted and homogeneous N-glycosylation by a tetracycline-inducible N-acetylglucosaminyltransferase I-negative HEK293S stable mammalian cell line. *Proc. Natl. Acad. Sci. USA* **99**, 13419-13424.

Risau,W. (1997). Mechanisms of angiogenesis. *Nature* **386**, 671-674.

Roskoski,R.Jr. (2007). Vascular endothelial growth factor (VEGF) signaling in tumor progression. *Crit Rev. Oncol. Hematol.* **62**, 179-213.

Rothlisberger,D., Honegger,A., and Pluckthun,A. (2005). Domain interactions in the Fab fragment: a comparative evaluation of the single-chain Fv and Fab format engineered with variable domains of different stability. *J. Mol. Biol.* **347**, 773-789.

Ruch,C., Skiniotis,G., Steinmetz,M.O., Walz,T., and Ballmer-Hofer,K. (2007). Structure of a VEGF-VEGF receptor complex determined by electron microscopy. *Nat. Struct. Mol. Biol.* **14**, 249-250.

Sakurai,Y., Ohgimoto,K., Kataoka,Y., Yoshida,N., and Shibuya,M. (2005). Essential role of Fik-1 (VEGF receptor 2) tyrosine residue 1173 in vasculogenesis in mice. *Proc. Natl. Acad. Sci. USA* **102**, 1076-1081.

Sarabipour,S., Ballmer-Hofer,K., and Hristova,K. (2016). VEGFR-2 conformational switch in response to ligand binding. *Elife* 5, e13876.

Sawano,A., Iwai,S., Sakurai,Y., Ito,M., Shitara,K., Nakahata,T., and Shibuya,M. (2001). Flt-1, vascular endothelial growth factor receptor 1, is a novel cell surface marker for the lineage of monocyte-macrophages in humans. *Blood* 97, 785-791.

Sawano,A., Takahashi,T., Yamaguchi,S., and Shibuya,M. (1997). The phosphorylated 1169-tyrosine containing region of flt-1 kinase (VEGFR-1) is a major binding site for PLCgamma. *Biochem. Biophys. Res. Commun.* 238, 487-491.

Scheidegger,P., Weiglhofer,W., Suarez,S., Kaser-Hotz,B., Steiner,R., Ballmer-Hofer,K., and Jaussi,R. (1999). Vascular endothelial growth factor (VEGF) and its receptors in tumor-bearing dogs. *Biol. Chem.* 380, 1449-1454.

Seetharam,L., Gotoh,N., Maru,Y., Neufeld,G., Yamaguchi,S., and Shibuya,M. (1995). A unique signal transduction from FLT tyrosine kinase, a receptor for vascular endothelial growth factor VEGF. *Oncogene* 10, 135-147.

Shalaby,F., Rossant,J., Yamaguchi,T.P., Gertsenstein,M., Wu,X.F., Breitman,M.L., and Schuh,A.C. (1995). Failure of blood-island formation and vasculogenesis in Flk-1- deficient mice. *Nature* 376, 62-66.

Shibuya,M. (2003). Vascular endothelial growth factor receptor-2: Its unique signaling and specific ligand, VEGF-E. *Cancer Sci.* 94, 751-756.

Shibuya,M. (2006). Vascular Endothelial Growth Factor (VEGF)-Receptor2: Its Biological Functions, Major Signaling Pathway, and Specific Ligand VEGF-E. *Endothelium* 13, 63-69.

Shibuya,M. (2011). Vascular Endothelial Growth Factor (VEGF) and Its Receptor (VEGFR) Signaling in Angiogenesis: A Crucial Target for Anti- and Pro-Angiogenic Therapies. *Genes Cancer* 2, 1097-1105.

Shibuya,M. (2014). VEGF-VEGFR Signals in Health and Disease. *Biomol. Ther.* 22, 1-9.

Shibuya,M., Yamaguchi,S., Yamane,A., Ikeda,T., Tojo,A., Matsushime,H., and Sato,M. (1990). Nucleotide sequence and expression of a novel human receptor- type tyrosine kinase gene (flt) closely related to the fms family. *Oncogene* 5, 519-524.

Shim,A.H., Liu,H., Focia,P.J., Chen,X., Lin,P.C., and He,X. (2010). Structures of a platelet-derived growth factor/propeptide complex and a platelet-derived growth factor/receptor complex. *Proc. Natl. Acad. Sci. USA* 107, 11307-11312.

Shinkai,A., Ito,M., Anazawa,H., Yamaguchi,S., Shitara,K., and Shibuya,M. (1998). Mapping of the sites involved in ligand association and dissociation at the extracellular domain of the kinase insert domain-containing receptor for vascular endothelial growth factor. *J. Biol. Chem.* 273, 31283-31288.

Shiote,M., Nagano,I., Ilieva,H., Murakami,T., Narai,H., Ohta,Y., Nagata,T., Shoji,M., and Abe,K. (2005). Reduction of a vascular endothelial growth factor receptor, fetal liver kinase-1, by antisense oligonucleotides induces motor neuron death in rat spinal cord exposed to hypoxia. *Neuroscience* 132, 175-182.

Shrimali,R.K., Yu,Z., Theoret,M.R., Chinnasamy,D., Restifo,N.P., and Rosenberg,S.A. (2010). Antiangiogenic agents can increase lymphocyte infiltration into tumor and enhance the effectiveness of adoptive immunotherapy of cancer. *Cancer Res.* **70**, 6171-6180.

Silacci,M., Brack,S., Schirru,G., Marlind,J., Ettore,A., Merlo,A., Viti,F., and Neri,D. (2005). Design, construction, and characterization of a large synthetic human antibody phage display library. *Proteomics* **5**, 2340-2350.

Smith,G.A., Fearnley,G.W., Harrison,M.A., Tomlinson,D.C., Wheatcroft,S.B., and Ponnambalam,S. (2015). Vascular endothelial growth factors: multitasking functionality in metabolism, health and disease. *J Inherit. Metab Dis.* **38**, 753-763.

Stacker,S.A., Caesar,C., Baldwin,M.E., Thornton,G.E., Williams,R.A., Prevo,R., Jackson,D.G., Nishikawa,S., Kubo,H., and Achen,M.G. (2001). VEGF-D promotes the metastatic spread of tumor cells via the lymphatics. *Nat Med* **7**, 186-191.

Stalmans,I., Ng,Y.S., Rohan,R., Fruttiger,M., Bouche,A., Yuce,A., Fujisawa,H., Hermans,B., Shani,M., Jansen,S., Hicklin,D., Anderson,D.J., Gardiner,T., Hammes,H.P., Moons,L., Dewerchin,M., Collen,D., Carmeliet,P., and D'Amore,P.A. (2002). Arteriolar and venular patterning in retinas of mice selectively expressing VEGF isoforms. *J. Clin. Invest.* **109**, 327-336.

Stuttfeld, E 2011, 'The structural and functional characterization of the extracellular domain of vascular endothelial growth factor receptors: Their role in receptor activation and use as therapeutic targets', PhD thesis, University of Basel.

Takahashi,H., and Shibuya,M. (2005). The vascular endothelial growth factor (VEGF)/VEGF receptor system and its role under physiological and pathological conditions. *Clin. Sci. (Lond)* **109**, 227-241.

Takahashi,T., Yamaguchi,S., Chida,K., and Shibuya,M. (2001). A single autophosphorylation site on KDR/Flk-1 is essential for VEGF-A-dependent activation of PLC-gamma and DNA synthesis in vascular endothelial cells. *EMBO J.* **20**, 2768-2778.

Tao,Q., Backer,M.V., Backer,J.M., and Terman,B.I. (2001). Kinase insert domain receptor (kdr) extracellular immunoglobulin-like domains 4-7 contain structural features that block receptor dimerization and vascular endothelial growth factor-induced signaling. *J. Biol. Chem.* **276**, 21916-21923.

Tchaikovski,V., Fellbrich,G., and Waltenberger,J. (2008). The molecular basis of VEGFR-1 signal transduction pathways in primary human monocytes. *Arterioscler. Thromb. Vasc. Biol.* **28**, 322-328.

Terman,B.I., Carrion,M.E., Kovacs,E., Rasmussen,B.A., Eddy,R.L., and Shows,T.B. (1991). Identification of a new endothelial cell growth factor receptor tyrosine kinase. *Oncogene* **6**, 1677-1683.

Thieltges,K.M., Avramovic,D., Piscitelli,C.L., Markovic-Mueller,S., Binz,H.K., and Ballmer-Hofer,K. (2018). Characterization of a drug-targetable allosteric site regulating vascular endothelial growth factor signaling. *Angiogenesis.* **21**, 533-543.

Tvorogov,D., Anisimov,A., Zheng,W., Leppänen,V.M., Tammela,T., Laurinavicius,S., Holnthoner,W., Helotera,H., Holopainen,T., Jeltsch,M., Kalkkinen,N., Lankinen,H., Ojala,P.M., and Alitalo,K. (2010). Effective Suppression of Vascular Network Formation by Combination of

Antibodies Blocking VEGFR Ligand Binding and Receptor Dimerization. *Cancer Cell* *18*, 630-640.

Verstraete,K., Vandriessche,G., Januar,M., Elegheert,J., Shkumatov,A.V., Desfosses,A., Svergun,D.I., Gutsche,I., Vergauwen,B., and Savvides,S.N. (2011). Structural insights into the extracellular assembly of the hematopoietic Flt3 signaling complex. *Blood* *118*, 60-68.

Waltenberger,J., Claesson-Welsh,L., Siegbahn,A., Shibuya,M., and Heldin,C.H. (1994). Different signal transduction properties of KDR and Flt1, two receptors for vascular endothelial growth factor. *J. Biol. Chem.* *269*, 26988-26995.

Wang,H.U., Chen,Z.F., and Anderson,D.J. (1998). Molecular Distinction and Angiogenic Interaction between Embryonic Arteries and Veins Revealed by ephrin-B2 and Its Receptor Eph-B4. *Cell* *93*, 741-753.

Wiesmann,C., Fuh,G., Christinger,H.W., Eigenbrot,C., Wells,J.A., and de Vos,A.M. (1997). Crystal structure at 1.7 Å resolution of VEGF in complex with domain 2 of the Flt-1 receptor. *Cell* *91*, 695-704.

Wise,L.M., Ueda,N., Dryden,N.H., Fleming,S.B., Caesar,C., Roufail,S., Achen,M.G., Stacker,S.A., and Mercer,A.A. (2003). Viral vascular endothelial growth factors vary extensively in amino acid sequence, receptor-binding specificities, and the ability to induce vascular permeability yet are uniformly active mitogens. *J. Biol. Chem.* *278*, 38004-38014.

Wise,L.M., Veikkola,T., Mercer,A.A., Savory,L.J., Fleming,S.B., Caesar,C., Vitali,A., Makinen,T., Alitalo,K., and Stacker,S.A. (1999). Vascular endothelial growth factor (VEGF)-like protein from orf virus NZ2 binds to VEGFR2 and neuropilin-1. *Proc. Natl. Acad. Sci. USA* *96*, 3071-3076.

Xia,P., Aiello,L.P., Ishii,H., Jiang,Z.Y., Park,D.J., Robinson,G.S., Takagi,H., Newsome,W.P., Jirousek,M.R., and King,G.L. (1996). Characterization of vascular endothelial growth factor's effect on the activation of protein kinase C, its isoforms, and endothelial cell growth. *J. Clin. Invest.* *98*, 2018-2026.

Yamazaki,Y., Matsunaga,Y., Tokunaga,Y., Obayashi,S., Saito,M., and Morita,T. (2009). Snake venom vascular endothelial growth factors (VEGF-Fs) exclusively vary their structures and functions among species. *J Biol Chem.* *284*, 9885-9891.

Yang,K., and Cepko,C.L. (1996). Flk-1, a receptor for vascular endothelial growth factor (VEGF), is expressed by retinal progenitor cells. *J. Neurosci.* *16*, 6089-6099.

Yang,W., Ahn,H., Hinrichs,M., Torry,R.J., and Torry,D.S. (2003). Evidence of a novel isoform of placenta growth factor (PlGF-4) expressed in human trophoblast and endothelial cells. *J. Reprod. Immunol.* *60*, 53-60.

Yang,Y., Xie,P., Opatowsky,Y., and Schlessinger,J. (2010). Direct contacts between extracellular membrane-proximal domains are required for VEGF receptor activation and cell signaling. *Proc. Natl. Acad. Sci. USA* *107*, 1906-1911.

Yang,Y., Yuzawa,S., and Schlessinger,J. (2008). Contacts between membrane proximal regions of the PDGF receptor ectodomain are required for receptor activation but not for receptor dimerization. *Proc. Natl. Acad. Sci. USA* *105*, 7681-7686.

Yuzawa,S., Opatowsky,Y., Zhang,Z., Mandiyan,V., Lax,I., and Schlessinger,J. (2007). Structural Basis for Activation of the Receptor Tyrosine Kinase KIT by Stem Cell Factor. *Cell* 130, 323-334.

Curriculum Vitae

Personal Details

Name Mayanka Asthana

Address 163 Addenbrookes Road, CB2 9BA Cambridge, UK

Education

09/11-present **PhD**, Laboratory of Biomolecular Research, Paul Scherer Institute

Thesis title: **Structural and functional characterization of extracellular domains of vascular endothelial growth factor receptor 1 and 2**

Supervisor: Prof. Dr. Kurt Balmer-Hofer

09/09-04/11 **M.Sc.**, Biology (Major in Biochemistry), ETH Zurich

Thesis title: **Substrate Identification of Atg1 Kinase in Autophagy in Yeast**

Supervisor: Prof. Dr. Matthias Peter

08/04-05/08 **B.Tech.**, Biotechnology, Vellore Institute of Technology University, India

Thesis title: **Comparison of Manual and Automated Techniques for Antibiotic Sensitivity Testing of Mycobacterial Strains Isolated from Victims of Bhopal Gas Disaster**

Work Experience

04/11-07/11 **Post Diploma Work**, Prof. Matthias Peters Lab, IBC, ETH Zurich

- **Project: Identifying native members of Atg1 complex in autophagy**

11/08-07/09 **Internship**, Department of Microbiology at Bhopal Memorial Hospital and Research Centre, Bhopal, India

- **Project: Prevalence of Tuberculosis-HIV Co-infection in Central India**

Publications

1. Markovic-Mueller,S., Stuttfeld,E., **Asthana,M.**, Weinert,T., Bliven,S., Goldie,K.N., Kisko,K., Capitani,G., and Ballmer-Hofer,K. (2017). Structure of the Full-length VEGFR-1 Extracellular Domain in Complex with VEGF-A. *Structure* 25, 341-352.
2. Kraft,C., Kijanska,M., Kalie,E., Siergiejuk,E., Lee,S.S., Semplicio,G., Stoffel,I., Brezovich,A., **Verma,M.**, Hansmann,I., Ammerer,G., Hofmann,K., Tooze,S., and Peter,M. (2012). Binding of the Atg1/ULK1 kinase to the ubiquitin-like protein Atg8 regulates autophagy. *EMBO J.* 31, 3691-3703.
3. Desikan,P., De,S., Pai,N.P., Mishra,P.K., Kumar,K., Panwalkar,N., **Verma,M.**, Hasan,Z.U., and Maudar,K.K. (2013). An HIV1/2 point of care test on sputum for screening TB/HIV co-infection in Central India - Will it work? *Asian Pac. J. Trop. Med.* 6, 216-219.
4. Desikan,P., De,S., Pai,N.P., Panwalkar,N., **Verma,M.**, and Jain,A. (2011). A pilot cross-sectional study to determine the utility of an oral HIV1/2 point of care test on sputum for screening TB/HIV co-infection in Central India. *Indian J. Med. Microbiol.* 29, 194-195.
5. Desikan,P., Kumar,Y., Pande,H.K., Jain,A., Panwalkar,N., **Verma,M.**, Bramhne,H.G., Yadav,A., and Mohapatra,S. (2009). Isolated ulcerative skin lesion caused by Salmonella Weltevreden. *J. Infect. Dev. Ctries.* 3, 569-571.
6. Desikan,P., De,S., Mishra,P., Jain,A., Panwalkar,N., **Verma,M.**, and Maudar,K.K. (2009). Comparison of performance characteristics of automated PCR systems with culture for detection of MTB complex from clinical samples in central India. *Indian J. Med. Microbiol.* 27, 277-278.